Provenance of Modern Soils of Middle Tennessee Assessed Using Zircon U-Pb Geochronology and Element Mass Fluxes

By

Nathan James Katsiaficas

Thesis

Submitted to the Faculty of the

Graduate School of Vanderbilt University

in partial fulfillment of the requirements

for the degree of

MASTER OF SCIENCE

In

Earth and Environmental Sciences

December, 2014

Nashville, Tennessee

Approved:

Professor John C. Ayers

Professor David J. Furbish

ACKNOWLEDGEMENTS

This study would not have been possible without financial support from Vanderbilt University's Department of Earth and Environmental Sciences and from the Geological Society of America Southeastern Section. I would especially like to thank Dr. John C. Ayers, Dr. Calvin F. Miller, and Dr. Lily Claiborne, my graduate committee, who have been highly supportive of my academic goals and provided much-needed guidance over the course of my graduate studies. I am deeply indebted to Dr. Ayers, my thesis advisor and committee chair, without whom I would not have had such an exciting venture. He is an exemplary research scientist, and as my mentor over the past two years, has helped me to grow both as a scientist and as a human being. In addition, I owe a great deal of gratitude to Dr. David J. Furbish, who provided me a new lens through which to view earth processes and offered invaluable advice and assistance over the course of this research endeavor.

Much of the data that is presented in this thesis would not be here without the tireless efforts of Ph.D. student and laboratory manager Aaron Covey who maintained the many instruments needed for the analyses in this study. Aaron was also an invaluable source of advice, knowledge, and humor, without whom, my experience as a graduate student would have been diminished. I am additionally grateful to department faculty Dr. Steven L. Goodbred, Dr. Guilherme Gualda, Dr. Daniel Morgan, and Dr. Molly F. Miller as well as visiting scholar Dr. Xiaomei Wang, postdoctoral-scholar Dr. Carol Wilson, and classmates, Dr. Susanne McDowell, Dr. Tamara Carley, Dr. Ayla Pamukcu, David Fry, and Tenley Banik, for their substantial assistance in the field, lab, or otherwise, throughout this project.

None of this would have been possible without the love and support of my family, especially my parents, Jim and Donna, and my siblings, Jacob and Caitlin. Thank you for pushing me to follow my dreams and pursue new challenges. Lastly, I want to thank the entire Earth and Environmental Sciences department as a whole—the staff, students, and faculty—you made those two years at Vanderbilt University some of the best of my life.

TABLE OF CONTENTS

LIST OF TABLES

LIST OF FIGURES

CHAPTER I

INTRODUCTION

Society depends on soil for food production, but little is known about soil formation (pedogenesis) in areas underlain by carbonate rocks, such as limestone and dolomite. Carbonate rocks comprise ~10% of the surficial geology of ice-free continents by area and ~20% of all Phanerozoic sedimentary rocks by volume (Ford and Williams, 2007). In the United States, carbonates are exposed over 17% of the surface area, with the majority occurring in the southeast (Davies et al., 1984). Despite the abundance of limestone exposed at the surface globally, there have been relatively few studies examining the origins of modern soils in limestone terranes. This soil provenance study was designed to characterize the parent material of soils forming atop limestone at two locations in Middle Tennessee using a novel application of zircon U-Pb geochronology, along with element mass fluxes and other geochemical methods. In the following I discuss soil development atop island carbonates and atop the more siliceous carbonates of Middle Tennessee.

I.1 Soil Development in Limestone Terranes

Island Carbonates

Weathering of very pure limestone should not produce soil, yet soils are commonly observed on limestone bedrock. Studies of terra rossa soils atop pure limestones in the Caribbean have shown that these soils were derived from aeolian input of dust from Africa (e.g. Muhs et al., 2007, 2012). While these studies support the development of soil from aeolian parent material rather than from insoluble residues, Muhs et al. (2007) suggest that this may be due to the general lack of significant impurities in island carbonates.

Siliceous Carbonates

In contrast to the high-purity island carbonates, a majority of the bedrock in Middle Tennessee is "dirty" limestone, reported to have a significant silt component (Holland and Patzkowsky, 1997).

Furthermore, African dust is not believed to be a significant soil input in Middle Tennessee. So, what is the parent material for Middle Tennessee soils? Candidates include: 1) loess; 2) alluvial sediments; 3) insoluble residue formed from the dissolution of "dirty" limestone; 4) volcanic material, including volcanic ash. Without volcanoes nearby to provide end-member (4), the southeastern US derives its soil from some combination of the first three end-members. All three are viable candidates for soil formation in Middle Tennessee.

According to the AGI Glossary of Geology (4th ed., 1997), loess is "windblown dust of Pleistocene age, carried from desert surfaces, alluvial valleys, and outwash plains, or from unconsolidated glacial or glaciofluvial deposits uncovered by successive glacial recessions but prior to invasion by a vegetation mat" (p. 375). Abundant loess is found in the Mississippi Valley—a region heavily dissected by dense drainage networks that transport large volumes of sediment. Huckemeyer (1999) examined soil formation atop terraces along a section of the Harpeth River in Middle Tennessee and concluded that the soils were polygenetic, derived primarily from the weathering of the underlying bedrock, but with a secondary loess component. Previous studies have documented massive, thick-bedded units of Mississippi Valley loess in West Tennessee (e.g. Rodbell, 1996 and Rodbell et al., 1997), but there have been no other published studies documenting the presence of this loess this far to the east in Middle Tennessee.

Rivers deposit alluvium in the floodplains along their banks. These floodplains are eventually abandoned as the river continues to incise into the bedrock and become river terraces that, with time, may develop soils atop them from weathering of the alluvium. During chemical weathering of limestone, the calcium carbonate component dissolves congruently, and is thus completely removed, leaving only a residuum containing siliciclastics from whatever silt fraction is present in the rock. While the silt fraction of the "dirty" limestone is probably dominated by quartz, feldspars, and other common silicate minerals, it may also contain heavy minerals, i.e., dense accessory minerals that are commonly used for geochronology such as zircon. Additionally, some of these units, such as the Hermitage Formation,

contain stylolites that formed by carbonate dissolution, which should concentrate zircon and other insoluble minerals.

The purpose of this study is to test the hypothesis that soils within the Middle Tennessee region are derived solely from insoluble residue left behind from the dissolution of the underlying limestone bedrock using zircon U-Pb age spectra, element mass fluxes, and other methods with soil-bedrock pairs collected from two different locations: 1) Atop a high terrace along the Harpeth River identified by Huckemeyer (1999); and 2) On a flat surface atop a road-cut exposure.

CHAPTER II

STUDY LOCATION AND SITE DESCRIPTIONS

II.1 Study Location and Geologic Setting

Middle Tennessee encompasses an area of more than 44,000 km^2 and is comprised of 41 different counties (Foster, 1923/2009). Its borders are geographically defined by a segment of the Tennessee River, which forms the western boundary of this region, and the Cumberland Plateau, which forms the eastern boundary. Middle Tennessee is predominantly comprised of Ordovician and Mississippian bedrock and may be divided into two physiographic provinces, the Nashville Basin (also known as the Central Basin), and the Highland Rim. The Ordovician bedrock, which is exposed in the Nashville Basin, consists of limestone interbedded with shale, whereas the Mississippian bedrock of the Highland Rim and surrounding areas is characterized by abundant chert—especially within the Fort Payne formation—and is less calcareous in composition (Fig. 1; Wilson, 1990).

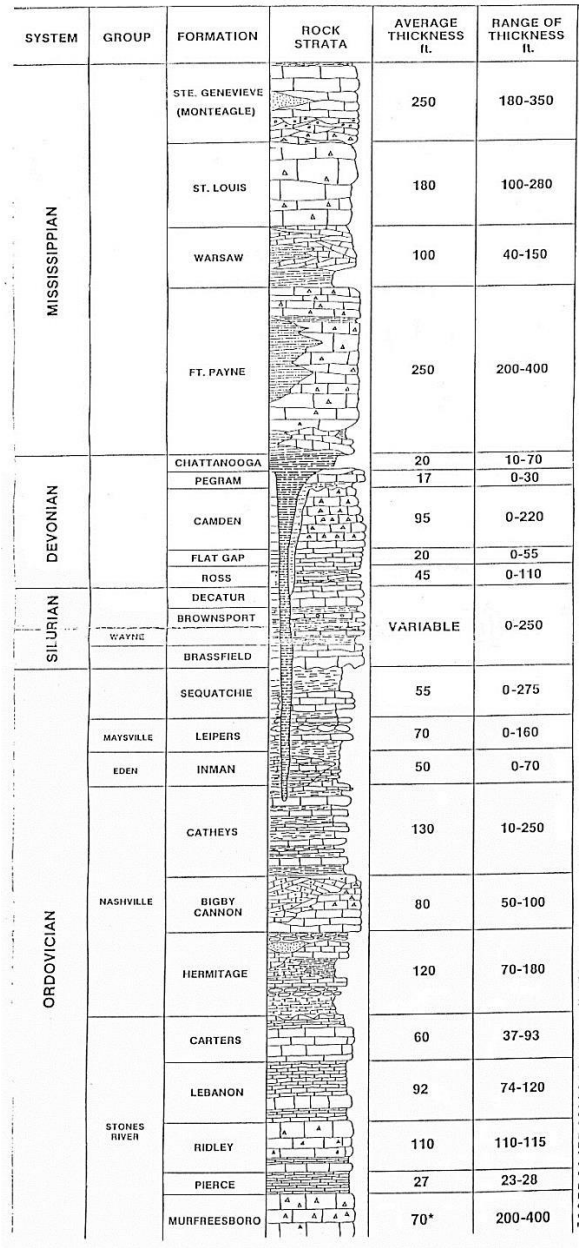

Figure 1 Stratigraphic column depicting the stratigraphy of Middle Tennessee created by Bob Beaver of Beaver Engineering, Inc. based on Wilson (1990).

II.2 Field Sites

For this study, the ideal field sites were topographically high, flat areas featuring unique juxtapositions of overlying soil and underlying bedrock units. Soils located at these higher elevations are less likely to have been disturbed by anthropogenic or fluvial processes. Similarly, the absence of steep slopes reduces the potential that the soils will have been disturbed. To best test soil derivation from

weathering of bedrock, it was important for the limestone bedrock to be relatively siliceous in composition. Based on the aforementioned specifications, two locations were chosen (Fig. 2).

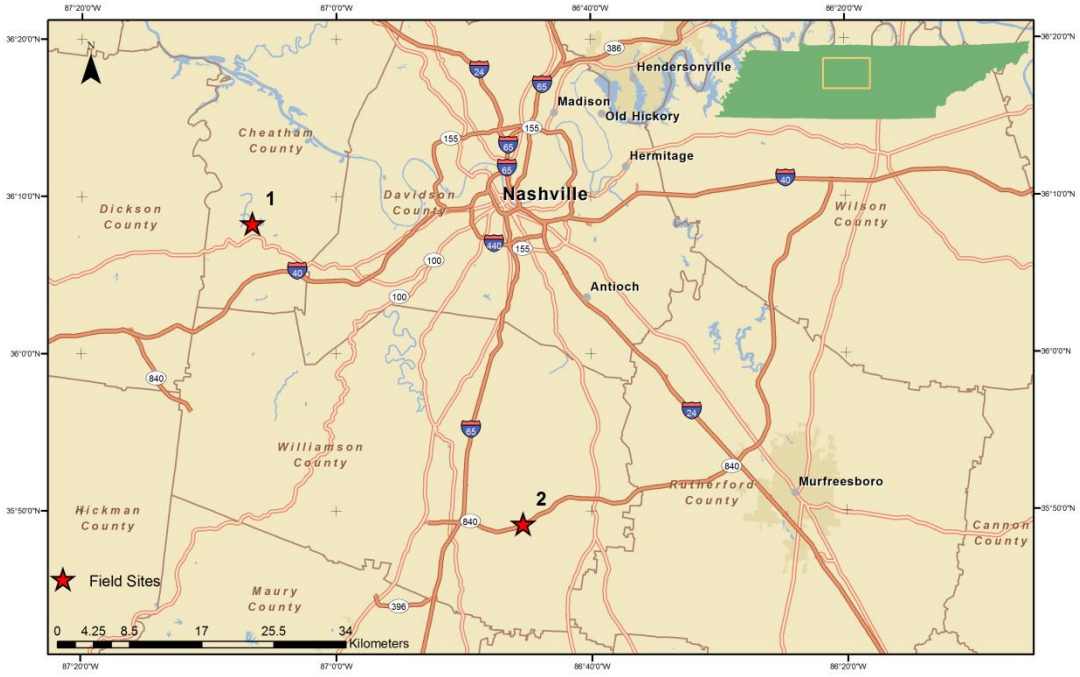

Figure 2 Map displaying the two locations from which samples of soil and bedrock were collected. Site 1 is located atop a bedrock terrace along the Harpeth River. Site 2 is located atop an outcrop along Highway 840.

Site 1: Harpeth River Terrace

Site 1 is located atop a late Pleistocene terrace along the Harpeth River in Cheatham County and features ultisols overlying cherty limestone bedrock of the Fort Payne Formation (Fig. 3; Nicholson et al., 2005).

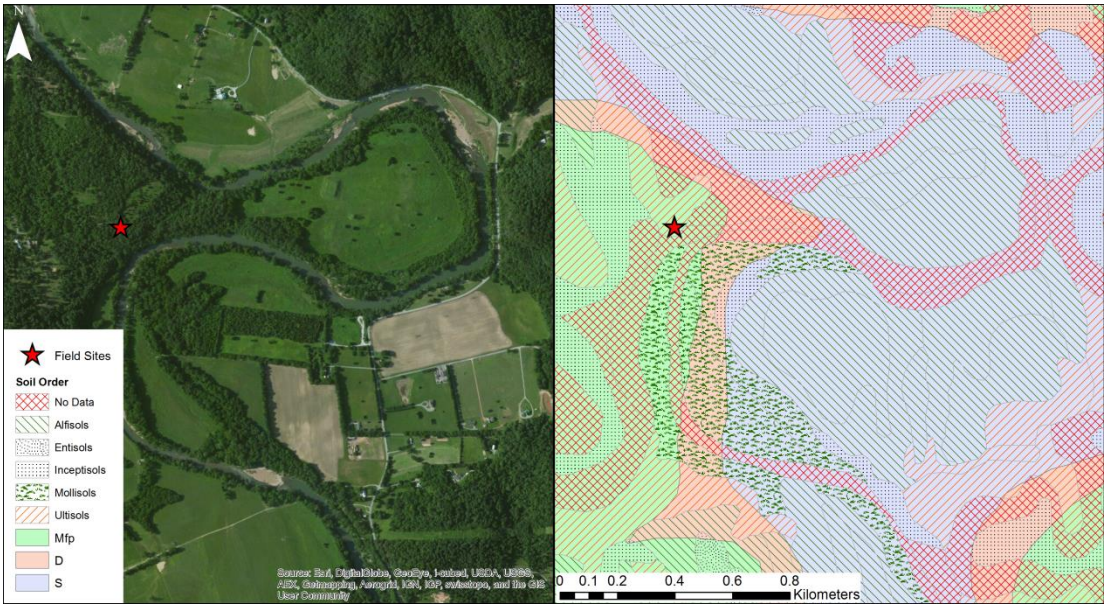

Figure 3 Maps depicting satellite imagery, soil order, and bedrock geology of the area around Site 1 along the Harpeth River. The geologic unit symbols "Mfp" and "D" refer to the Mississippian Fort Payne Formation, and the Devonian Pegram Formation, respectively, and "S" refers to Silurian rock units, including the Brassfield Limestone, Wayne Group, and Brownsport Formation. The site marked on the map is located at approximately 36.138746° N, 87.109788° W. Geological data from Nicholson et al. (2005). Soil data from NRCS (2012).

Within the field area, the bedrock is predominantly chert, with little or no calcium carbonate component present. This terrace and the soils that sit atop it were examined in the Master's Thesis study of Vanderbilt University student Jessica Huckemeyer. Huckemeyer (1999) investigated soil formation along the upper 40 km of the Harpeth River. While the soils in the valley are mainly comprised of chert and quartz (Brietburg et al., 1996)—the residual materials left behind from dissolution of the limestone bedrock—Huckemeyer (1999) suggests that soils atop multiple late Pleistocene terrace levels contain a loess component. Huckemeyer (1999) claimed to have observed a loess mantle more than 25 cm thick within the soils atop the terrace at Site 1, and correlated the surface to the Hatchie Terrace of Saucier (1987), a Sangamon Prairie Terrace equivalent (~128 to ~75 ka). Sangamon age surfaces in the southeastern United States have experienced two episodes of loess deposition (Huckemeyer, 1999). The first corresponds to deposition of the Roxana Silt (60 to 26 ka; Rodbell et al., 1997). The second and most recent event corresponds to deposition of the Peoria Loess (26 to 12 ka; Rodbell et al., 1997), which was

deposited during the last glacial period across a broad region of the mid-continent throughout the Mississippi Valley (Fig. 2 from Bettis et al., 2003).

Although a Sangamon age terrace would have likely experienced both episodes of loess deposition, Huckemeyer (1999) interpreted the loess mantle as correlating to 25 cm of Peoria Loess deposition. As for the Roxana Silt, Huckemeyer (1999) determined that soil development had masked any loess deposition that occurred during that time period. A thickness on the order of 10's of cm for the Peoria Loess along the Harpeth is in agreement with an eastward-decrease in thickness from several-meter thick loess deposits at localities in West Tennessee observed by Rodbell et al. (1997).

Informed by Huckemeyer (1999), I sought to determine if soils atop this Sangamon age terrace did indeed reflect derivation from multiple sources, or instead formed solely from weathering of the cherty limestone bedrock.

Site 2: Highway 840 Outcrop

Site 2 is located atop a road-cut exposure along Tennessee State Route 840. The outcrop features alfisols overlying limestone of the Hermitage Formation (Fig. 5; Nicholson et al., 2005).

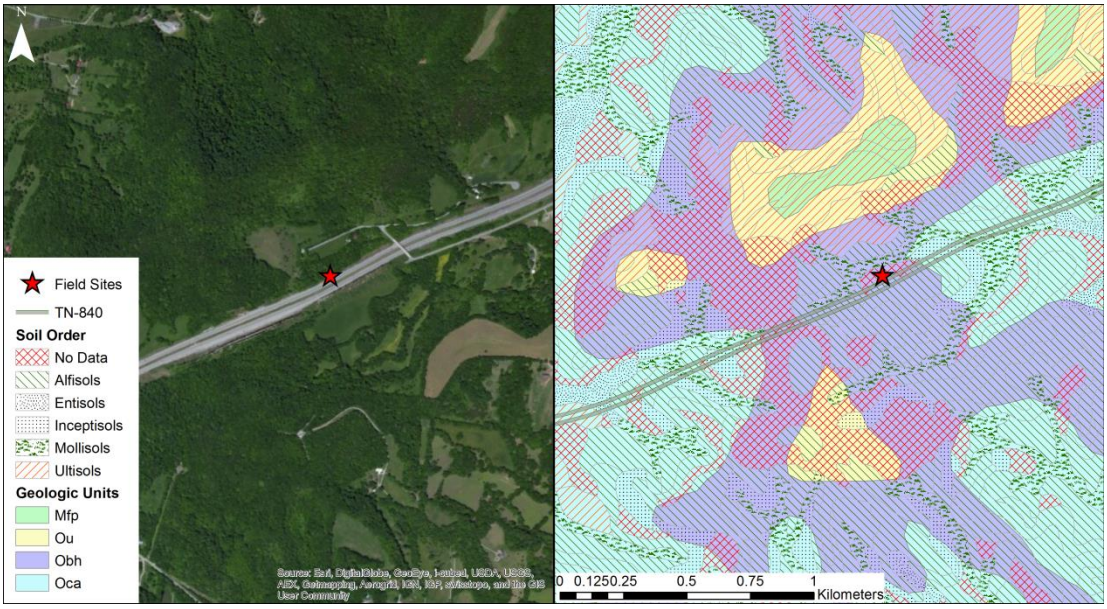

Figure 4 Maps depicting satellite imagery, soil order, and bedrock geology of the area around Site 2 along TN-840. The geologic symbols "Mfp" and "Oca" denote the Mississippian Fort Payne Formation and the Ordovician Carters Limestone, respectively, "Ou" refers to the Ordovician Liepers and Catheys formations, and "Obh" refers to the Ordovician Bigby-Cannon and Hermitage formations. The site marked on the map is at approximately 35.81993° N, 86.755888° W. Geological data from Nicholson et al. (2005). Soil data from NRCS (2012).

Due to the high proportion of siliciclastics characteristic of the Hermitage Formation, dissolution of the bedrock over long periods of time should yield abundant insoluble residuum from which soils may form. Additionally, the bedrock at Site 2, being more calcareous in composition than that of the first field location, is more representative of the limestone bedrock found in Middle Tennessee. An understanding of the process of soil formation atop the limestone bedrock at this field site can inform us about this same process atop other Ordovician limestone units in the region. I anticipated that this site would support the hypothesis of soil derivation from weathering of the underlying bedrock.

CHAPTER III

METHODS

To determine if weathering of the underlying bedrock had yielded the overlying, modern-day soil, soil-bedrock pairs were analyzed for their chemical compositions and zircon U-Pb age spectra. The soil-bedrock pairs feature different soil taxa representing different stages of soil development, and different types of bedrock, encompassing some of the variation of soil types and bedrock geology within the broader Middle Tennessee region. Samples were collected in June and November of 2013.

III.1 Sample Collection

At each of the two sites, a trench was excavated down to the impermeable saprolite layer. Soil profiles were logged based on the cross-sectional view revealed by the trench. For each soil horizon, the Munsell color, relative amount of organic matter and clay, texture, and other observations were recorded. If one or more well-defined B-horizons were present, several gallons of each horizon were taken. In the absence of well-developed soil horizons, a composite sample of the A and B horizons was collected. At Site 1, samples of the B1 and B2 horizon were collected and are henceforth referred to as "B1" and "B2." At Site 2, a composite sample of the A and B horizons was collected and is henceforth referred to as "840W."

For each sampled soil horizon, an additional sample to measure the bulk density was collected using a small piece of metal tubing with a known volume. The metal tubing was pounded horizontally into the wall of the excavated trench, and then carefully unearthed to minimize any loss of material from the tubing or compression of the soil. The sample was weighed to calculate bulk density upon return to the lab.

Several kilograms of bedrock were collected from each site using a 4 lb. sledge hammer. The sampled bedrock was collected from exposures that were no more than 10 m away from the soil trench. Great efforts were made to collect a representative sample of the rock from each of the two locations to

account for any small-scale heterogeneities that might have been present. Bedrock that was already weathered was avoided. At Site 1 a sample of the Fort Payne Formation—henceforth referred to by its USGS map designation, "Mfp"—was collected. At Site 2 a sample of the Hermitage Formation—henceforth referred to by its USGS designation, "Oh"—was collected.

III.2 Sample Preparation

Once the samples were collected, they were prepared following different sets of procedures that were tailored to the specific characteristics of the sample itself.

Soil Samples

Soils were all processed following the same set of methods. Sample preparation procedures for soil samples are outlined in Figure 5.

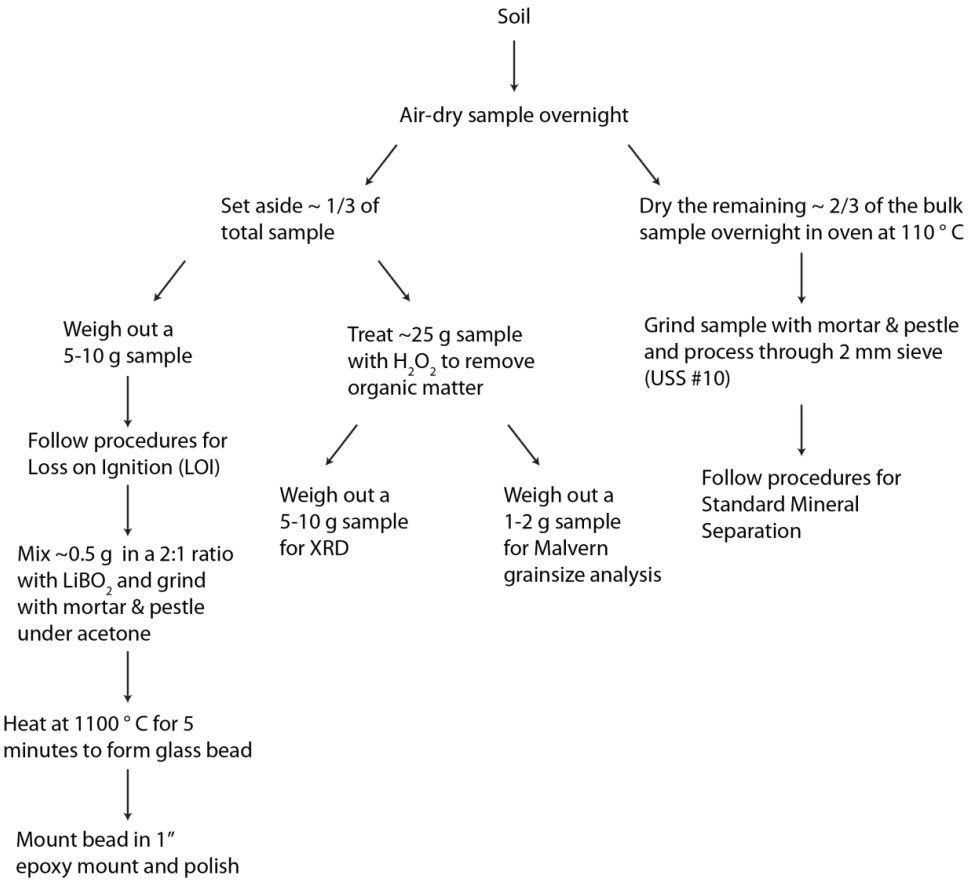

Figure 5 Flow chart outlining the preparation steps for soil samples for different analyses.

First, soil samples were allowed to air dry overnight, after which ~1/3 of each sample was set aside. The remaining material, representing ~2/3 of the overall sample (~2-3 kg) was dried in an oven at 110 °C. The dried soil was then ground in a mortar and pestle and sieved using a 2 mm (USS #10) mesh sieve. This sieved material was then set aside to undergo standard mineral separation procedures described in Section III.5.

Two subsamples were taken from the air-dried portion of each soil, measuring ~5-10 g and ~25 g respectively. Following Tan (2005, p. 448), a 25 g sample was treated with 200 – 300 mL of H_2O_2 to remove any organic material. From the remaining material, a sample of ~5-10 g was taken to be sent away for XRD analysis (Sect. III.4). A 1-2 g sample was taken to analyze grain size using a Malvern Mastersizer 2000E. For grain size analysis, a 0.5 g portion of the sample was wet-sieved through a 1 mm sieve (USS #18).

The 5-10 g sample was processed through the loss on ignition (LOI) procedures (Sect. III.3). Approximately 0.5 g of the remaining material was combined in a 2:1 ratio with $LiBO_2$ and ground in a mortar and pestle under acetone. Once dry, a small portion of the soil-$LiBO_2$ mixture, typically ~0.2 g, was heated in a graphite crucible at 1100 °C for 5 minutes to fuse the material into a homogeneous glass bead. The bead was then mounted in a 1" epoxy mount and polished in preparation for analysis in the SEM and LA-ICP-MS.

Bedrock Samples

Sample preparation steps for bedrock samples are outlined in Figure 6.

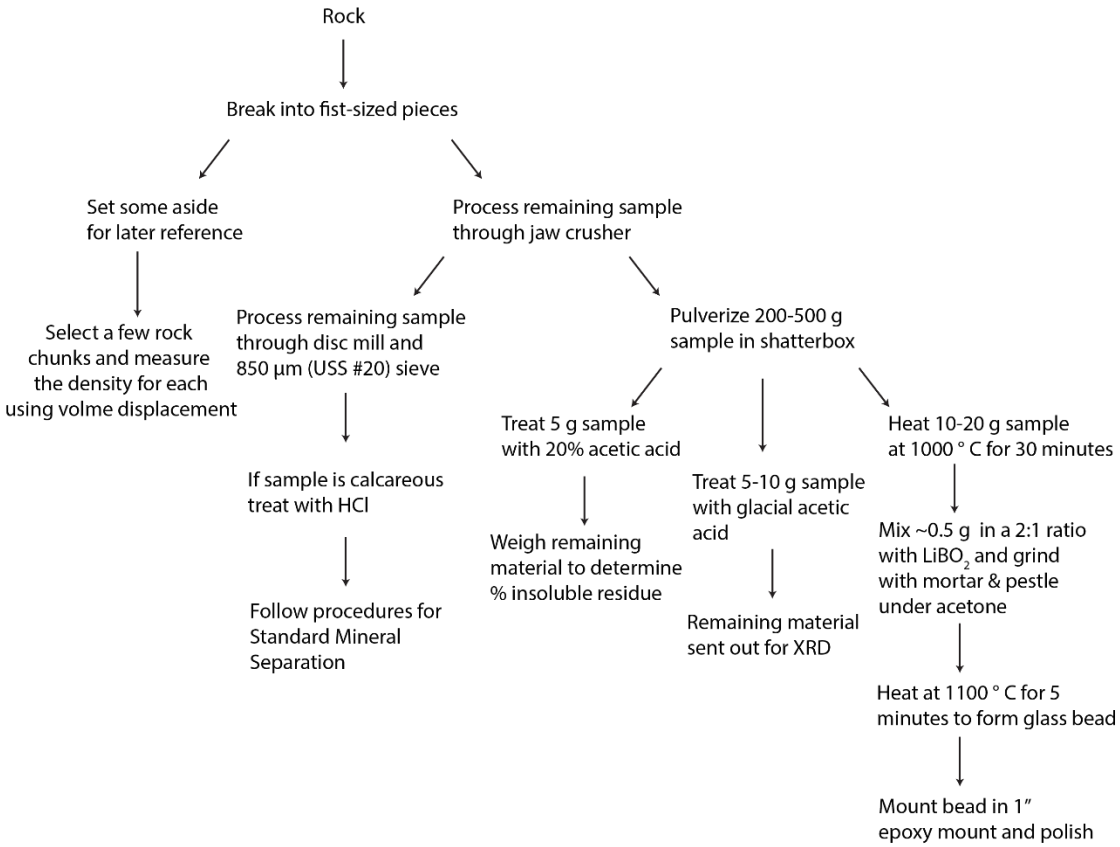

Figure 6 Flow chart outlining the preparation steps for bedrock samples for different analyses.

Rock sample preparation consisted of reducing the large boulders that were collected to smaller sized material for different analyses. A sledge hammer was first used to break the rocks into more manageable pieces that were fist-sized or smaller. A representative sample of these rock chunks was set aside for later use. The rest of the broken-up rock was processed through a jaw crusher to further reduce the size of the material. A 200 – 500 g portion of the resulting material was processed with a SPEX shatterbox to produce a rock powder. From this material, three samples, measuring 5 g, 5-10 g, and 10-20 g respectively, were taken. The 5 g sample was treated with 20% acetic acid to dissolve carbonate. At the end of the dissolution, the remaining material was dried and weighed to estimate the percent insoluble residue. The 5-10 g sample was treated with full strength glacial acetic acid. The undissolved material was sent out for XRD analysis. The 10-20 g sample was heated in a graphite crucible at 1000 °C for 30 minutes to remove the carbonate component. From the remaining material, 0.5 g was mixed in a 2:1 ratio

with $LiBO_2$ and ground in a mortar and pestle under acetone. Just as with the soil preparation procedures, ~0.2 g of this mixture was heated in a graphite crucible at 1100 °C to fuse the material into a glass bead. The bead was then mounted in a 1" epoxy mount and polished to prepare it for SEM and LA-ICP-MS analyses.

The remaining crushed material was reduced to smaller particles in a disc mill. Next, the disc-milled material was sieved with an 850 µm (USS #20) sieve. If the sample was found to be devoid of any dissolvable $CaCO_3$—e.g. the Mfp bedrock sample—the material was processed using standard mineral separation procedures (Sect. III.5). Alternatively, if the rock contained enough calcium carbonate to effervesce with the addition of hydrochloric acid, it was treated with acid to remove this component. A majority of the dissolution was carried out using 10% hydrochloric acid, but the concentration was increased to ~36% towards the end of the dissolution. The resulting material was then also processed through standard mineral separation procedures (Sect. III.5).

Finally, from the rock material set aside for later use as a reference, a few representative pieces were selected for measurement of their density by volume displacement. The rock chunks were weighed one by one, before being immersed in water in a large graduated cylinder, at which point the volume displaced by each was noted. Their densities were calculated and averaged to find one density value for each sample.

III.3 Loss on Ignition (LOI)

As indicated in Figure 5, a 5-10 g sample of each soil was processed through loss on ignition (LOI) procedures to estimate the proportions of different components. The temperature-steps used in this procedure were chosen based on the findings in Ball (1964). Each sample was initially weighed before being dried overnight at 110 °C. Once cooled, samples were weighed again to estimate the adsorbed water content. Next, samples were heated at 375 °C for 4 hours, cooled, and weighed again to estimate total organic carbon. The samples were then heated at 600 °C for 2 hours, cooled, and weighed to estimate structural water content. Finally, the samples were heated at 1000 °C for 30 minutes, allowed to cool, and weighed to estimate carbonate content.

III.4 X-ray Diffraction (XRD)

In preparation for XRD analysis, a 5-10 g portion of each soil and rock sample was set aside and treated with glacial acetic acid or H_2O_2 respectively (Figs. 5-6). For each soil and rock, a 1-2 g subsample of the resulting material was bottled and sent to China University of Geosciences (Wuhan) for quantitative analysis in a PANalytical X'pert Pro Powder XRD for identification of diagnostic minerals. The instrument was run at a voltage of 40 kV with a current of 40 mA, and used Cu K_α radiation, with a wavelength of 0.15416 nm. The scanning was conducted for from 3° to 65° in continuous step scan mode at 0.417782 °/s with a step size of 0.017°.

III.5 Standard Mineral Separation

After being prepared using the methods described in Section II.2, samples were processed using a combination of different methods to separate out the fraction of the sample containing zircon and other heavy minerals. These procedures are outlined in Figure 7.

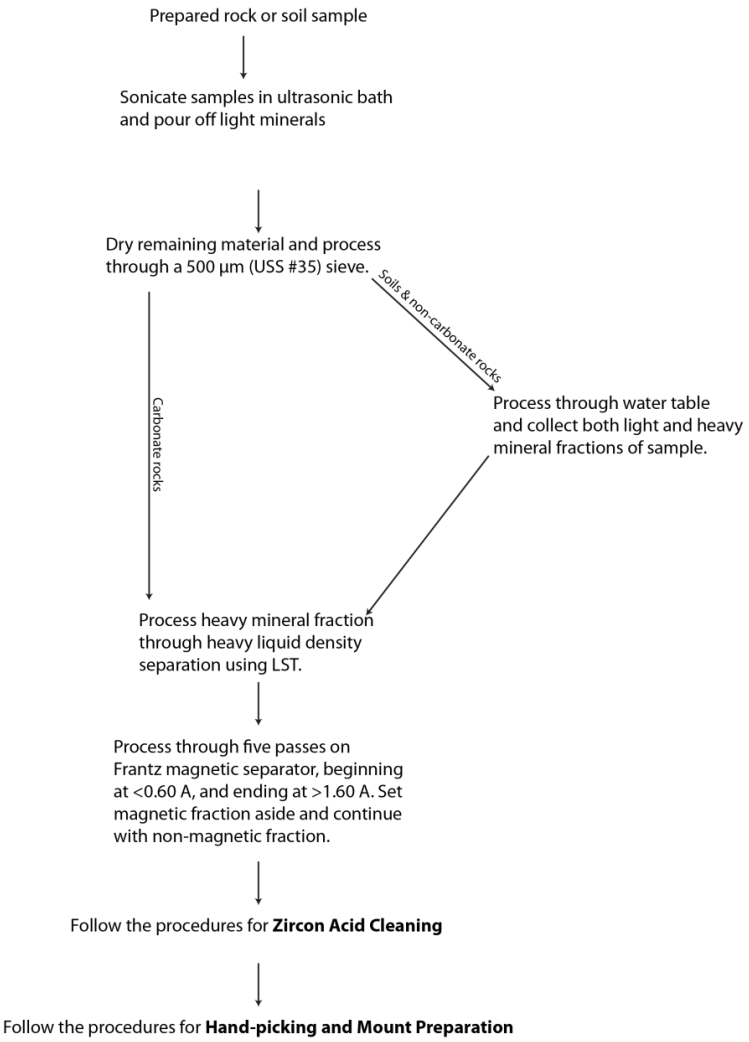

Figure 7 Flow chart displaying the steps for standard mineral separation of zircon. Bold text indicates title of section describing the specific steps for the method in more detail.

First, the samples were distributed between several 1 L beakers, which were then filled with water. The beakers were placed in an ultrasonic bath and sonicated to break clays and other light minerals off of the surfaces of zircon and other heavy minerals. Beakers were removed from the bath every 15-20 minutes to pour off the light minerals. Rock samples were sonicated for at least 90 minutes. Soils were sonicated for at least 180 minutes. Once dried, samples were sieved through a 500 µm (USS #35) sieve. Soils and non-calcareous rock samples underwent separation on an AMS M7 Micron Mill Wave Table. During this step of the process, heavy minerals were allowed to concentrate in pockets before being extracted with a vacuum pump. The remaining light materials were collected and set aside. For rocks that

had been treated with hydrochloric acid to remove calcium carbonate during preparation, this process was skipped.

The remaining heavy materials or undissolved residue next underwent heavy liquid density separation, using a lithium heteropolytungstate (LST) solution following Larsen et al. (2014). Once dried, the heavy fraction of the sample underwent magnetic separation in a Frantz magnetic separator. During this process, the material was subjected to increasing magnetic charges over the course of five runs. At the end of each run, the magnetic fraction was set aside. The electrical currents used for the five runs were < 0.60 A, 0.60-0.90 A, 0.90-1.20 A, 1.20-1.60 A, and > 1.6 A respectively. The final run was necessary to better remove the mineral apatite from the non-magnetic fraction of the sample. By the end of these separation procedures, what had begun as several kilograms of material was reduced to a non-magnetic fraction weighing a few grams at most.

III.6 Zircon Acid Cleaning

Despite the numerous steps carried out to separate non-magnetic heavy minerals, much of what remained—typically 90% or more by weight—was comprised of amorphous silica and other unwanted material. This greatly complicated the task of identifying and extracting zircon. In addition, there was no surefire means to discern if a zircon had been hydrothermally altered until after the grain-mount preparation process. To address both the need to expedite the hand-picking process, and remove as much of the hydrothermally altered zircon as possible, the samples were treated with several acids.

First as a precaution, any samples that had not yet been treated with hydrochloric acid were submerged in a 10% solution of the acid for 10-15 minutes before being decanted and rinsed in deionized water. Next, following the procedures of Lackey (2005), all samples were treated with full strength nitric acid and heated on a hot plate for 1-2 hours at 85 °C. After cooling, the nitric acid was pipetted off, and the sample was rinsed three times with deionized water. Next, the samples were immersed in 15-20 mL of full strength hydrofluoric acid, partially covered, and left in a fume hood overnight for 12-16 hours. The following morning, the acid was pipetted off and samples were rinsed once again before being submerged in 40 mL of full strength hydrochloric acid and heated on a hot plate for 1 hour. After the acid was

pipetted off and the samples were rinsed in deionized water, they were rinsed twice more in isopropyl alcohol to speed up the drying process.

III.7 Hand-picking and Mount Preparation

Once dry, the acid-cleaned samples were examined under 50x magnification on a Zeiss Stemi 2000-C stereo microscope under both transmitted and reflected light. While only one hundred zircon grains per sample were desired, two hundred potential grains were picked from each to account for any misidentification during hand-picking and for any potential complications that might occur during the mount-making process. Each of the two hundred mineral grains were individually plucked from a glass slide and placed into rows within a 15 mm diameter circle on double-sided tape. A 1" plastic mold was affixed to the tape so that the circle containing the sample lay directly in the center. Epoxy was poured into each mount and allowed to harden for ~24 hours before being removed, lathed, ground, and polished. Samples were then carbon-coated in preparation for SEM analysis.

III.8 Analytical Methods

Soil and rock samples were analyzed using several different methods. Polished carbon-coated epoxy mounts of glass beads and zircon were examined using both a Tescan Vega 3 LM Variable Pressure SEM and an iCAP Q ICP-MS equipped with a Photon-Machines Excite 193 nm LA system. The zircon epoxy mounts were analyzed using U-Pb geochronological methods on the LA-ICP-MS. Grain size was analyzed for soil samples using the Malvern Mastersizer 2000E.

Trace Element Analyses

The glass beads were examined using electron dispersive spectroscopy (EDS) on the SEM for major element concentrations. The average measured concentration of SiO_2 in the glasses was used as an internal standard in subsequent analyses on the LA-ICP-MS for major and trace element concentrations. The glass standard NIST SRM 612 was used as the external standard in the LA-ICP-MS analyses. Additionally, glass beads of USGS reference materials BCR-2, RGM-1, QLO-1, BIR-1, GSP-2, AGV-2, and BHVO-1 were created for use as secondary standards. After analyses were completed, the data was reduced using the 'GLITTER' software package.

Geochronological Methods

Cathodoluminescence (CL) and backscattered electron (BSE) images were collected for each of the zircon grain mounts using the SEM. Based on the CL images, zircon grains exhibiting younger rims surrounding an older core were not sampled. Although some of the samples contained zircon grains measuring as small as 20-30 µm in width, a 50 x 50 µm spot size was chosen to ensure enough material would be ablated to capture an adequate signal for geochronological measurements. Due to the spot size, larger-sized zircon grains were chosen when possible. Spots were chosen to avoid sampling any visible inclusions. At least 100 zircon grains were analyzed for U-Pb ages and trace element concentrations for each sample. NIST SRM 612 was used as a primary standard for trace element measurements in zircon, and RGM-1 was used as a secondary standard. For U-Pb age measurements, Zircon 91500 (Jochum et al, 2005) was used as a primary standard, and Zirconia (NC) from Braun et al. (2009) and Covey et al. (2012) as a secondary standard. Data was reduced using the 'GLITTER' software package and age spectra were constructed. Age spectra for concordant $^{206}Pb/^{238}U$ ages were plotted as kernel density values calculated using the program Density Plotter (Vermeesch, 2012).

CHAPTER IV

RESULTS

IV.1 Soil Characteristics

At each field site, soil pits were excavated down to the saprolite layer. Soil horizons were identified based on field observations, including changes in clay and organic matter content, and color. Soil profiles for Site 1 and Site 2 are shown in Figure 8.

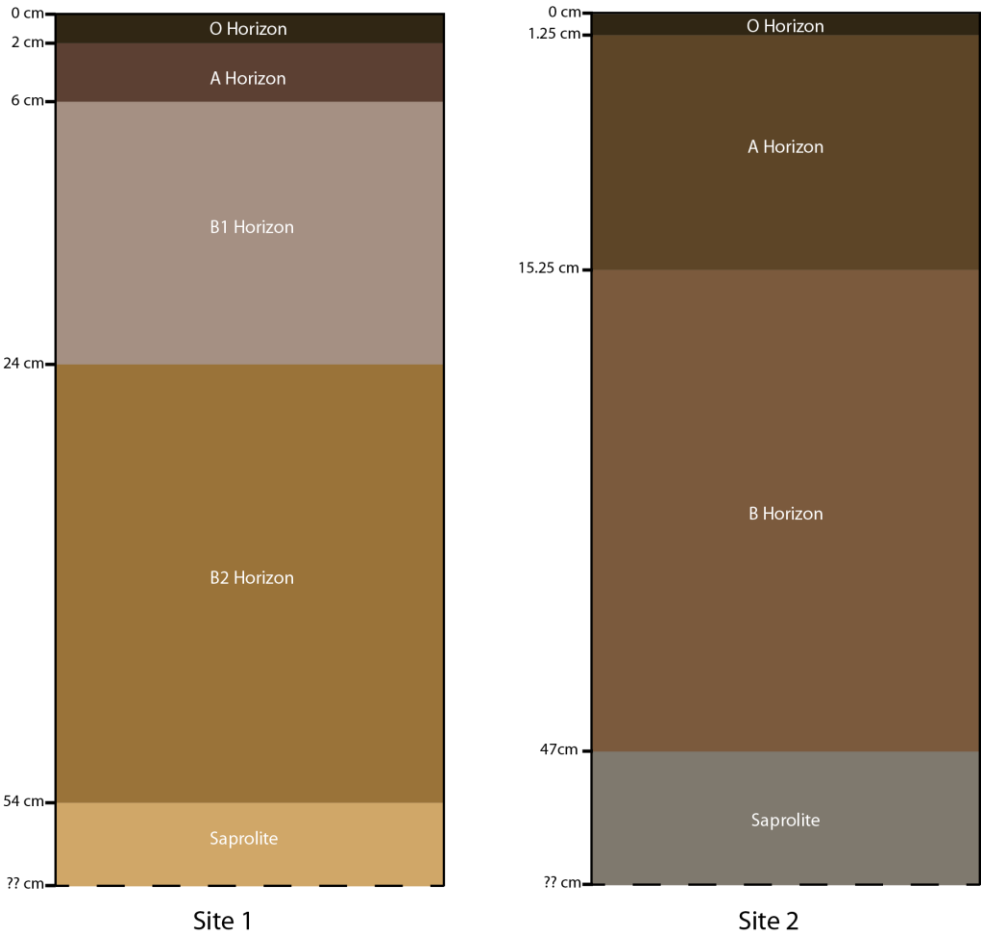

Figure 8 Soil profiles from Site 1 and Site 2 depicting the thickness and Munsell color for each of the identified soil horizons. The Munsell color of the underlying bedrock is used to depict the color of the saprolite layer.

The ultisol soils found at Site 1 exhibited well-developed soil horizons, displaying a 4 cm thick A horizon overlying an 18 cm thick B1 horizon, and a 30 cm thick B2 horizon. The transition between the B1 and B2 horizons is quite readily visible (Fig. 9).

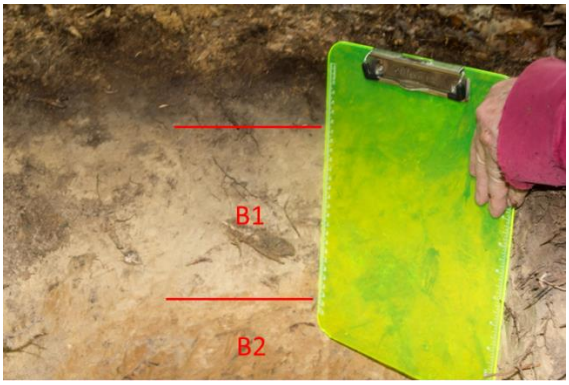

Figure 9 Photograph of the inner-wall of the soil pit at Site 1 showing the transition between the B1 and B2 horizons.

The B1 horizon is characterized by pale brown material that is clay-rich with poorly developed peds. The B2 horizon is yellowish brown in color and contains a significantly greater proportion of clay than in B1, with moderate peds.

The alfisol soils at Site 2 (Fig. 8) were very young and displayed poorly developed soil horizons. The transition between the A and B horizons was gradational, and not clearly defined (Fig. 10). The A horizon was estimated to be 14 cm thick, and the B horizon 31.75 cm thick. The A horizon is dark yellowish brown with a high proportion of organic material. The B horizon is brown and characterized by a relatively clay-rich composition with moderate-strong subangular peds.

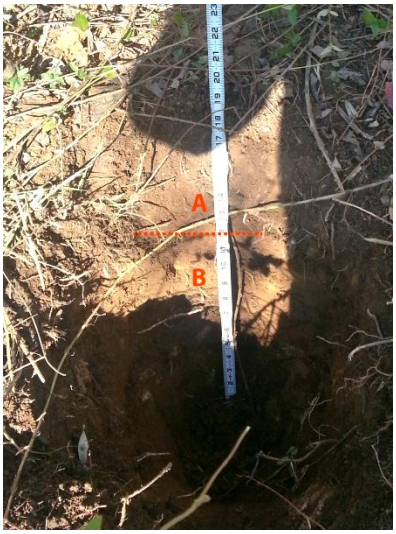

Figure 10 Photograph of soil pit at Site 2 showing approximate transition between the A and B horizons.

IV.2 Bulk Properties

Several properties were measured for the soil and rock samples, including the bulk density, mean grain size (for soils), percent insoluble residue (for rocks), chemical index of alteration (CIA), and Munsell color. These properties are listed for each sample in Table 1.

Table 1 Munsell color, bulk density with 1σ error, surface- and volume-weighted mean grain sizes, USDA soil texture, percent insoluble residue, volume strain ($\epsilon_{Zr,\,w}$), and chemical index of alteration (CIA) values for the rock and soil samples.

Sample	Munsell Color	Bulk Density (g/cm^3)	Surface-weighted mean grain size (µm)	Volume-weighted mean grain size (µm)	Soil Texture (USDA)	% Insoluble Residue	$\epsilon_{Zr,\,w}$	CIA
B1	10YR 6/3	1.5 ± 0.2	10.964	43.044	Silt	NA	0.809	73
B2	10YR 5/6	1.5 ± 0.2	9.388	19.856	Silt	NA	0.758	82
840W	7.5YR 5/4	1.8 ± 0.2	6.412	29.348	Silt Loam	NA	0.678	76
Mfp	10YR 7/6	2.2 ± 0.6	NA	NA	NA	98.8%	NA	71
Oh	2.5Y 5/1	2.5 ± 0.1	NA	NA	NA	27.7%	NA	80

Grain size distributions of the soil samples from particle size analyses on the Malvern Mastersizer are shown in Figure 11.

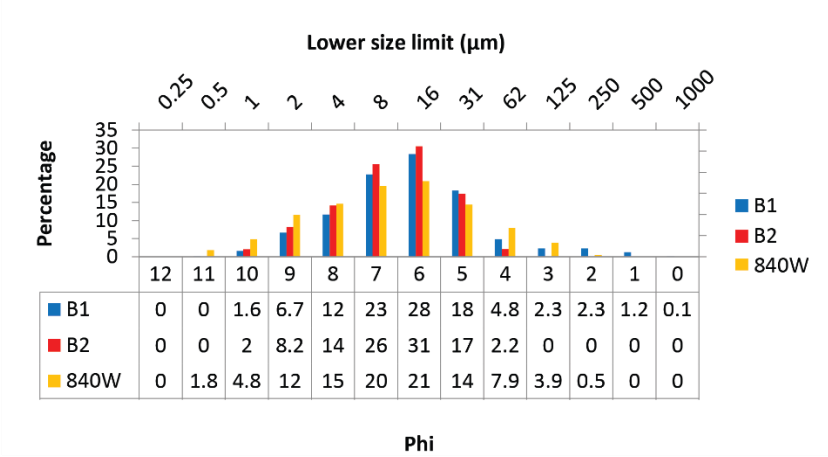

	12	11	10	9	8	7	6	5	4	3	2	1	0
B1	0	0	1.6	6.7	12	23	28	18	4.8	2.3	2.3	1.2	0.1
B2	0	0	2	8.2	14	26	31	17	2.2	0	0	0	0
840W	0	1.8	4.8	12	15	20	21	14	7.9	3.9	0.5	0	0

Figure 11 Histogram of grain size distributions from particle size analyses on the Malvern Mastersizer 2000E. Lower limits of bins are labeled in units of µm and Phi. The table below the histogram shows the exact percentages of the samples for each of the bins.

Grain mounts were made for each soil sample and photographed to characterize the degree of angularity or roundness of the grains (Fig. 12).

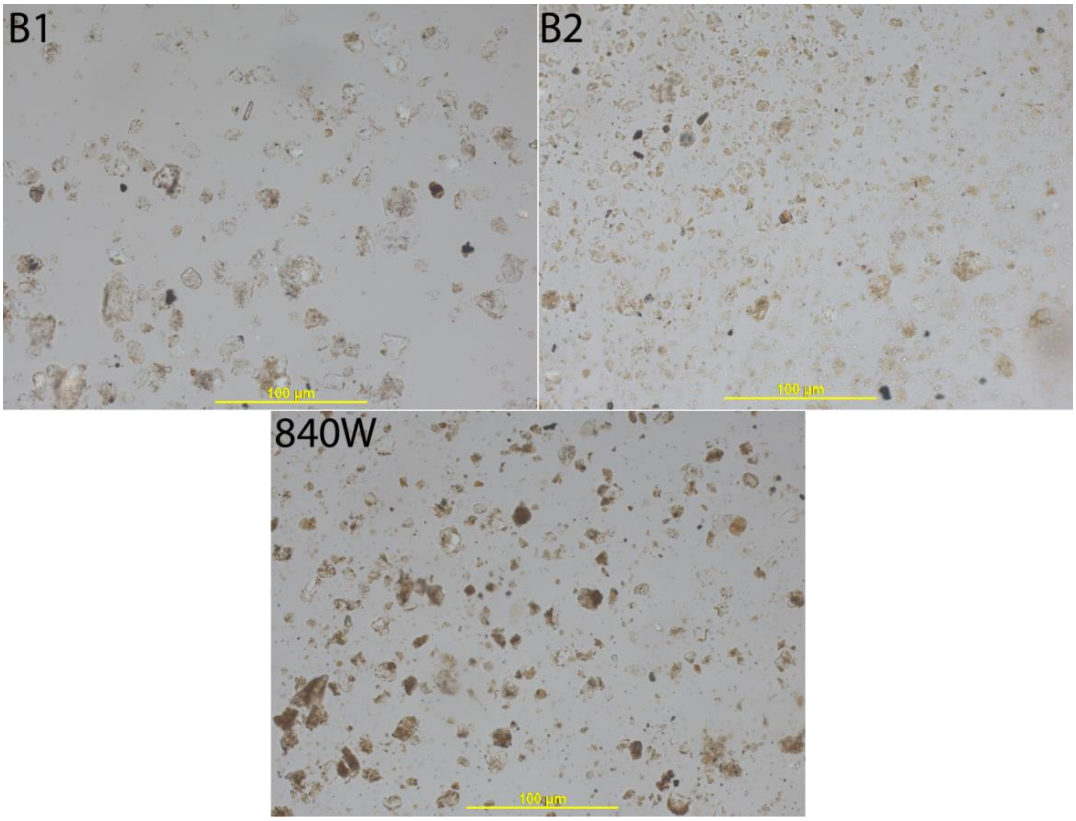

Figure 12 Photomicrographs of grain mounts of B1, B2, and 840W soil samples immersed in oil with an index of refraction of 1.54. Images captured at 200X magnification in plane polarized light.

IV.3 XRD Analyses

XRD analyses were conducted for all samples to identify diagnostic minerals. Clay minerals were not analyzed for. The results of these analyses are shown in Table 2.

Table 2 XRD results as volume % for all five samples.

Sample	Quartz	Plagioclase	Apatite	Chlorite	Illite
B1	95	5			
B2	95	3		2	
Mfp	>98				
840W	92	4	4		
Oh	78	4	8		10

IV.4 Zircon U-Pb Geochronological Analyses

More than one hundred zircon grains were analyzed from each of the five samples. However, in some cases, less than half of the analyses for a sample yielded $^{206}Pb/^{238}U$ ages that were concordant within 1σ error. Due to the relatively large spot size, some of the grains analyzed were found to have been ejected during the ablation. These analyses were discarded during the data reduction phase. The complete dataset of ages, including discordant analyses, can be found in Appendix A, Table A2.

Cathodoluminescence Imaging

Cathodoluminescence images were captured on the department's SEM to aid in identifying potential age domains and inclusions. The zircon grains shown in Figure 13 all yielded concordant $^{206}Pb/^{238}U$ ages.

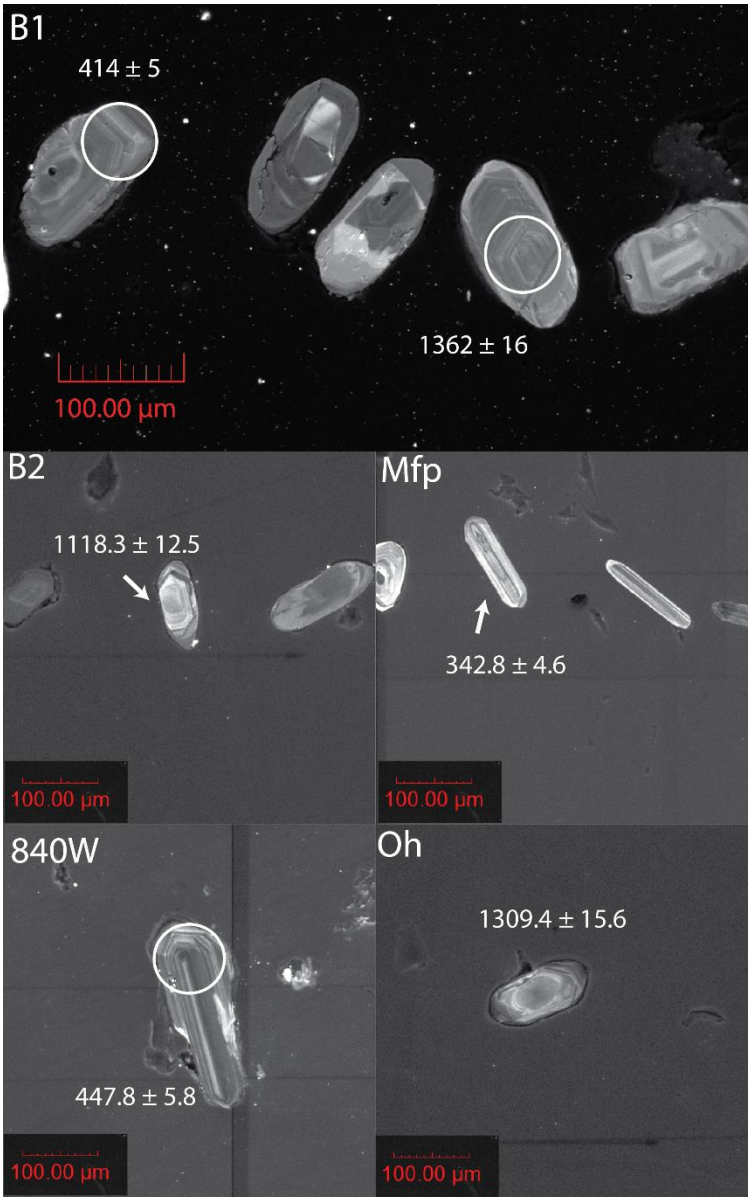

Figure 13 Cathodoluminescence images of zircon grains from the B1, B2, Mfp, Oh, and 840W samples. The labeled grains yielded concordant $^{206}Pb/^{238}U$ ages within 1σ error. These ages are shown with 1σ uncertainty. The ellipses mark the approximate analysis spot for larger grains.

Zircon REE Concentrations and U-Pb Concordia

Concentrations of trace elements were measured for each spot analyzed. Some of the zircon grains analyzed were found to be enriched in light rare earth elements (LREE). This was likely the result of unknowingly sampling inclusions of other minerals in the analyzed spots. As a precaution, if the analysis exhibited LREE concentrations significantly higher than those of the other zircon analyses within

a given sample, the analysis was filtered out of the dataset. Similarly, any analysis that yielded a $^{206}Pb/^{238}U$ age that was outside of 1σ error of the $^{207}Pb/^{235}U$ age was filtered out as discordant. The full dataset of concordant and discordant analyses is included in Appendix A (Table A2). The median concentrations of rare earth elements (REE) for the filtered analyses are shown in Figure 14 and the $^{207}Pb/^{206}Pb$ and $^{206}Pb/^{238}U$ ratios are plotted on Tera-Wasserburg concordia diagrams in Figure 15.

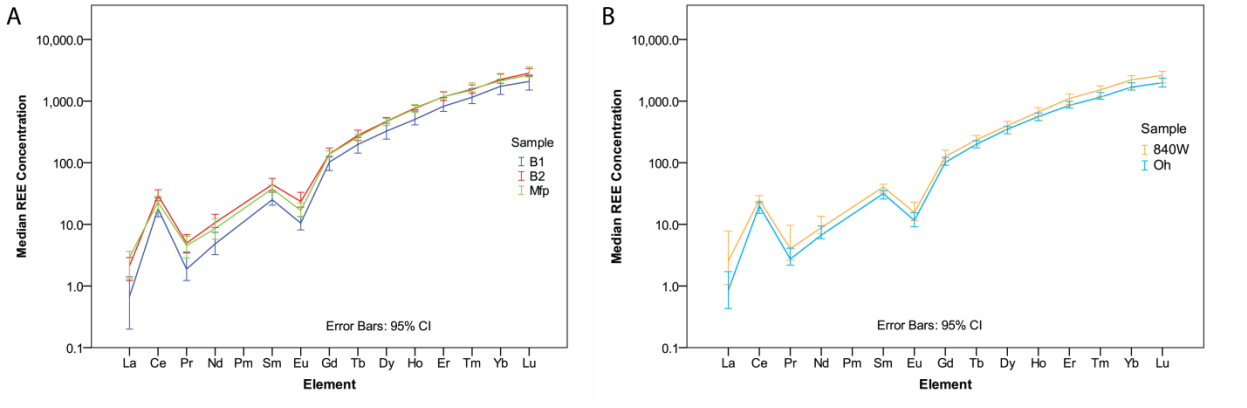

Figure 14 Median REE concentrations in zircon for the samples from Site 1 (A) and Site 2 (B) with error bars corresponding to 95% confidence limits.

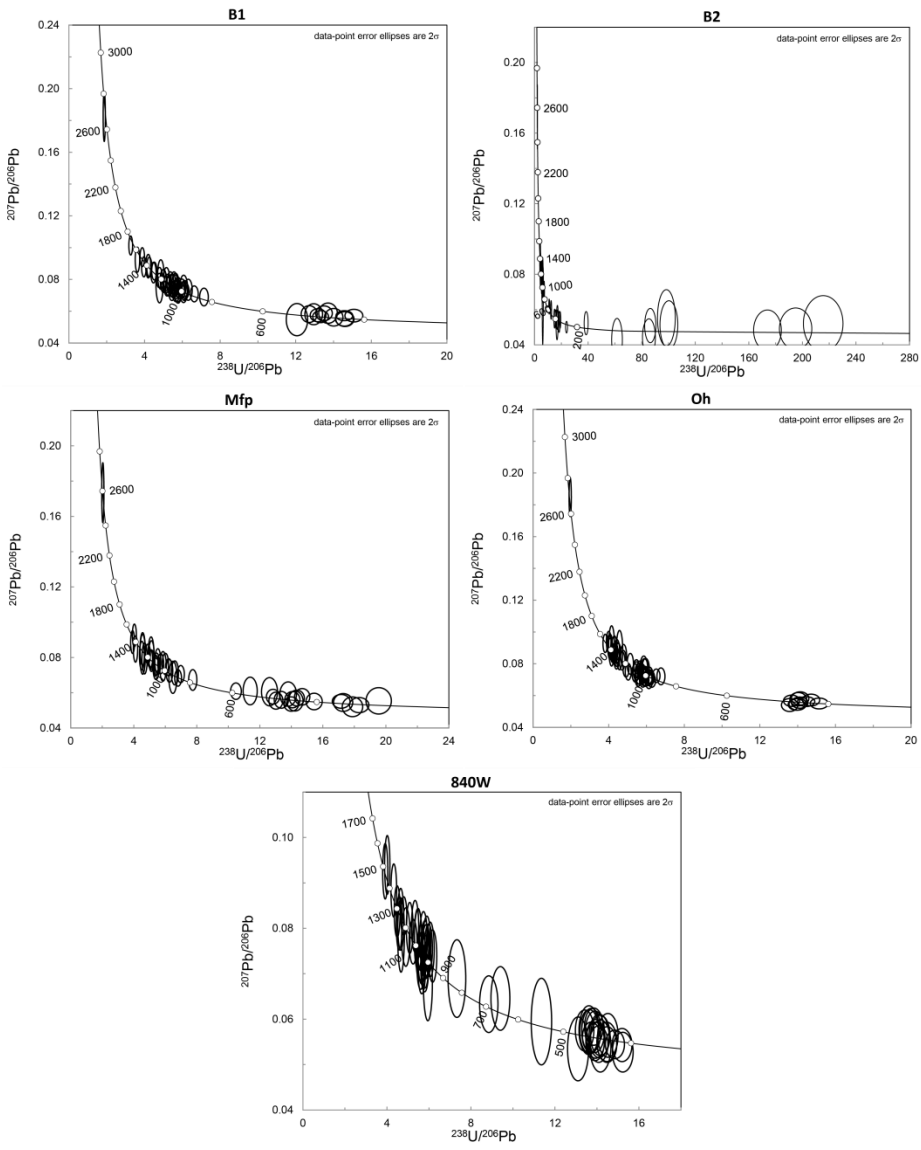

Figure 15 Tera-Wasserburg concordia diagrams for each of the five samples. The ellipses represent the 2σ uncertainty for each of the plotted analyses.

Age Spectra

Age spectra were constructed from the filtered dataset of zircon analyses for the samples collected (Fig. 16).

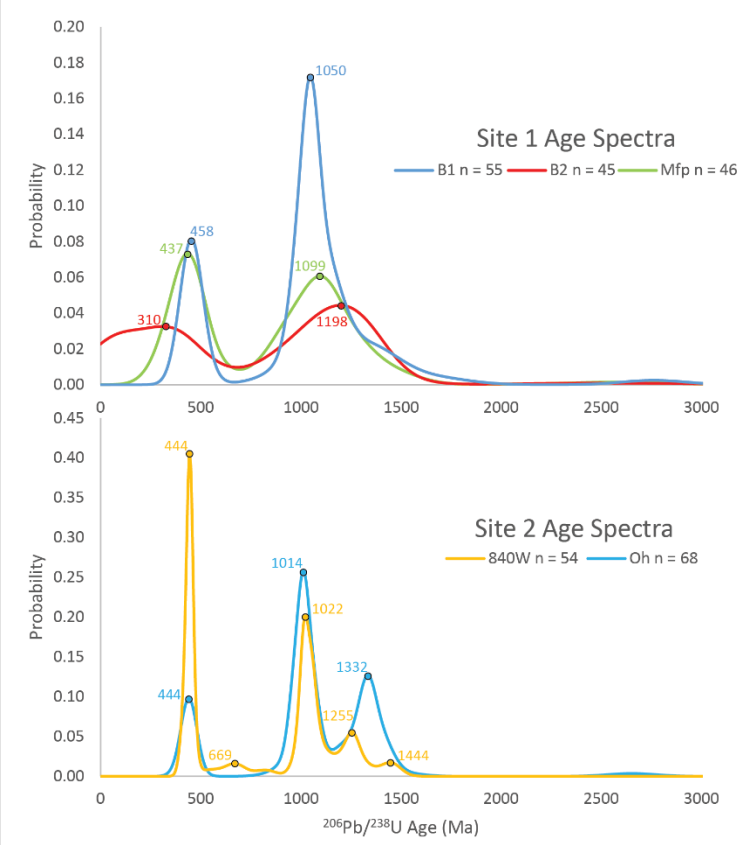

Figure 16 Age spectra displaying the distributions of zircon $^{206}Pb/^{238}U$ ages for all samples plotted as kernel density estimates calculated using the Java-based program Density Plotter created by Vermeesch (2012). Age modes within the distributions are labeled with their corresponding age.

IV.5 $LiBO_2$ Glass Analyses

Standard Analyses

Glass beads created from the powdered USGS reference materials BCR-2, RGM-1, QLO-1, BIR-1, GSP-2, AGV-2, and BHVO-1, were analyzed to test the viability of the $LiBO_2$ fusion method for measuring bulk sample major and trace element concentrations. In order to further analyze $LiBO_2$ glasses using the LA-ICP-MS, it was first necessary to establish the concentration of Si in each sample using EDS. The results from EDS analyses of the secondary standards are shown below in Figure 17.

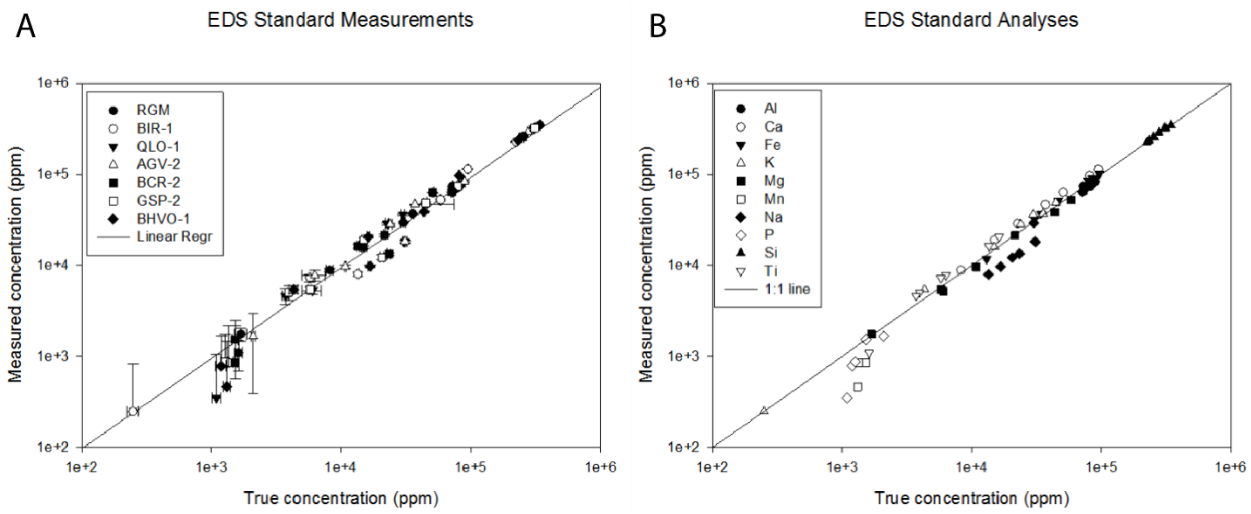

Figure 17 A. Measured concentrations from EDS analysis of rock standard glass beads vs true concentrations from Govindaraju (1994) and Wilson (1997; 1998a; 1998b). Error bars are 2σ. B. Measured concentrations of specific elements from the same analyses shown in A to illustrate the limitations in the accuracy of EDS analyses for specific elements.

With the average concentration of Si in each sample now known, the standard glass beads were analyzed using the department's new LA-ICP-MS to test its accuracy and precision with samples prepared in this manner. The EDS-measured Si concentration of each standard was used as an internal standard for each analysis. The concentrations measured in these analyses are shown with the accepted values for comparison in Figure 18. For a majority of the analyses, the measured concentrations are within error of the true concentrations so that the markers plot along the 1:1 line, indicating the analyses are both precise and accurate.

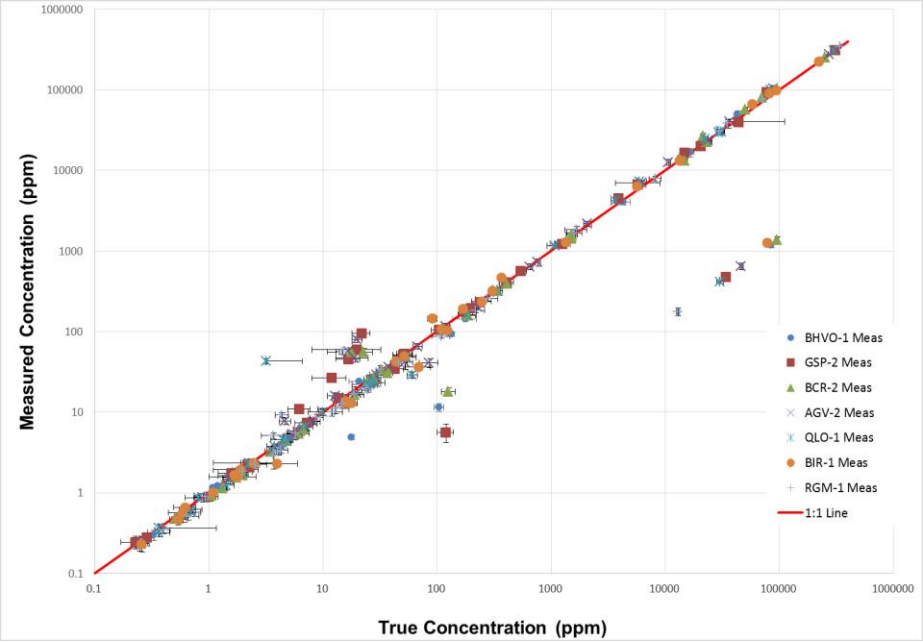

Figure 18 Measured concentrations from LA-ICP-MS analyses of rock standard glass beads vs. accepted values with 2σ error bars. Accepted values for RGM-1, QLO-1, BIR-1, and BHVO-1 are from Govindaraju (1994). Accepted values for BCR-2, AGV-2, and GSP-2 are from Wilson (1997; 1998a; 1998b).

Sample Analyses

The glass beads created from the soil and rock samples were analyzed on a LA-ICP-MS for major and trace element concentrations. Element concentrations in samples from Site 1 are shown in Figure 19. Element concentrations in Site 2 samples are shown in Figure 20.

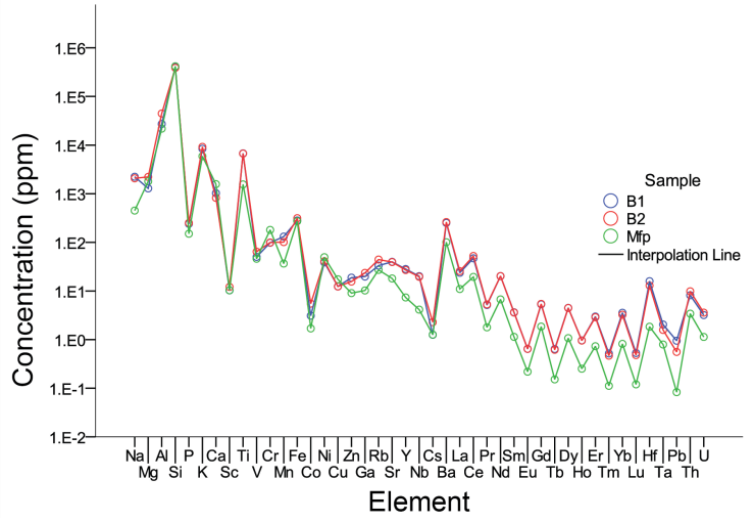

Figure 19 Concentrations of major and trace elements in the glass beads created from the samples from Site 1.

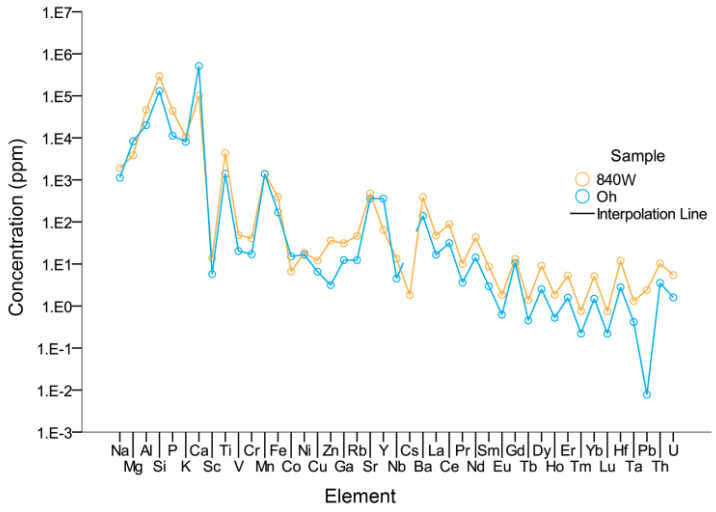

Figure 20 Concentrations of major and trace elements in the glass beads created from the samples from Site 2.

The close similarity of major and trace element patterns within the soil-bedrock pairs (Figs.19-20) strongly suggests that the soils were derived from weathering of the underlying bedrock and that bedrock composition was not highly variable.

Volume Strain and Element Mass Flux

Using the densities of the soil and rock samples (Table 1) and the concentrations of major and trace elements from the glass beads (Figs. 19-20), it is possible to calculate a mass flux for each element to determine how immobile the element is. However, one element must be assumed to be perfectly immobile for this method to be used. Following Brimhall et al. (1991), I assume that Zr is perfectly immobile. With Zr as the index element, the volume strain (ϵ) can be calculated from the equation:

$$\epsilon_{Zr,w} = \frac{(V_w - V_p)}{V_p} = \frac{\rho_p C_{Zr,p}}{\rho_w C_{Zr,w}} - 1 \qquad (1)$$

Where the subscript, *w*, denotes the weathered material, i.e. soil, the subscript, *p*, denotes parent material, and V, ρ, and C_{Zr}, denote volume, density, and concentration of zirconium respectively. Assuming only one parent material for a soil, the volume strain approximates the amount of parent material that would need to be weathered to arrive at an observed volume of soil. The resulting volume strain allows for calculation of the mass flux, $\delta_{j,w}$, for each element other than Zr using:

$$\delta_{j,w} = \frac{\rho_w C_{j,w}\left(\epsilon_{Zr,w} + 1\right) - \rho_p C_{jp}}{100} \quad (2)$$

Where $\delta_{j,w}$ is in units of g cm^{-3} for a specific element of interest, *j*. Positive values of $\delta_{j,w}$ require external input—i.e. a second parent material—whereas negative values of $\delta_{j,w}$ suggest that only one parent supplied material to the soil (Brimhall et al., 1991). However, at both sites the presence of zircon age peaks within the soils that are not found within the age spectra for the underlying bedrock (Fig. 16) requires an exotic zircon component.

To account for this exotic component, some modifications were necessary for the calculation of mass fluxes for the soils. To estimate the volume fraction of exotic material in each soil, the age spectra of the soil and bedrock samples from each site were normalized so that the sum of the probabilities equaled one. Next, the age spectrum of the exotic component was determined for each soil and underlying bedrock sample set by calculating the difference between their normalized age spectra. The sum of the probabilities for the exotic component was assumed to equal its fraction in the soil. This is equivalent to the fraction of measured zircon ages in the soil that do not match zircon age peaks in the bedrock, which can be determined by simply counting the number of ages that do and do not match. Using these calculations, the soils from Site 1and Site 2 were found to contain an exotic component that comprised ~25% of the ages within the soil age spectra. Therefore, rather than assuming the entirety of Zr in the soil was derived from weathering of the underlying bedrock, it was instead assumed that only 75% of the Zr came from the bedrock, following Brimhall et al. (1991). In Eq. 1, the concentration of Zr in the soil, $C_{Zr,w,}$ was multiplied by 0.75 to account for the possibility of external input adding 25% of the total concentration of Zr in the soil (Figs. 21-22). Values for the volume strain are given for the soil samples in Table 1.

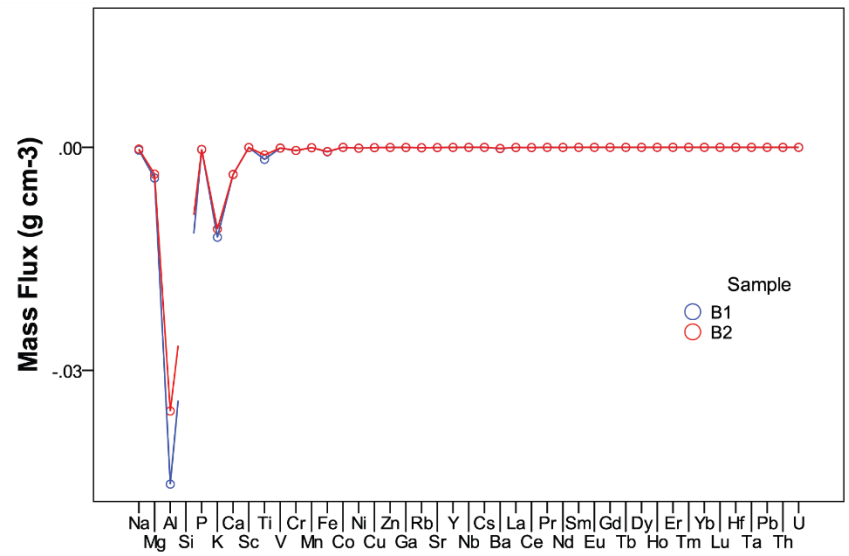

Figure 21 Element mass flux values for B1 and B2 soils at Site 1. Calculations assume that the weathering of the underlying bedrock (Mfp) supplies 75% of the Zr present in the soil, with the other 25% being sourced by an exotic component.

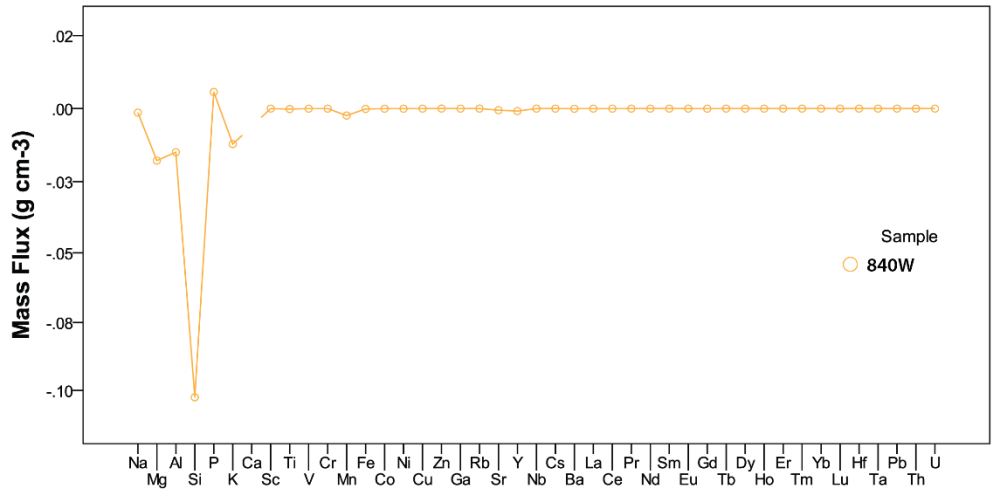

Figure 22 Element mass flux values for the 840W soil at Site 2. Calculations assume that 75% of the Zr in the soil was derived from weathering of the underlying bedrock (Oh), with the other 25% being sourced by an exotic component.

CHAPTER V

DISCUSSION

V.1 Do the Results Indicate Soils Formed Solely by Chemical Weathering of Underlying Bedrock?

To address the question of whether the soils at the two field sites formed solely by chemical weathering of the underlying bedrock, several lines of evidence from the previous chapter are examined in the section below.

Percent Insoluble Residue, Chemical Index of Alteration (CIA), XRD, and Grain Size and Shape

The percent insoluble residue and the chemical index of alteration (CIA) are both useful as qualitative measures for the role of bedrock weathering in soil formation. Percent insoluble residue is a measure of the soil forming potential of a rock—the higher the percentage, the greater the amount of material available to form soil. The percent insoluble residue values for the two bedrock samples are given in Table 1. Of the two samples, the Fort Payne has the highest percentage of insoluble constituents, as might be expected given its cherty composition. The Hermitage sample has a far lower percentage of insoluble residue due to its calcareous nature, and therefore less material available to chemically weather to form soil.

CIA is a measure for the degree to which a sediment has been weathered. CIA values are calculated from molar concentrations of Al_2O_3, CaO, Na_2O, and K_2O using the formula:

$$CIA = \frac{Al_2O_3}{(Al_2O_3 + CaO^* + Na_2O + K_2O)} \times 100 \qquad (3)$$

Where CaO* is the fraction of CaO associated with the silicate fraction of the sample (Nesbitt and Young, 1982). Unweathered granites and granodiorites have CIA values of 45-55, whereas average shales have CIA values of 70-75 and illites, beidellites, and montmorillonites have values of 75-85 (Nesbitt and Young, 1982).

The CIA values for the soils from the two sites (Table 1) are all greater than 70, with two of the three falling between 75 and 85. These high CIA values indicate that these soils are not first-cycle sediments, and were likely derived from a recycled sedimentary source that had experienced a high degree of weathering. The CIA values for the Mfp and Oh bedrock samples are 70 and 80 respectively, suggesting that, much like the soils, both contain a significant proportion of recycled sedimentary material that has undergone a high degree of weathering. If bedrock weathering is the dominant process in soil formation at a particular field site, the overlying soil should have a CIA value that is at least equal to that of the underlying rock, if not greater than it. This is the case with the soils from Site 1, both of which have greater CIA values than the underlying Mfp bedrock. However, at Site 2, the overlying soil has a CIA of 76, which is significantly lower than that of the underlying Oh bedrock, which is 80. This may be an indication that the Oh bedrock was not the only source from which the 840W soil was derived.

The results from XRD analyses of the samples (Table 2) provide another lens through which the derivation of soils from the underlying bedrock may be tested. If a species of mineral is present in the soil, but absent in the underlying bedrock, and is not a secondary mineral formed from weathering of a primary mineral in the bedrock, the soil must not have formed from bedrock weathering alone. At Site 1, chlorite is present in the B2 soil, and plagioclase in both soils, but both of these minerals are absent from the underlying bedrock. The bedrock from Site 2 contains illite, but this mineral is not found in the overlying soil. During the weathering process, it is probable that illite would have been altered to another clay mineral, such as montmorillonite, which would not have been detected by the type of XRD analysis performed on the samples, making its absence rather ambiguous.

In soils, the shape of a mineral grain can reveal the degree to which it has or has not been transported. During transport, particles advance by the process of saltation as they are carried either by wind or water. In this process, particles move along the surface in small hops, impacting with other particles and with their surroundings along the way. These impacts act to abrade the particles, giving them a more rounded shape (e.g. Brimhall et al., 1994) and may break individual particles into many smaller ones that, due to their smaller size, might be lofted higher and suspended in the transport medium over

longer distances before being deposited. If a soil has formed exclusively from in situ weathering of the underlying bedrock, mineral grains should be more angular. The size of a mineral grain can limit which agent of transport could have played a role. Grain size is particularly important when considering the possibility of an aeolian input of material as wind may transport grains measuring anywhere from >2 μm to 100μm in diameter over long distances (Gatehouse et al., 2001). The grain shape of the soils from the two sites was characterized by examining grain mounts (Fig. 12) of the samples. Within the B1 soil, many of the mineral grains appear to be mostly angular to subangular, though there is a small proportion of subrounded to rounded particles. Similarly, B2 also has a majority of angular to subangular mineral grains, but there is a higher proportion of subrounded to rounded particles than in B1. The 840W soil from Site 2 contains mineral grains that are much more angular than those at Site 1. No rounded grains were observed in this sample. The presence of rounded grains in soils at Site 1 could suggest an external input, but it is impossible to rule out derivation from the siliciclastic fraction of the underlying Fort Payne bedrock, which may contain mineral grains that were rounded by sedimentary transport. While the three soils contain particles within the grain size range transportable by wind, the shapes of a majority of the particles do not require that they were transported and it is entirely possible, based on the size and shape of the grains alone, for in situ weathering of the underlying bedrock to have formed these soils.

Age Distributions and K-S Tests

A population of zircon grains found within a soil that was derived from a single bedrock source should yield a U-Pb age distribution that is similar to that of the zircon population in the bedrock. In such a scenario, the age distributions, plotted as kernel density estimates (Fig. 16) for the soil-bedrock pair, should have modes close to or at the same ages. To identify zircon ages of soil and bedrock that match we used frequency-weighted averages of the ages contributing to each KDE age-peak. If the bedrock was the sole parent source for the soil, then each peak in the soil's age spectra, represented by a weighted average and standard deviation, should overlap with the frequency-weighted average and standard deviation associated with a peak in the bedrock's age spectra. The weighted averages and standard deviations for the samples are given in Table 3 (Site 1) and Table 4 (Site 2).

Table 3 Weighted averages and standard deviations of $^{206}Pb/^{238}U$ zircon ages in Ma contributing to specific KDE age-peaks in the age-spectra (Fig. 16) for the samples from Site 1.

Mfp Wt. Avg	Wt. Std. Dev.	B1 Wt. Avg	Wt. Std. Dev.	B2 Wt. Avg	Wt. Std. Dev.
436.4	92.2	455.9	53.6	297.1	174.2
1098.9	165	1116.9	146.1	1142.9	195.1

Table 4 Weighted averages and standard deviations of $^{206}Pb/^{238}U$ zircon ages in Ma contributing to specific KDE age-peaks in the age-spectra (Fig. 16) for the samples from Site 2.

Oh Wt. Avg	Wt. Std. Dev.	840W Wt. Avg	Wt. Std. Dev.
439.6	37.8	442.9	22.2
		657.7	40.7
1017.9	56.1	1043.5	47.9
1328.4	78.3	1260.2	49.7
		1439.5	35.2

As might have been anticipated from the visible resemblance of their age spectra (Fig. 16), the B1 soil and Mfp bedrock have similar age-peaks, with weighted averages that are within error of each other at ~440 Ma and ~1100 Ma. The similarity of their zircon U-Pb age distributions seems to support the derivation of the B1 soil solely from weathering of the Mfp bedrock. At the same location, the B2 soil doesn't appear to share the same degree of similarity with the underlying bedrock. While the weighted averages for B2 are within error of those of the Mfp bedrock, there is much greater error associated with them. Examination of the B2 age spectrum (Fig. 16) reveals that, in contrast to age peaks in B1 and Mfp, the young age peak in the B2 age spectrum is not normally distributed. The cause of the age spectra's abnormal shape is the presence of several Pb^{206}/U^{238} ages that far postdate the Lower Mississippian

depositional age of the Mfp bedrock of ~347-358 Ma (Wilson, 1990), including ages as young as 29.8 ± 0.9 Ma and 33 ± 0.8 Ma. Because the age distribution of B2 is not Gaussian, comparison of the weighted averages for its two age-peaks to those of Mfp would not be meaningful. However, the presence of such young ages in the B2 soil suggest that weathering of the Mfp rock was not the only source for the B2 soil. Because B2 directly underlies B1, it would be expected that similarly young ages would be present in B1 soil as well. It is not clear why these young ages do not appear in that soil.

The age spectra of the 840W soil and Oh rock (Fig. 16) show several similarities to each other, as do the weighted averages and deviations associated with several age-peaks (Table 4), with age-peaks matching within error at ~440 Ma and in the vicinity of ~1030 Ma. However, it is unclear which age-peak of the 840W soil corresponds to the third age-peak of the Oh bedrock, which has an associated weighted average of 1328.4 ± 78.3 Ma, as the overlying soil's age spectra has two separate age-peaks that are both within 1σ error. Most importantly, the 840W soil has an age-peak corresponding to a weighted average of 657.7 ± 40.7 Ma that does not show up within the zircon population in the Oh bedrock. Therefore, it is very possible the 840W soil might not have been derived solely from chemical weathering of the Oh bedrock.

For a soil formed only by chemical weathering of the underlying bedrock, the zircon U-Pb age spectra should not only appear to be visibly similar, they should also be statistically similar. It is possible to measure how similar the populations of U-Pb ages are between a soil and the underlying bedrock by comparing the cumulative age distributions using the nonparametric Kolmogorav-Smirnov (K-S) test. The K-S test was used to test the null hypothesis that the overlying soil displayed the same distribution of U-Pb ages as the underlying bedrock. A significance level of < 0.05 was required to reject the null hypothesis. If a soil was derived solely from weathering of the underlying bedrock, a significance level greater than 0.05 would be expected. Cumulative probability distributions for the filtered datasets for the three soil-bedrock pairs are shown in Figure 23 along with the significance levels from the K-S test comparing them.

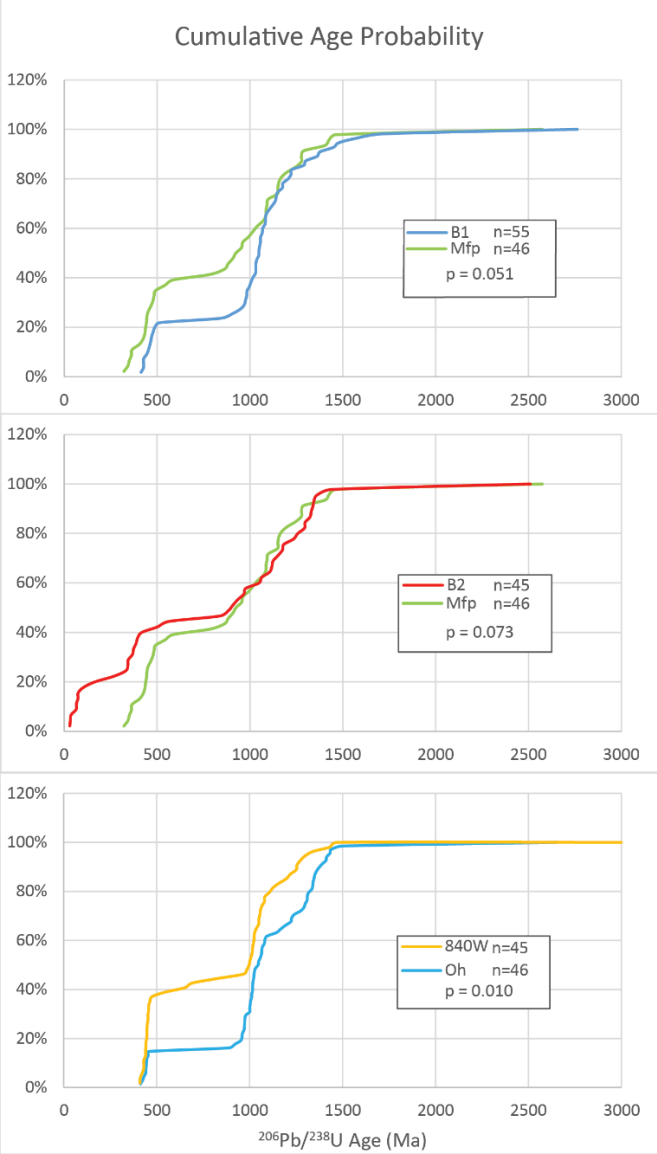

Figure 23 Cumulative probability plots displaying 206Pb/238U ages for each soil and underlying bedrock. In each plot, the p-values reflect the probability that the soil and bedrock samples have the same 206Pb/238U age distributions.

Of the three soil-bedrock pairs, the only one that has a significance level at or below the required threshold of 0.05 to reject the null hypothesis is the pair from Site 2, with a significance level of 0.01. For Site 1, the K-S test significance level for the B1-Mfp pair is just barely above the cutoff, at 0.051, while the B2-Mfp significance level is slightly higher, at 0.073. Therefore for these two soils from Site 1, the null hypothesis in the K-S test is accepted. It is easy to envision that with additional zircon U-Pb analyses, the significance level could change enough for B1 and Mfp to exhibit significantly different age

distributions, however it is unclear if the same could occur for B2 and Mfp. Based on the K-S test results, the B1 and B2 soils were both derived from chemical weathering of the Mfp bedrock, whereas the 840W soil must have had some other source of parent material in addition to the underlying Oh bedrock.

Deconvolution of Age Components

Due to the detrital nature of the zircon within the samples, and associated multiple age components, definitively identifying all of the different age modes from within each sample's U-Pb age population is very difficult. The weighted averages and standard deviations (Tables 3-4) discussed previously are one potential approach to this issue, but they have large errors associated with them. To better address this challenge, a routine called "Unmix" from the Isoplot software package (Ludwig, 2009) was used. Unmix uses an algorithm based on the Sambridge and Compston (1994) "mixture modeling" method to deconvolute multiple age components, assigning age peaks and proportions for each component based on an assumed number of components input by the user. For each of the five samples, the number of components was increased until a stable solution was obtained. For the samples from Site 1, the Unmix routine revealed significant age peaks at 416.5 ± 1.4, 967.3 ± 3.2, and 1253 ± 4.5 Ma in the Mfp bedrock, 450 ± 1.7, 1012.1 ± 2.5, 1182.3 ± 4.4, and 1440 ± 7.4 Ma in the B1 soil, and 33.1 ± 0.5, 81.1 ± 0.8, 361.7 ± 1.4, 940.9 ± 4.3, and 1239.6 ± 3.6 Ma in the B2 soil. The Oh bedrock has significant Unmix age peaks at 438.8 ± 1.7, 954.5 ± 4.6, 1042.8 ± 2.9, and 1328.6 ± 3.2, whereas the overlying 840W soil has peaks at 442.2 ± 1.3, 1035.6 ± 2.8, and 1234.7 ± 5.7. The age peaks and associated probability density plots included below in Figure 24 (Site 1) and Figure 25 (Site 2).

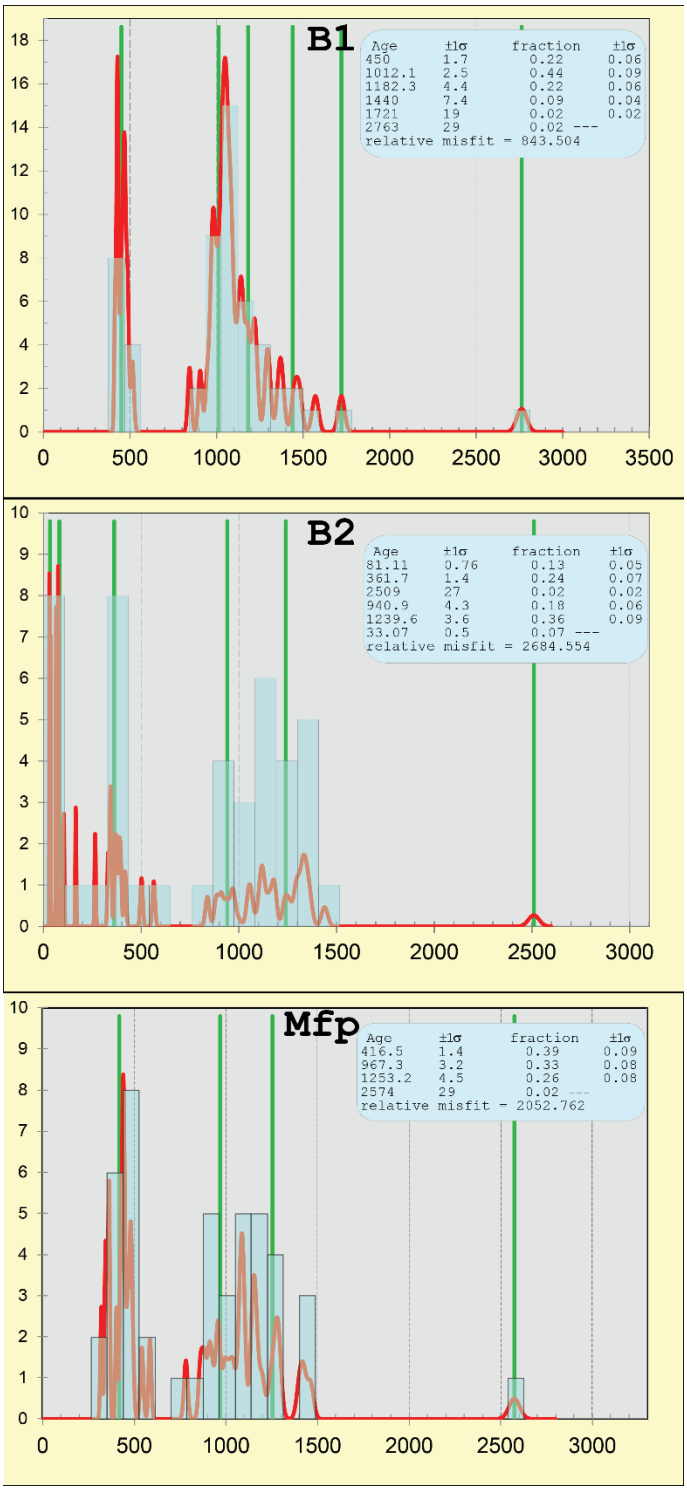

Figure 24 Unmix results for the three samples from Site 1. Unmix age peaks are marked in green on each probability density plot and listed along with the fraction of the sample represented by each peak in the included tables.

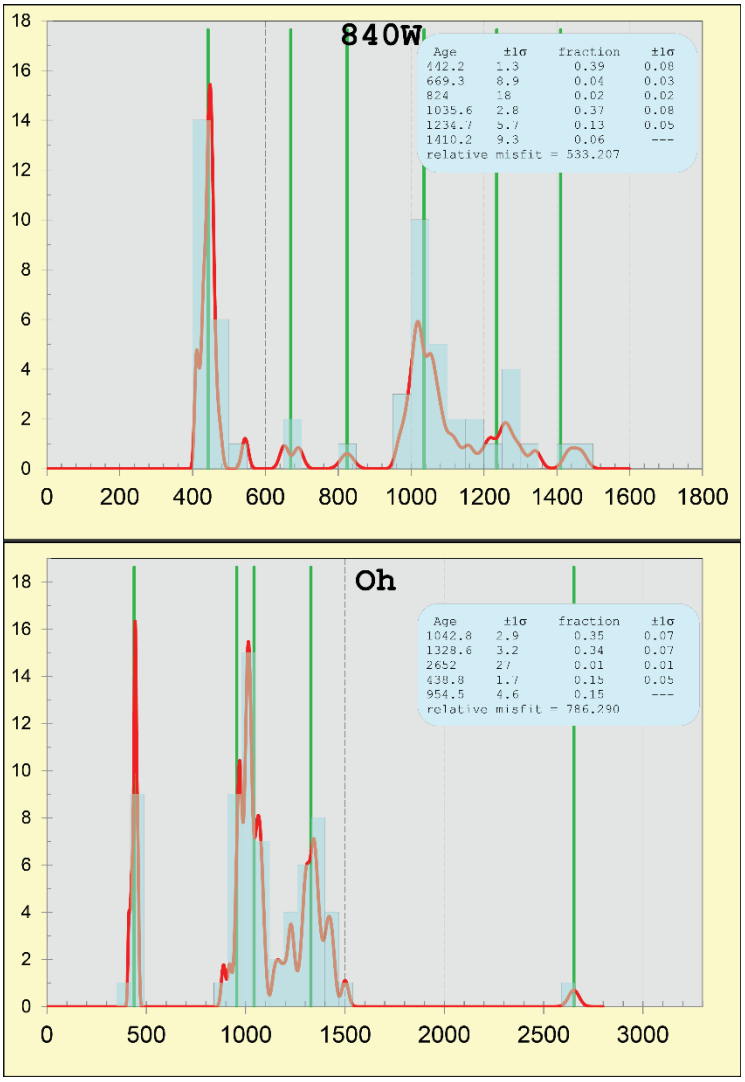

Figure 25 Unmix results for the two samples from Site 2. Unmix age peaks are marked in green on each probability density plot and listed along with the fraction of the sample represented by each peak in the included tables.

Many of the Unmix age peaks are in agreement with the peaks of the kernel density estimation and their weighted averages. For the B2 soil, the Unmix routine picks up on age populations that are missed by the KDE peaks and weighted averages, including a population at 33.1 ± 0.5 and 81.1 ± 0.8. The Unmix peak in B1 and Mfp around ~440 Ma is at the same location as the KDE peak, and suggests some component of bedrock weathering of Mfp to produce the B1 soil. The Unmix peaks at 940.9 ± 4.3 and 1239.6 ± 3.6 are close to the Mfp Unmix peaks at 967 ± 3.2 and 1253 ± 4.5, suggesting that some component of the B2 soil was derived from the Mfp bedrock. The younger Unmix peaks in B2 that are too young to be derived from the Mississippian make sense given the KDE distribution, and suggest that

some component of the B2 soil was not derived from Mfp. The Unmix peaks identified in the 840W soil are all similar to the Oh bedrock except for one at 1234.7 ± 5.7. Overall the Unmix ages do not refute the clear genetic relationship between the 840W and Oh bedrock, but the presence of an apparent age population in the soil that is not in the bedrock suggests that weathering of the Hermitage alone could not have produced the soil.

Potential Source Terranes for U-Pb Age Peaks in Bedrock and Comparisons to Price Fm. and Martinsburg Fm.

The zircon U-Pb ages from the bedrock can be used to learn about the tectonic setting in which a rock was deposited. Cawood et al. (2014) examined detrital zircon U-Pb ages in different sedimentary rock formations and found that by subtracting the maximum depositional age of the bedrock from the crystallization ages of zircon grains, the tectonic setting in which the formation was deposited could be identified. The exact timing of deposition of the Fort Payne Formation in the Middle Tennessee region is not known, though most—e.g. Wilson (1990)—consider it to be a Lower Mississippian rock unit. In contrast, the age of the Hermitage Formation is well-constrained to a depositional age of 453 ± 1 Ma by Holland and Patzkowsky (1997). Following Cawood et al. (2014), the deposition age was subtracted from zircon U-Pb ages from Mfp and Oh bedrock samples, approximating the depositional age of the Fort Payne Formation as 350 Ma, and using 453 Ma (Holland and Patzkowsky, 1997) for the depositional age of the Hermitage Formation (Fig. 26).

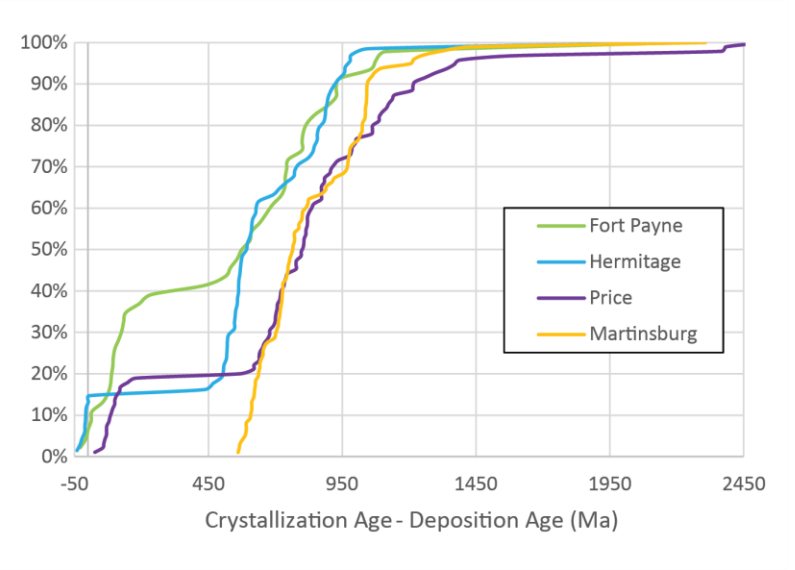

Figure 26 Cumulative probability plots of zircon U-Pb crystallization age minus the deposition age of the bedrock. Price Formation (Caldwell, WV) and Martinsburg Formation (Fincastle, VA) zircon U-Pb ages from Park et al. (2010).

The distributions shown in Figure 26 plot in the same area as detrital zircon from sedimentary rocks deposited in the Appalachian foreland basin, as shown by the distributions of the Lower Mississippian Price Formation (sample from Caldwell, WV) and Middle Ordovician Martinsburg Formation (sample from Fincastle, VA) (Park et al., 2010). This places the Mfp and Oh bedrock into a collisional tectonic setting of deposition. Zircon within the Oh and Mfp bedrock samples record several of the major orogenic events from the latest Proterozoic to early Phanerozoic that occurred in Laurentian and Gondwanan provinces. Both rock samples contain multiple zircon grains with ages corresponding to the Eastern Granite-Rhyolite Province (ca. 1300 – 1500 Ma), Grenville Orogeny (ca. 900 – 1300 Ma), and Taconic Orogeny (ca. 490-440 Ma) (Park et al., 2010). Zircon from the Mfp bedrock also record the Acadian Orogeny (ca. 350-390; Becker et al., 2005). Although the Price and Martinsburg formations of Park et al. (2010) are located in West Virginia and Virginia respectively—far from the sampling sites for the Mfp and Oh bedrock in Middle Tennessee—U-Pb ages from detrital zircon within these sedimentary rock units form age spectra with peaks that are at relatively similar locations to the Middle Tennessee samples (Fig. 27).

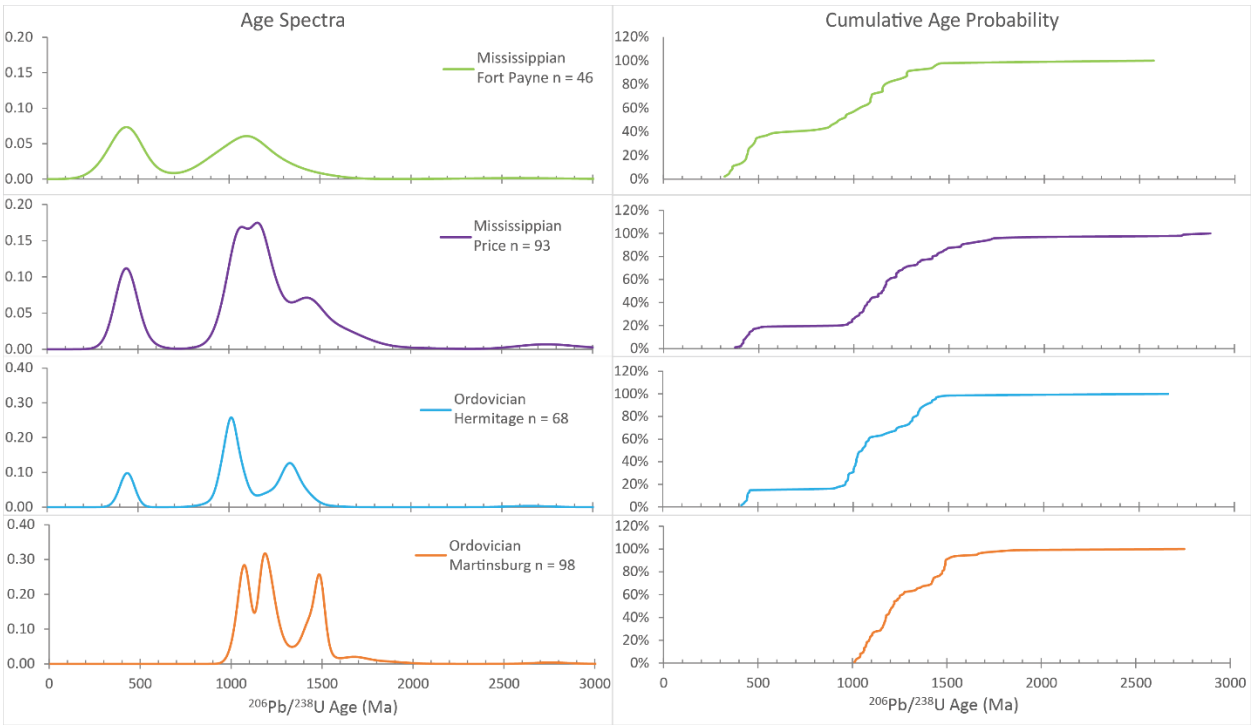

Figure 27 Comparison of Fort Payne and Hermitage zircon U-Pb age spectra and cumulative probability plots to those of the Price and Martinsburg formations from Park et al. (2010).

The two Lower Mississippian rock samples and two Middle Ordovician rock samples shown in Figure 27 have age spectra with some parallels in the ages at which peaks are located, but distinctly different shapes. In contrast, portions of the cumulative probability plots between the two Mississippian rocks and the two Ordovician rocks are alarmingly similar in shape. It is conceivable that two geographically distant rock units deposited over the same time period, within the same foreland basin, receiving detritus from the same massive geologic provinces as one another would contain zircon populations with similar U-Pb age modes, corresponding to major regional and global tectonic events related to the assemblage and rifting of super continents and continent-scale orogenesis. K-S tests were performed to determine if there was any statistically significant similarity between each pair. The Fort Payne-Price pairing was found to have dissimilar age distributions with a significance level of 0.001. The Hermitage-Martinsburg pairing had the same result, but with a significance level of 0. Despite the commonalities in where and when detritus was being sourced from, and the regional and tectonic setting

in which it was being deposited, the two Middle Tennessee samples are significantly different from their approximately coeval, central Appalachian counterparts.

Potential Lead-loss in Zircon

Over time, the decay of uranium and thorium within a zircon grain damages the crystal lattice through a process called metamictization. This can result in the zircon losing lead. If a zircon crystallized shortly before it was deposited, a small amount of lead loss would decrease its U-Pb age significantly below the depositional age. It would be hard to detect the lead loss on a Terra-Wasserburg concordia plot in such a situation because the trajectory of the zircon's U-Pb composition would be almost parallel to the concordia line. In Figure 26 there are a few cases where the zircon U-Pb age minus the depositional age yields negative values for the two bedrock samples, possibly because such lead loss has occurred. Two zircon grains from the Fort Payne sample give negative values from this equation, the most negative being -28.4 Myrs. There are eight zircon U-Pb ages in the Hermitage sample younger than the unit's deposition age, but the most negative difference returned is -40.6 Myrs. None of these appear to be discordant because the age at which they formed is so close to the deposition age of the bedrock unit. This is not an issue for this study as absolute U-Pb ages are not crucial to identifying the soil's provenance. For the purposes of comparing the age distributions between a soil and the underlying bedrock, such lead loss will not affect the outcome.

Element Concentrations, Element Mass Flux, and Volume Strain

For a soil forming only from chemical weathering of an underlying bedrock parent, mass fluxes for all elements should be negative—though negative flux values do not require that a soil formed from only one parent. Positive mass fluxes, on the other hand, do require at least one additional parent material souce. Element mass flux values are presented in Figures 21-22 and in Table A1. Positive mass flux values that were within 1σ of a zero value were disregarded. For the samples from Site 1, most of the mass fluxes are negative, but both the B1 and B2 soils had a positive mass flux for Pb. At Site 2, the 840W soil had a positive mass flux for uranium, as well as REE Dy, Ho, Er, and Yb. However, these mass flux values were calculated assuming only 75% of the Zr in the soil was derived from the bedrock,

the other 25% being contributed by some exotic source of parent material. Therefore, the positive mass fluxes that were calculated in this manner are rather inconclusive for determining if there was more than one parent material source. Removing the exotic component does not change the positive mass flux of Pb in both soils from Site 1. Therefore these soils may have had some external component that contributed additional Pb, but seem to have formed mostly from chemical weathering of the underlying bedrock. The positive flux of Pb in the soils might relate to lead particulates from leaded gasoline. In contrast, removing the exotic component results in mass fluxes that are negative for all elements in the soil at Site 2, suggesting that the Hermitage bedrock alone could have formed the overlying soil there.

The volume strain may also be used with the measured thickness of the soil horizon to estimate the original height of the bedrock, B_p, prior to the weathering that produced the observed soils. Following Brimhall (1988), B_p and the height of the weathered soil section, B_w, may be substituted into Eq. 1, which can be rearranged to obtain:

$$B_{Zr,p} = \frac{B_{Zr,w}}{(1 + \epsilon_{Zr,w})} \quad (4)$$

For the B1 and B2 samples, this equation returned $B_{Zr,\,p}$ values of 0.92 m and 1.21 m respectively. The overall thickness of bedrock that was dissolved to form the B1 and B2 soils can found by subtracting the sum of the two $B_{Zr,\,w}$ values from the sum of the two $B_{Zr,\,p}$ values. This yields an estimate of 1.65 m for the total height of bedrock dissolved to form the observed soils. Assuming a median age of 100 ka from the 128-75 ka Sangamon surface age range (Huckemeyer, 1999), this corresponds to an estimated denudation rate of 17 m/Myr for the Fort Payne Fm., which is of the same order of magnitude as a previous denudation rate estimate of 11 m/Myr in Reesman and Godfrey (1981). These calculations once again assume 25% of the total Zr concentration in the soil was derived from an exotic source. Removal of the exotic component from the formula used to calculate $\epsilon_{Zr,\,w}$ in Eq. 4 changes the estimated total height of bedrock removed to 2.36 m, and the denudation rate further away from the estimate of Reesman and Godfrey (1981), to 23.6 m/Myr. The calculations in Eq. 4 were not carried out for the soil at Site 2 because there is no correlated age for the bedrock surface.

Input of Exotic Material?

While weathering of the underlying bedrock seems to be the dominant source of parent material to the soils based on all the evidence presented, an additional exotic component is required at both sites. At Site 1, the B1 and B2 soils contained plagioclase, which was not found in the underlying Fort Payne bedrock. K-S tests show that the soils' zircon U-Pb ages are not significantly different from those of the bedrock; however, for the B1 soil, the significance level of this test is just barely (0.01) above the cutoff. With additional U-Pb age analyses, the K-S test may determine that B1 and Mfp are significantly different in U-Pb age distributions. The presence of young zircon in the B2 soil that far post-date the depositional age of the Fort Payne—the youngest being 29.8 ± 0.9 Ma—cannot be explained by lead loss, and based on the wide spread in Cenozoic ages of other young zircon grains in this soil, contamination is also unlikely. The positive mass flux of Pb does require an external input, but may be derived from leaded gasoline.

At Site 2, the 840W soil has a lower CIA value than the underlying Hermitage bedrock, suggesting it is less chemically weathered than the underlying rock. This seems to indicate the presence of some secondary source of parent at this site that is less weathered than both the soil and Hermitage rock. The K-S test of zircon U-Pb ages in the 840W soil and Hermitage bedrock found a significant difference in their age populations such that the soil could not have come from the bedrock alone.

Therefore, for soils at both sites, it would appear that there is some exotic parent material that was not derived from the underlying bedrock. However, there is a predominant bedrock signature in all three soil samples from their associated underlying rock unit, suggesting that weathering of any exotic component would be minor in proportion to bedrock weathering. I will explore potential sources of exotic material for each of the two sites in the next section.

V.2 What are the Potential Sources of Exotic Parent Material for the Soils?

While weathering the underlying bedrock seems to be a dominant source of parent material for soils at the two sites, as discussed in the last section, weathering of other rock units, of different

composition than the underlying bedrock, could be a source of exotic material. In addition, it is possible for alluvium or loess deposition to have contributed an exotic component to soils in the region. These potential sources will be evaluated for each of the two sites in the section that follows to determine which are most likely comprising an exotic component in each locale.

Potential Sources of Exotic Parent Material for Soils at Site 1

As previously mentioned in Section II.2, Site 1 is located atop a terrace along the Harpeth River that Huckemeyer (1999) correlated to a Sangamon age equivalent surface. Terrace surfaces that originated during the Sangamon interglacial period in the Southeastern United States have experienced two or more episodes of loess deposition (Huckemeyer, 1999). Huckemeyer (1999) described the terrace at Site 1 as experiencing the two most recent of these episodic loess depositions, the Roxana Silt and the Peoria Loess, with the Roxana incorporated into the existing soil, and the Peoria present as a 25 cm-thick mantle atop the B-horizon. Despite excavating a soil pit down to the saprolite, no loess mantle was identified at Site 1. However, this does not rule out the presence of either or both loess units in the soils at this site as the majority of both the B1 and B2 soils are comprised of particles small enough to be transported by wind (>2 μm to 100μm; Gatehouse et al., 2001). While the majority of the grains are angular to subangular, B2 especially has numerous rounded and subrounded grains that could reflect wind transport.

Thick loess bluffs on the order of 25 m or more have been documented along the banks of the Mississippi River in West Tennessee (e.g. Rodbell, 1996; Rodbell et. al, 1997), but aside from Huckemeyer (1999), no published studies have identified Peoria Loess in Middle Tennessee. Due to the relatively old age of the terrace at Site 1, it is very likely that there was some loess deposition. Huckemeyer (1999) estimates 0.37-0.75 m of deposition on this terrace, split between the Roxana Silt and Peoria Loess. However, assuming a median age of 100 ka once again, and assuming that all 25% of the exotic input estimated earlier was from loess, I estimate a maximum of 0.43 m of total loess deposition—a number much closer to the lower end of the range given in Huckemeyer (1999). For 0.75 m of loess to have been deposited—the upper end of the range estimated in Huckemeyer (1999)— ~43% exotic input is required, which is hardly the minor exotic component supported by the exotic zircon ages, XRD results,

mass flux values, and other lines of evidence discussed earlier. Instead, I would propose that if loess comprises the majority of the exotic component, the overall deposition of Roxana and Peoria combined would be much closer to the 37 cm estimated by Huckemeyer (1999), and possibly even lower.

It may prove difficult to deconvolute both a Roxana and Peoria loess signature from the soil. However, the presence of loess is required to produce the young ages observed in the B2 soil. There are no rock units in the Harpeth's watershed, or even in the entirety of Tennessee that could contribute zircon with such young ages. Unless the Harpeth is carrying loess that was blown in and deposited on the floodplain, alluvium can't explain the young ages in B2 either. This would support the presence of loess documented by Huckemeyer (1999), though it is not clear if the B1 and B2 soils record both a Peoria Loess and Roxana Silt signature.

As the soils at Site 1 sit atop the a high, flat terrace, some twenty or more meters above the active floodplain of the Harpeth River, any recent deposition of alluvium is highly improbable. If alluvium were to have contributed at any time during the development of the ultisol soils that sit atop the terrace, such contributions would have occurred around the time at which the bedrock surface and then-floodplain was abandoned by the Harpeth. Once abandoned, it is possible that alluvium might have been left atop the surface. Any major flooding events that might have occurred over the next several thousand years could have added additional river sediments to the terrace.

Well-developed soils like those at Site 1 typically require a timescale on the order of tens of thousands of years to form (Birkeland, 1999). If flooding occurred long after the surface was abandoned, there would be traces of fluvial reworking within the soil profile. No such reworking was observed in our excavated profile nor was any observed by Huckemeyer (1999) atop other surfaces at this terrace level elsewhere along the Harpeth River. Therefore, any contribution of alluvium as parent material should be relatively insignificant in comparison to that of the underlying Fort Payne bedrock. It is unclear if the presence of an appreciable quantity of alluvium would even be discernable from the other soil constituents as much of the geology surrounding the Harpeth River is comprised of the Fort Payne Formation or the stratigraphically-higher Warsaw Formation.

The terrace at Site 1 is located near the middle of the Fort Payne Formation stratigraphically. The nearest exposure of the Warsaw Formation is 3 km away and > 75 m higher in elevation than the terrace. The Fort Payne Formation is 61 m thick on average in Tennessee (Nicholson et al., 2005). Over the past 100 kyrs, it is highly improbable that the 1.1 to 1.7 m of overlying rock weathered away had extended up into the Warsaw. Therefore, it is highly unlikely that any bedrock unit other than the Fort Payne Formation could have contributed to the soil. There are no other bedrock units that could have provided an exotic component to the soil.

Potential Sources of Exotic Parent Material for Soils at Site 2

As discussed in Section II.2, Site 2 sits atop an outcrop of Hermitage Formation limestone along Tennessee State Route 840. The alfisols atop this high flat surface are much younger than the ultisols at Site 1, having formed over the past several hundred to a few thousand years (Birkeland, 1999). Because they are so young, loess deposition is not considered to be a viable source for exotic material at this site. While this surface sits more than 10 m above the active floodplain of the Harpeth River, the possibility that alluvium might have been contributed by the Harpeth during the timescale of soil development at this site cannot be ruled out at this time. Characterization of the Harpeth River alluvium and its zircon U-Pb age spectra are needed to better address this question.

The other potential source of exotic material that could have contributed is the weathering of a bedrock unit that is compositionally different from the underlying Hermitage Formation bedrock. The next unit up from the Hermitage is the Bigby-Cannon Formation, which outcrops above the Hermitage along TN-840 approximately 0.15 km away from Site 2. Stratigraphically, Site 2 sits within the upper Hermitage Formation. Therefore, based on the stratigraphic position of Site 2 within this formation, and its proximity to an outcrop of the Bigby-Cannon Formation, it is very plausible that there might have been weathering of this other bedrock unit to contribute an exotic component to the soils at Site 2 over the past several hundred to few thousand years. The Bigby-Cannon Formation is a phosphatic limestone rock unit that is somewhat similar geochemically to the Hermitage Formation. If an exotic component was contributed by this rock unit, it may only be detectable via zircon U-Pb geochronology.

CHAPTER VI

CONCLUSIONS

From a methods standpoint, this is the first of any known published studies to successfully recover zircon from limestone. We had attempted to recover monazite, another useful accessory mineral and geochronometer, from the limestone and soils but were unsuccessful either because it was not present in the sediment at the time of deposition, unidentifiable, or destroyed by weathering during the past few hundred million years since the rocks formed. Based on the results presented in this study, zircon U-Pb geochronology appears to be a powerful and effective tool for use in determining soil provenance in limestone terranes provided that adequate populations of zircon grains are analyzed for each sample. In most of our samples, 50% or more of the analyzed grains yielded discordant $^{206}Pb/^{238}U$ ages. Therefore, it is recommended that at least 200 zircon grains be analyzed for each sample, instead of the ~100 grains per sample analyzed in this study. If numerous potential end-members are being considered, it is recommended that even more than 200 grains be analyzed per sample.

We utilized KDE plots, weighted averages and the Unmix routine to try to identify age populations within each sample. The most useful of these three was the Unmix routine, which identified age populations with a much lower degree of uncertainty than the other methods. The K-S test proved to be invaluable for making meaningful comparisons of age distributions between the soil and underlying bedrock. The K-S test results from the comparison of each bedrock sample's zircon U-Pb age distribution to that of a different rock unit hundreds of kilometers away that was deposited around the same time, in the same tectonic setting, receiving the sediment from the same orogenic sequence, illustrate how well-suited this method is for this type of problem. While zircon U-Pb geochronology was useful in addressing the question of soil provenance in Middle Tennessee, this one method alone is not enough to answer it. Other methods are needed to fill in the gaps and corroborate what the geochronological results suggest.

One of these other methods, mass flux, was difficult to use for determining soil provenance because of the large degree of uncertainty associated with the calculations. Some of this uncertainty was related to measurement of the rock density. Another component of it was due to the error associated with the concentration measurements.

From our analyses performed the soils and bedrock at both sites, it is evident that weathering of bedrock is the dominant soil-forming process in Middle Tennessee. Much of this weathering is of the underlying bedrock unit, though it is possible for stratigraphically higher rock units to contribute materials to the soils as well. If the latter scenario holds true, but the rock is not very different from the underlying unit geochemically, was deposited soon after the underlying unit, and has a similar environment of deposition such that its zircon age distribution is similar, it may be impossible identify its presence in the soil using any method.

In Middle Tennessee, there is no doubt that alluvium plays a role in contributing parent material to form soils along the many rivers dissecting the region, but it doesn't appear to have played much of a role at either of the sites examined in this study. There are no rock units in the lands drained by these rivers or even in the state as a whole that could have contributed the young ages found in the soils atop the terrace. At Site 1, Cenozoic zircon U-Pb ages require that this exotic material be derived from loess—likely either Peoria Loess or Roxana Silt, which are otherwise found in West Tennessee. This would be the furthest East in Middle Tennessee that their presence has been confirmed. At Site 2 it is possible that the Bigby-Cannon Formation has contributed material to the soils. Additional work is already underway by PI John C. Ayers and collaborator Xiaomei Wang to complete additional zircon analyses for the samples in this study and to characterize the geochemistry and zircon U-Pb age spectra of different potential end-members in the region, including alluvium from the Harpeth and Cumberland rivers, Peoria Loess, Roxana Silt, and Bigby-Cannon Formation. With this additional work, we anticipate being able to more firmly identify the exotic component or components present in the soils at each of the two sites. The characterization of these different end-members will facilitate future studies of soil provenance at other locations, either along more recently active terraces or foodplains, or atop other bedrock units.

REFERENCES

Ball, D.F. (1964). Loss on ignition as an estimate of organic matter and organic carbon in noncalcareous soils. *Journal of Soil Science*, 15(1), 84-92.

Becker, T. P., Thomas, W. A., Samson, S. D., & Gehrels, G. E. (2005). Detrital zircon evidence of Laurentian crustal dominance in the lower Pennsylvanian deposits of the Alleghanian clastic wedge in eastern North America. *Sedimentary Geology*, 182(1-4), 59–86.

Bettis, E. A., Muhs, D. R., Roberts, H. M., & Wintle, A. G. (2003). Last Glacial loess in the conterminous USA. *Quaternary Science Reviews*, 22(18-19), 1907-1946.

Birkeland, P. W. (1999). *Soils and Geomorphology* (3rd ed., p. 430). Oxford University Press.

Braun, S. A., Bream, B. R., & Gualda, G. A. R. (2009). Age and chemistry of megacrystic zircons from Zirconia, North Carolina. *GSA Abstracts with Programs*, 41(7), 671.

Brimhall, G. H., Christopher, J. L., Ford, C., Bratt, J., Taylor, G., & Warin, O. (1991). Quantitative geochemical approach to pedogenesis: importance of parent material reduction, volumetric expansion, and eolian influx in lateritization. *Geoderma*, 54(1-4), 51-91.

Brimhall, G. H., Lewis, C. J., Ague, J. J., Dietrich, W. E., Hampel, J., Teague, T., & Rix, P. (1988). Metal enrichment in bauxites by deposition of chemically mature aeolian dust. *Nature*, 333(6176), 819–824.

Cawood, P. A., Hawkesworth, C. J., & Dhuime, B. (2012). Detrital zircon record and tectonic setting. *Geology*, 40(10), 875–878.

Covey, A. K., Braun, S. A., Gualda, G. A. R., Bream, B. R., Fisher, C., Wooden, J. L., & Schmitz, M. D. (2012). Zirconia (NC) zircon as a potential standard. *2012 Fall Meeting*, AGU, San Francisco, CA, 3-7 Dec.

Davies, W. E., Simpson, J. H., Ohlmacher, G. C., Kirk, W. S., & Newton, E. G. (1984). Engineering aspects of karst. *U.S. Geological Survey National Atlas*, scale 1:7,5000.

Ford, D., & Williams, P. (2007). *Karst Hydrogeology and Geomorphology* (2nd ed.). Chichester, UK, John Wiley & Sons Ltd, pp. 9.

Foster, A. P. (2009). *Counties of Tennessee*. Baltimore, MD: Genealogical Publishing Inc., 124 p. (Original work published 1923)

Gatehouse, R. D., Williams, I. S., & Pillans, B. J. (2001). Fingerprinting windblown dust in south-eastern Australian soils by uranium-lead dating of detrital zircon. *Soil Research*, 39(1), 7–12.

Govindaraju, K. (1994). 1994 Compilation of Working Values and Descriptions for 383 Geostandards. *Geostandards Newsletter*, 18, 1–158.

Holland, S. M., & Patzkowsky, M. E. (1997). Distal orogenic effects on peripheral bulge sedimentation: Middle and Upper Ordovician of the Nashville Dome. *Journal of Sedimentary Research*, 67(2), 250–263.

Huckemeyer, J. L. (1999). *Late Quaternary Alluvial Stratigraphy and Soil Development Along the Harpeth River, Central Tennessee*. Nashville, TN, Vanderbilt University Press, 192 p.

Jackson, J.A., editor, 1997, Glossary of Geology: Alexandria, VA, American Geological Institute, 4th ed., 769 p.

Jochum, K. P., Nohl, U., Herwig, K., Lammel, E., Stoll, B., & Hofmann, A. W. (2005). GeoReM: A New Geochemical Database for Reference Materials and Isotopic Standards. *Geostandards and Geoanalytical Research*, 29(3), 333–338.

Lackey, J. S. (2005). *The magmatic and alteration history of the Sierra Nevada batholith as recorded by oxygen isotope ratios in zircon, titanite, garnet, and quartz*. Unpub. PhD thesis, University of Wisconsin, 345 p.

Larsen, I. J., Almond, P. C., Eger, A., Stone, J. O., Montgomery, D. R., & Malcolm, B. (2014). Rapid Soil Production and Weathering in the Southern Alps, New Zealand. *Science*, 343(6171), 637–640.

Ludwig, K. R. (2009), Isoplot v.4 for Excel 2007, Berkeley Geochronology Center, Berkeley, CA.

Muhs, D. R., Budahn, J. R., Prospero, J. M., & Carey, S. N. (2007). Geochemical evidence for African dust inputs to soils of western Atlantic islands: Barbados, the Bahamas, and Florida. *Journal of Geophysical Research*, 112(F2), F02009.

Muhs, D. R., Budahn, J. R., Prospero, J. M., Skipp, G., & Herwitz, S. R. (2012). Soil genesis on the island of Bermuda in the Quaternary: The importance of African dust transport and deposition. *Journal of Geophysical Research*, 117(F3), F03025.

Nesbitt, H., & Young, G. (1982). Early Proterozoic climates and plate motions inferred from major element chemistry of lutites. *Nature*, 299, 715-717.

Nicholson, S. W., Dicken, C. L., Horton, J. D., Labay, K .A., Foose, M.P., and Mueller, J. A. L.(2005). *Preliminary integrated Geologic Map Databases for the United States: Kentucky, Ohio, Tennessee, and West Virginia*. U.S. Geological Survey Open-File Report 2005–1324.

NRCS. (2012). *Gridded Soil Survey Geographic (gSSURGO) Database for Tennessee*. Retrieved March, 10, 2013 from United States Department of Agriculture, National Resources Conservation Council Data Gateway, http://datagateway.nrcs.usda.gov.

Park, H., Barbeau Jr., D. L., Rickenbaker, A., Bachmann-Krug, D., & Gehrels, G. E. (2010). Application of Foreland Basin Detrital-Zircon Geochronology to the Reconstruction of the Southern and Central Appalachian Orogen. *The Journal of Geology*, 118(1), 23–44.

Reesman, A. L., & Godfrey, A. E. (1981). Development of the Central Basin of Tennessee by chemical denudation. *Zeitschrift Fur Geomorphologie*, 25, 437–456.

Rodbell, D. T. (1996). Subdivision, subsurface stratigraphy, and estimated age of fluvial-terrace deposits in northwestern Tennessee. *U.S. Geological Survey Bulletin 2128*, 1-24.

Rodbell, D. T., Forman, S. L., Pierson, J., & Lynn, C. W. (1997). Stratigraphy and chronology of Mississippi Valley loess in western Tennessee. *Geological Society of America Bulletin*, 109(9), 1134-1148.

Sambridge, M., & Compston, W. (1994). Mixture modeling of multi-component data sets with application to ion-probe zircon ages. *Earth and Planetary Science Letters*, 128, 373–390.

Saucier, R. T. (1987). Geomorphological interpretations of late Quaternary terraces in western Tennessee and their regional tectonic implications. *U.S. Geological Survey Professional Paper 1336-A*, 1-19.

Tan, K. H. (2005). *Soil Sampling, Preparation, and Analysis* (2nd ed.). Boca Raton, FL: CRC Press, 623 p.

Vermeesch, P. (2012). On the visualisation of detrital age distributions. *Chemical Geology*, 312, 190–194.

Wilson, C. W. (1990). *Pre-Chattanooga Stratigraphy in Central Tennessee* (2nd ed.). State of Tennessee, Department of Conservation, Division of Geology, 415p.

Wilson, S A. (1997). The collection, preparation and testing of USGS reference material BCR-2, Columbia River Basalt. *U.S. Geological Survey Open-File Report* 98-00x.

Wilson, S. A. (1998a). Data compilation and statistical analysis of intralaboratory results for AGV-2. *U.S. Geological Survey Open-File Report* (in-progress).

Wilson, S. A. (1998b). Data compilation for USGS reference material GSP-2, Granodiorite, Silver Plume, Colorado. *U.S. Geological Survey Open-File Report* (in-progress).

APPENDIX A

Table A1 Mass fluxes (g/cm3; grams of a specific element per volume of rock) for the B1-Mfp, B2-Mfp, and 840W-Oh soil-bedrock pairs with standard deviations. Calculations assume 25% of Zr in soils was sourced from an exotic source, rather than the bedrock.

Element	δB1	S.D.	δB2	S.D.	δ840	S.D.
Na	-0.000313	0.265	-0.000198	0.156	-0.00136	0.503
Mg	-0.00349	3.959	-0.00304	3.414	-0.0177	5.019
Al	-0.0389	614.606	-0.0304	468.137	-0.0149	73.083
Si	-0.781	216978.902	-0.755	206178.142	-0.103	7658.766
P	-0.000253	0.0314	-0.000230	0.0278	0.00562	0.237
K	-0.0103	46.581	-0.00931	40.96	-0.0120	18.313
Ca	-0.00308	3.554	-0.00308	3.076	-1.198	269.812
Sc	-0.0000192	0.000135	-0.0000177	0.000122	-0.0000039	0.0000111
Ti	-0.00136	3.514	-0.000863	2.086	-0.000161	0.179
V	-0.0000842	0.00269	-0.0000751	0.00235	-0.0000138	0.000130
Cr	-0.000359	0.0396	-0.000351	0.0385	-0.0000115	0.000540
Mn	-0.0000402	0.00208	-0.0000412	0.00200	-0.00236	0.0507
Fe	-0.000504	0.0939	-0.000470	0.0856	-0.000123	0.00645
Co	-0.00000274	0.00000419	-0.00000161	0.00000235	-0.0000328	0.0000178
Ni	-0.0000953	0.00302	-0.0000915	0.00286	-0.0000276	0.000255
Cu	-0.0000338	0.000373	-0.0000328	0.000358	-0.0000072	0.0000218
Zn	-0.0000139	0.000120	-0.0000137	0.000112	0.0000197	0.0000757
Ga	-0.0000163	0.000150	-0.0000133	0.000118	-0.0000071	0.0000249
Rb	-0.0000486	0.000957	-0.0000419	0.000802	0.0000047	0.0000814
Sr	-0.0000272	0.000481	-0.0000243	0.000410	-0.000537	0.00358
Yb	-0.00000754	0.0000827	-0.00000582	0.0000602	-0.000850	0.00400
Nb	-0.00000297	0.0000227	-0.00000162	0.0000116	-0.0000011	0.0000038

Cs	-0.00000235	0.00000202	-0.00000187	0.00000158		
Ba	-0.000143	0.0153	-0.000119	0.0121	-0.0000518	0.00217
La	-0.0000167	0.000176	-0.0000141	0.000143	-0.0000053	0.0000215
Ce	-0.0000281	0.000569	-0.0000224	0.000433	-0.0000118	0.0000937
Pr	-0.00000234	0.00000494	-0.00000189	0.00000377	-0.0000014	0.0000012
Nd	-0.00000851	0.0000706	-0.00000694	0.0000541	-0.0000031	0.0000108
Sm	-0.00000138	0.00000208	-0.00000111	0.00000159	-0.0000007	0.0000005
Eu	-0.00000028	0.00000008	-0.00000023	0.00000006	-0.0000002	0.0000000
Gd	-0.00000243	0.00000539	-0.00000197	0.00000414	-0.0000168	0.0000150
Tb	-0.00000014	0.00000003	-0.00000010	0.00000002	-0.0000001	0.0000000
Dy	-0.00000099	0.00000174	-0.00000065	0.00000106	0.0000006	0.0000004
Ho	-0.00000026	0.00000010	-0.00000019	0.00000007	0.0000001	0.0000000
Er	-0.00000070	0.00000080	-0.00000050	0.00000055	0.0000001	0.0000000
Tm	-0.00000009	0.00000002	-0.00000007	0.00000001	0.0000000	0.0000000
Yb	-0.00000071	0.00000100	-0.00000055	0.00000072	0.0000002	0.0000001
Lu	-0.00000010	0.00000002	-0.00000008	0.00000002	0.0000000	0.0000000
Hf	0.00000071	0.00000412	0.00000083	0.00000451	0.0000021	0.0000055
Ta	-0.00000111	0.00000095	-0.00000112	0.00000092	0.0000000	0.0000000
Pb	0.00000010	0.00000003	0.00000003	0.00000001		
Th	-0.00000495	0.0000174	-0.00000370	0.00001243	-0.0000011	0.0000015
U	-0.00000150	0.00000200	-0.00000111	0.00000139	0.0000002	0.0000001

Table A2 Complete data output from 'GLITTER' software package including U-Pb ratios and ages with 1σ uncertainties for both concordant (highlighted) and discordant analyses. If zircon grain was ejected during ablation, the analysis is excluded from this table.

Anal. #	$^{207}Pb/^{206}Pb$	1 σ	$^{207}Pb/^{235}U$	1 σ	$^{206}Pb/^{238}U$	1 σ	rho	$^{208}Pb/^{232}Th$	1 σ	$^{207}Pb/^{206}Pb$ Age (Ma)	1 σ	$^{207}Pb/^{235}U$ Age (Ma)	1 σ	$^{206}Pb/^{238}U$ Age (Ma)	1 σ	$^{208}Pb/^{232}Th$ Age (Ma)	1 σ
840W_017	0.0760	0.0014	1.7739	0.0473	0.1690	0.0021	0.475	0.0533	0.0010	1095.3	36.8	1036.0	17.3	1006.3	11.8	1049.9	18.2
840W_018	0.0809	0.0014	2.2294	0.0557	0.1931	0.0024	0.500	0.0510	0.0007	1219.7	33.4	1190.3	17.5	1137.9	13.0	1004.7	13.9
840W_019	0.0902	0.0019	2.9713	0.0986	0.2278	0.0030	0.393	0.0648	0.0012	1428.6	39.3	1400.3	25.2	1322.8	15.6	1268.6	22.1
840W_020	0.0804	0.0016	2.0126	0.0576	0.1823	0.0023	0.444	0.0491	0.0009	1206.3	38.0	1119.8	19.4	1079.4	12.6	968.4	18.2
840W_021	0.0981	0.0020	3.4893	0.1103	0.2432	0.0031	0.406	0.0735	0.0011	1589.0	36.7	1524.8	25.0	1403.1	16.2	1433.7	21.0
840W_022	0.0759	0.0029	1.6669	0.0927	0.1577	0.0025	0.279	0.0371	0.0009	1092.3	73.8	996.0	35.3	943.8	13.7	735.3	17.2
840W_023	0.0741	0.0015	1.6266	0.0477	0.1559	0.0020	0.433	0.0306	0.0006	1043.1	40.6	980.5	18.5	933.7	11.0	609.2	11.0
840W_024	0.0589	0.0017	0.5793	0.0214	0.0733	0.0010	0.366	0.0216	0.0004	564.7	61.9	464.0	13.8	456.2	6.0	431.0	8.1
840W_025	0.0895	0.0018	3.2274	0.0996	0.2491	0.0032	0.412	0.0716	0.0012	1415.6	38.2	1463.8	23.9	1433.8	16.3	1397.1	22.3
840W_026	0.0578	0.0017	0.5778	0.0214	0.0728	0.0010	0.364	0.0214	0.0004	520.3	61.7	463.0	13.7	453.2	5.9	427.4	7.9
840W_035	0.0735	0.0016	1.7620	0.0555	0.1784	0.0023	0.408	0.0499	0.0009	1026.9	43.3	1031.6	20.4	1058.3	12.5	984.7	17.3
840W_036	0.0787	0.0017	1.9383	0.0603	0.1705	0.0022	0.411	0.0438	0.0008	1164.9	41.5	1094.4	20.8	1015.0	12.0	866.5	15.8
840W_037	0.0789	0.0017	2.0342	0.0652	0.1846	0.0024	0.401	0.0496	0.0010	1168.9	42.3	1127.0	21.8	1091.8	12.9	978.7	18.4
840W_038	0.0770	0.0016	1.9867	0.0614	0.1826	0.0023	0.413	0.0555	0.0010	1119.8	41.6	1111.0	20.9	1080.9	12.7	1091.4	18.9
840W_039	0.0848	0.0020	2.4292	0.0885	0.2149	0.0028	0.363	0.0626	0.0012	1311.6	45.5	1251.3	26.2	1254.8	15.1	1227.1	22.0
840W_040	0.0731	0.0017	1.6499	0.0568	0.1620	0.0021	0.381	0.0489	0.0009	1016.3	47.5	989.5	21.8	967.7	11.8	965.2	18.2
840W_041	0.0775	0.0028	1.8361	0.1013	0.1662	0.0025	0.277	0.0483	0.0016	1134.0	70.9	1058.5	36.3	991.1	14.1	953.1	31.6
840W_042	0.0566	0.0015	0.5508	0.0187	0.0718	0.0009	0.386	0.0208	0.0004	474.7	56.4	445.5	12.3	446.8	5.7	416.4	7.8
840W_043	0.0775	0.0020	1.7525	0.0646	0.1643	0.0022	0.362	0.0511	0.0011	1134.0	49.4	1028.1	23.8	980.4	12.1	1007.4	21.6
840W_044	0.0750	0.0018	1.7157	0.0604	0.1652	0.0022	0.373	0.0499	0.0010	1068.0	48.2	1014.4	22.6	985.3	12.0	984.3	18.6
840W_053	0.0533	0.0024	0.5626	0.0315	0.0763	0.0012	0.279	0.0218	0.0005	343.1	99.0	453.2	20.5	474.3	7.1	436.5	10.5
840W_054	0.0795	0.0019	1.8628	0.0653	0.1743	0.0023	0.375	0.0533	0.0011	1183.7	45.4	1068.0	23.2	1035.6	12.6	1048.9	20.2
840W_055	0.0584	0.0021	0.5269	0.0242	0.0706	0.0010	0.318	0.0207	0.0005	546.3	77.4	429.8	16.1	439.9	6.2	415.0	9.5
840W_056	0.0706	0.0018	1.6427	0.0613	0.1774	0.0024	0.358	0.0482	0.0010	944.3	50.3	986.8	23.5	1053.0	13.0	950.5	18.3
840W_057	0.0777	0.0019	1.9474	0.0744	0.1824	0.0025	0.353	0.0546	0.0011	1138.4	48.9	1097.5	25.6	1079.9	13.4	1074.3	21.9
840W_058	0.0577	0.0016	0.5358	0.0201	0.0689	0.0009	0.364	0.0227	0.0005	518.2	59.0	435.7	13.3	429.4	5.6	454.5	9.6
840W_059	0.0909	0.0021	2.4306	0.0880	0.2021	0.0027	0.369	0.0537	0.0010	1443.9	44.0	1251.7	26.0	1186.8	14.5	1056.8	19.4
840W_060	0.0825	0.0022	2.0943	0.0861	0.1861	0.0026	0.337	0.0539	0.0012	1256.6	50.7	1146.9	28.2	1100.0	14.0	1060.5	22.8

Anal. #	$^{207}Pb/^{206}Pb$	1 σ	$^{207}Pb/^{235}U$	1 σ	$^{206}Pb/^{238}U$	1 σ	rho	$^{208}Pb/^{232}Th$	1 σ	$^{207}Pb/^{206}Pb$ Age (Ma)	1 σ	$^{207}Pb/^{235}U$ Age (Ma)	1 σ	$^{206}Pb/^{238}U$ Age (Ma)	1 σ	$^{208}Pb/^{232}Th$ Age (Ma)	1 σ
840W_061	0.0768	0.0022	1.7632	0.0762	0.1722	0.0024	0.327	0.0526	0.0013	1117.1	55.1	1032.0	28.0	1024.1	13.4	1036.3	25.5
840W_062	0.0733	0.0019	1.6960	0.0672	0.1775	0.0025	0.348	0.0435	0.0010	1021.6	51.2	1007.0	25.3	1053.5	13.4	860.5	18.8
840W_071	0.0580	0.0017	0.5504	0.0206	0.0709	0.0010	0.370	0.0164	0.0003	531.0	64.2	445.3	13.5	441.6	5.9	329.0	6.0
840W_072	0.0570	0.0019	0.5829	0.0238	0.0734	0.0010	0.347	0.0212	0.0004	489.3	71.1	466.3	15.2	456.8	6.2	423.8	8.1
840W_073	0.0722	0.0017	1.5958	0.0554	0.1699	0.0023	0.383	0.0518	0.0010	991.5	47.5	968.6	21.7	1011.6	12.4	1019.8	18.6
840W_074	0.0723	0.0017	1.6688	0.0586	0.1610	0.0021	0.379	0.0477	0.0010	993.1	47.6	996.7	22.3	962.3	11.9	941.3	18.4
840W_075	0.0721	0.0014	1.7461	0.0507	0.1717	0.0022	0.439	0.0502	0.0009	987.9	39.9	1025.7	18.8	1021.5	12.1	989.6	16.5
840W_076	0.0548	0.0015	0.5240	0.0182	0.0691	0.0009	0.387	0.0214	0.0004	405.6	58.1	427.8	12.2	430.7	5.6	428.5	7.5
840W_077	0.0899	0.0018	2.8162	0.0844	0.2312	0.0030	0.429	0.0607	0.0010	1423.4	37.2	1359.9	22.5	1340.9	15.5	1191.4	19.8
840W_078	0.0726	0.0015	1.8231	0.0560	0.1798	0.0023	0.420	0.0534	0.0009	1002.1	41.4	1053.8	20.2	1065.9	12.7	1051.3	18.0
840W_079	0.0810	0.0017	2.0778	0.0657	0.1873	0.0024	0.410	0.0584	0.0011	1222.1	40.8	1141.5	21.7	1106.7	13.2	1147.4	20.0
840W_080	0.0712	0.0016	1.7889	0.0620	0.1767	0.0023	0.382	0.0524	0.0010	961.8	46.4	1041.4	22.6	1048.7	12.8	1032.1	18.9
840W_089	0.0837	0.0017	2.5726	0.0784	0.2229	0.0028	0.418	0.0654	0.0011	1286.1	38.0	1292.9	22.3	1297.4	15.0	1280.3	21.1
840W_090	0.0575	0.0016	0.5675	0.0200	0.0719	0.0010	0.379	0.0228	0.0004	510.0	60.3	456.4	12.9	447.8	5.8	455.7	8.0
840W_091	0.0747	0.0015	1.8560	0.0563	0.1778	0.0023	0.419	0.0601	0.0012	1059.9	40.8	1065.6	20.0	1054.7	12.4	1178.7	22.9
840W_092	0.0647	0.0024	0.6076	0.0284	0.0718	0.0011	0.321	0.0223	0.0005	763.0	77.1	482.0	18.0	447.2	6.5	446.0	9.3
840W_093	0.0698	0.0015	1.6156	0.0488	0.1725	0.0022	0.420	0.0518	0.0009	921.4	42.0	976.3	18.9	1026.0	12.0	1020.0	17.1
840W_094	0.0552	0.0013	0.5179	0.0167	0.0691	0.0009	0.400	0.0175	0.0003	419.9	52.9	423.7	11.2	430.4	5.4	350.9	6.1
840W_095	0.0739	0.0017	1.7963	0.0625	0.1679	0.0022	0.375	0.0527	0.0010	1037.4	46.6	1044.1	22.7	1000.6	12.1	1037.5	19.8
840W_096	0.0774	0.0018	1.9149	0.0651	0.1756	0.0023	0.381	0.0555	0.0010	1131.7	44.7	1086.3	22.7	1042.6	12.5	1091.9	19.8
840W_097	0.0862	0.0019	2.4393	0.0817	0.1999	0.0026	0.384	0.0559	0.0010	1342.4	42.2	1254.3	24.1	1174.9	13.8	1098.9	19.2
840W_098	0.0903	0.0020	2.8180	0.0962	0.2154	0.0028	0.378	0.0603	0.0011	1432.3	42.2	1360.3	25.6	1257.5	14.7	1183.7	21.2
840W_107	0.0732	0.0014	1.7901	0.0502	0.1705	0.0021	0.445	0.0547	0.0010	1019.2	38.1	1041.9	18.3	1014.9	11.7	1077.1	18.2
840W_108	0.0769	0.0020	1.7783	0.0675	0.1695	0.0023	0.353	0.0530	0.0009	1118.1	50.0	1037.6	24.7	1009.6	12.5	1042.9	16.3
840W_109	0.0820	0.0015	2.0755	0.0565	0.1819	0.0023	0.458	0.0563	0.0009	1246.0	35.5	1140.7	18.7	1077.6	12.4	1107.3	17.4
840W_110	0.0760	0.0016	1.7392	0.0542	0.1638	0.0021	0.411	0.0501	0.0008	1094.3	41.8	1023.2	20.1	978.0	11.7	987.2	15.6
840W_111	0.0816	0.0018	2.1221	0.0718	0.1845	0.0024	0.386	0.0597	0.0011	1235.0	42.7	1156.0	23.4	1091.3	13.1	1172.5	20.3
840W_112	0.0793	0.0016	2.1722	0.0683	0.1967	0.0025	0.409	0.0591	0.0011	1179.7	40.4	1172.2	21.9	1157.7	13.6	1160.3	21.2
840W_113	0.0933	0.0018	3.2589	0.0972	0.2553	0.0033	0.428	0.0751	0.0012	1494.7	35.9	1471.3	23.2	1465.9	16.7	1463.0	22.4
840W_114	0.0589	0.0017	0.6134	0.0238	0.0717	0.0010	0.357	0.0222	0.0004	562.3	63.1	485.7	15.0	446.2	6.0	443.9	8.2
840W_115	0.0741	0.0017	1.7620	0.0614	0.1708	0.0023	0.382	0.0523	0.0010	1042.7	46.0	1031.6	22.6	1016.3	12.5	1029.3	19.3
840W_116	0.0558	0.0014	0.5493	0.0191	0.0706	0.0009	0.382	0.0195	0.0004	444.6	55.1	444.5	12.6	440.0	5.7	390.1	7.2
840W_125	0.1008	0.0018	3.6469	0.1036	0.2592	0.0033	0.447	0.0810	0.0012	1638.1	33.0	1559.8	22.7	1485.9	16.9	1574.7	22.1

Anal. #	$^{207}Pb/^{206}Pb$	1 σ	$^{207}Pb/^{235}U$	1 σ	$^{206}Pb/^{238}U$	1 σ	rho	$^{208}Pb/^{232}Th$	1 σ	$^{207}Pb/^{206}Pb$ Age (Ma)	1 σ	$^{207}Pb/^{235}U$ Age (Ma)	1 σ	$^{206}Pb/^{238}U$ Age (Ma)	1 σ	$^{208}Pb/^{232}Th$ Age (Ma)	1 σ
840W_126	0.0789	0.0016	2.1606	0.0639	0.1815	0.0023	0.432	0.0551	0.0009	1168.9	38.8	1168.5	20.5	1075.4	12.7	1083.4	17.7
840W_127	0.0827	0.0024	2.1476	0.0958	0.1813	0.0026	0.319	0.0606	0.0013	1261.3	55.0	1164.3	30.9	1073.9	14.1	1188.4	25.3
840W_129	0.0566	0.0016	0.5911	0.0206	0.0746	0.0010	0.386	0.0227	0.0004	475.2	59.7	471.6	13.1	463.6	6.0	454.2	8.1
840W_130	0.0746	0.0016	1.7421	0.0555	0.1673	0.0022	0.405	0.0478	0.0009	1056.7	43.8	1024.2	20.6	997.3	12.0	944.1	17.7
840W_131	0.0519	0.0012	0.5170	0.0155	0.0706	0.0009	0.426	0.0202	0.0003	279.9	51.4	423.1	10.4	439.4	5.4	403.5	6.7
840W_132	0.0749	0.0016	1.7415	0.0521	0.1645	0.0021	0.424	0.0513	0.0009	1065.0	41.1	1024.0	19.3	981.6	11.6	1011.2	18.1
840W_133	0.0780	0.0022	2.3188	0.1039	0.2142	0.0030	0.312	0.0600	0.0013	1147.5	55.7	1218.0	31.8	1251.0	15.9	1177.4	25.1
840W_134	0.0704	0.0016	1.7024	0.0542	0.1778	0.0023	0.403	0.0517	0.0010	940.6	44.4	1009.4	20.4	1055.1	12.5	1018.8	19.0
840W_144	0.0747	0.0014	2.0268	0.0608	0.1907	0.0028	0.492	0.0558	0.0010	1060.4	37.6	1124.6	20.4	1125.3	15.2	1098.3	19.3
840W_145	0.0795	0.0015	2.6554	0.0818	0.2461	0.0038	0.503	0.0629	0.0011	1184.7	35.8	1316.1	22.7	1418.1	19.7	1232.7	21.5
840W_146	0.0792	0.0018	2.1970	0.0827	0.2041	0.0034	0.445	0.0624	0.0014	1177.7	44.5	1180.1	26.3	1197.2	18.3	1222.9	26.5
840W_147	0.0949	0.0020	4.3514	0.1724	0.3412	0.0060	0.446	0.0985	0.0021	1525.2	39.6	1703.2	32.7	1892.5	29.0	1897.9	38.6
840W_148	0.0635	0.0021	0.9468	0.0459	0.1064	0.0021	0.403	0.0313	0.0008	724.2	67.8	676.4	23.9	651.6	12.1	623.8	15.9
840W_149	0.0622	0.0016	0.9864	0.0444	0.1130	0.0023	0.448	0.0352	0.0009	682.0	53.0	696.9	22.7	690.3	13.2	699.4	16.6
840W_150	0.1021	0.0022	6.4380	0.3170	0.4299	0.0093	0.437	0.1265	0.0033	1663.4	39.8	2037.5	43.3	2305.4	41.7	2407.1	58.4
840W_151	0.0653	0.0017	1.2965	0.0724	0.1364	0.0032	0.420	0.0438	0.0013	783.2	54.7	844.2	32.0	824.3	18.2	866.0	24.5
840W_152	0.0962	0.0024	5.3394	0.3400	0.3870	0.0099	0.401	0.1196	0.0038	1551.1	45.5	1875.2	54.5	2108.8	45.9	2283.2	69.3
840W_161	0.0770	0.0015	1.9158	0.0546	0.1612	0.0020	0.433	0.0494	0.0008	1121.9	37.9	1086.6	19.0	963.2	11.0	974.2	15.4
840W_162	0.1800	0.0031	13.1093	0.4939	0.4859	0.0061	0.335	0.1349	0.0020	2653.1	28.4	2687.6	35.5	2552.7	26.6	2557.8	35.5
840W_163	0.0620	0.0020	0.5914	0.0238	0.0724	0.0010	0.343	0.0232	0.0005	672.7	67.9	471.8	15.2	450.3	6.0	464.3	9.0
840W_164	0.0553	0.0014	0.5338	0.0175	0.0710	0.0009	0.391	0.0220	0.0004	425.1	56.0	434.4	11.6	442.3	5.5	439.1	7.2
840W_165	0.0522	0.0015	0.4775	0.0174	0.0657	0.0009	0.364	0.0215	0.0004	294.5	65.6	396.3	12.0	410.0	5.3	429.6	7.6
840W_166	0.0680	0.0018	1.5512	0.0614	0.1717	0.0023	0.337	0.0477	0.0010	869.4	54.8	951.0	24.5	1021.2	12.6	941.8	18.6
840W_167	0.0520	0.0014	0.5462	0.0186	0.0719	0.0009	0.380	0.0218	0.0004	287.3	59.1	442.5	12.2	447.5	5.6	436.6	8.0
840W_168	0.0829	0.0017	2.4423	0.0792	0.2183	0.0028	0.390	0.0597	0.0010	1266.5	40.4	1255.2	23.4	1272.7	14.6	1172.2	18.8
840W_169	0.0569	0.0013	0.4927	0.0149	0.0658	0.0008	0.418	0.0158	0.0003	488.5	48.7	406.7	10.1	410.9	5.0	316.7	5.2
840W_170	0.0725	0.0017	1.7340	0.0597	0.1768	0.0023	0.373	0.0528	0.0012	1000.9	46.2	1021.2	22.2	1049.4	12.5	1039.5	22.1
840W_179	0.0555	0.0012	0.5053	0.0135	0.0673	0.0008	0.467	0.0209	0.0003	432.1	45.9	415.3	9.1	420.0	5.1	418.9	6.5
840W_180	0.0560	0.0013	0.5499	0.0163	0.0679	0.0009	0.428	0.0204	0.0003	453.4	51.1	445.0	10.7	423.6	5.2	408.7	6.7
840W_181	0.0878	0.0017	2.7743	0.0857	0.2207	0.0028	0.408	0.0520	0.0008	1377.2	36.8	1348.6	23.1	1285.8	14.7	1025.0	16.0
840W_182	0.0807	0.0013	2.3739	0.0576	0.2082	0.0025	0.501	0.0590	0.0009	1213.4	32.0	1234.8	17.3	1219.2	13.5	1158.3	16.2
840W_183	0.0656	0.0023	1.5767	0.0826	0.1681	0.0025	0.282	0.0491	0.0011	792.8	72.2	961.1	32.5	1001.8	13.7	967.9	21.4
840W_184	0.0594	0.0032	0.7221	0.0489	0.0881	0.0015	0.258	0.0240	0.0008	583.3	114.0	551.9	28.9	544.1	9.1	478.3	16.2

Anal. #	$^{207}Pb/^{206}Pb$	1 σ	$^{207}Pb/^{235}U$	1 σ	$^{206}Pb/^{238}U$	1 σ	rho	$^{208}Pb/^{232}Th$	1 σ	$^{207}Pb/^{206}Pb$ Age (Ma)	1 σ	$^{207}Pb/^{235}U$ Age (Ma)	1 σ	$^{206}Pb/^{238}U$ Age (Ma)	1 σ	$^{208}Pb/^{232}Th$ Age (Ma)	1 σ
840W_185	0.0554	0.0012	0.5630	0.0153	0.0728	0.0009	0.460	0.0211	0.0003	426.7	45.1	453.5	9.9	453.2	5.5	422.5	6.3
840W_186	0.0595	0.0015	0.5809	0.0183	0.0722	0.0009	0.413	0.0214	0.0004	586.2	52.3	465.1	11.8	449.5	5.7	428.7	7.5
840W_187	0.0812	0.0017	2.3430	0.0743	0.2175	0.0028	0.404	0.0645	0.0010	1225.5	39.7	1225.4	22.6	1268.8	14.8	1264.1	19.1
840W_188	0.0702	0.0014	1.6821	0.0502	0.1726	0.0022	0.425	0.0520	0.0008	935.5	41.0	1001.8	19.0	1026.3	12.1	1023.9	16.1
840W_189	0.0766	0.0019	1.5717	0.0557	0.1441	0.0019	0.376	0.0465	0.0008	1111.0	47.5	959.1	22.0	867.6	10.8	919.5	15.7
Oh_017	0.0707	0.0013	1.6136	0.0420	0.1679	0.0020	0.467	0.0483	0.0008	947.3	37.2	975.5	16.3	1000.5	11.3	953.0	15.0
Oh_018	0.0756	0.0012	1.9510	0.0439	0.1823	0.0022	0.531	0.0337	0.0006	1085.0	31.6	1098.8	15.1	1079.6	11.9	669.3	12.4
Oh_019	0.0854	0.0019	2.6129	0.0955	0.2265	0.0029	0.354	0.0622	0.0012	1325.1	43.5	1304.3	26.8	1316.2	15.4	1219.2	22.3
Oh_020	0.0535	0.0012	0.5169	0.0144	0.0737	0.0009	0.444	0.0209	0.0003	351.8	50.0	423.1	9.6	458.4	5.5	418.2	6.0
Oh_021	0.0754	0.0012	1.7129	0.0387	0.1687	0.0020	0.530	0.0463	0.0006	1078.7	32.1	1013.4	14.5	1005.1	11.2	915.1	12.1
Oh_022	0.0783	0.0016	1.9481	0.0576	0.1927	0.0024	0.422	0.0544	0.0009	1155.6	39.2	1097.8	19.8	1135.8	13.0	1070.1	17.0
Oh_023	0.0764	0.0015	1.7378	0.0508	0.1716	0.0021	0.427	0.0519	0.0009	1105.9	39.8	1022.6	18.9	1020.7	11.8	1021.7	17.2
Oh_024	0.0572	0.0013	0.5431	0.0156	0.0709	0.0009	0.436	0.0196	0.0003	497.6	49.4	440.4	10.3	441.6	5.4	392.5	5.9
Oh_025	0.0891	0.0018	2.9081	0.0949	0.2323	0.0030	0.389	0.0604	0.0009	1405.4	38.9	1384.0	24.7	1346.5	15.4	1184.8	17.4
Oh_026	0.0720	0.0016	0.6938	0.0204	0.0682	0.0009	0.435	0.0237	0.0004	986.4	44.7	535.1	12.2	425.1	5.2	473.9	7.1
Oh_035	0.0588	0.0014	0.5745	0.0166	0.0699	0.0009	0.435	0.0209	0.0003	558.1	49.7	460.9	10.7	435.8	5.3	418.4	6.1
Oh_036	0.0855	0.0015	2.4236	0.0603	0.2095	0.0026	0.490	0.0346	0.0005	1326.8	32.5	1249.6	17.9	1226.1	13.6	687.5	9.7
Oh_038	0.0890	0.0015	2.8078	0.0686	0.2300	0.0028	0.496	0.0707	0.0010	1403.0	31.4	1357.6	18.3	1334.2	14.6	1381.2	18.2
Oh_039	0.0750	0.0013	1.8003	0.0462	0.1834	0.0022	0.476	0.0541	0.0009	1067.1	35.5	1045.6	16.7	1085.6	12.2	1064.3	16.6
Oh_040	0.1027	0.0017	3.9632	0.1014	0.2964	0.0036	0.476	0.0806	0.0012	1672.7	30.8	1626.7	20.7	1673.2	17.9	1566.0	22.0
Oh_041	0.0849	0.0017	2.9184	0.0928	0.2584	0.0033	0.396	0.0670	0.0011	1312.8	38.6	1386.7	24.0	1481.6	16.7	1310.7	21.4
Oh_042	0.0897	0.0016	3.0547	0.0829	0.2582	0.0032	0.453	0.0719	0.0011	1419.5	34.0	1421.4	20.8	1480.4	16.2	1404.0	20.5
Oh_043	0.0950	0.0018	3.2456	0.0962	0.2499	0.0031	0.420	0.0762	0.0012	1528.8	35.7	1468.1	23.0	1437.8	16.0	1484.5	22.9
Oh_044	0.1861	0.0033	12.9721	0.3858	0.5090	0.0063	0.415	0.1376	0.0021	2707.7	29.3	2677.6	28.0	2652.2	26.8	2604.8	37.2
Oh_053	0.0790	0.0013	2.2112	0.0547	0.1956	0.0024	0.492	0.0580	0.0009	1171.1	32.8	1184.6	17.3	1151.8	12.8	1140.0	16.2
Oh_054	0.0722	0.0014	1.5322	0.0413	0.1534	0.0019	0.460	0.0456	0.0011	992.7	37.8	943.4	16.6	920.0	10.6	902.1	21.3
Oh_055	0.0541	0.0013	0.5383	0.0161	0.0718	0.0009	0.423	0.0222	0.0003	374.4	52.6	437.3	10.7	446.8	5.5	442.8	6.8
Oh_056	0.0720	0.0014	1.6138	0.0437	0.1630	0.0020	0.458	0.0505	0.0007	984.7	37.6	975.6	17.0	973.3	11.2	996.1	14.1
Oh_057	0.0707	0.0013	1.6989	0.0438	0.1724	0.0021	0.477	0.0500	0.0007	948.0	35.9	1008.1	16.5	1025.5	11.7	985.2	14.3
Oh_058	0.0880	0.0029	3.0267	0.1776	0.2406	0.0037	0.260	0.0687	0.0018	1381.6	62.8	1414.4	44.8	1390.0	19.1	1342.4	33.4
Oh_059	0.0747	0.0014	1.8628	0.0524	0.1794	0.0022	0.444	0.0499	0.0008	1060.3	37.6	1068.0	18.6	1063.5	12.3	983.4	16.3
Oh_060	0.0844	0.0017	2.3925	0.0752	0.2121	0.0027	0.407	0.0552	0.0009	1300.6	39.1	1240.4	22.5	1240.1	14.4	1086.3	17.4
Oh_061	0.0747	0.0016	1.8029	0.0573	0.1689	0.0022	0.404	0.0495	0.0010	1059.9	42.0	1046.5	20.8	1006.1	12.0	975.9	18.3

Anal. #	$^{207}Pb/^{206}Pb$	1 σ	$^{207}Pb/^{235}U$	1 σ	$^{206}Pb/^{238}U$	1 σ	rho	$^{208}Pb/^{232}Th$	1 σ	$^{207}Pb/^{206}Pb$ Age (Ma)	1 σ	$^{207}Pb/^{235}U$ Age (Ma)	1 σ	$^{206}Pb/^{238}U$ Age (Ma)	1 σ	$^{208}Pb/^{232}Th$ Age (Ma)	1 σ
Oh_062	0.0755	0.0015	1.9088	0.0582	0.1734	0.0022	0.418	0.0504	0.0009	1083.0	39.9	1084.2	20.3	1031.1	12.1	993.5	16.9
Oh_071	0.0699	0.0018	1.7851	0.0671	0.1797	0.0024	0.354	0.0484	0.0010	924.3	51.0	1040.0	24.5	1065.1	13.1	954.4	19.3
Oh_072	0.0714	0.0013	1.6580	0.0415	0.1746	0.0022	0.494	0.0517	0.0008	968.3	35.6	992.6	15.9	1037.3	11.8	1019.1	14.7
Oh_073	0.0892	0.0016	3.1387	0.0900	0.2454	0.0031	0.437	0.0724	0.0010	1408.8	34.4	1442.2	22.1	1414.7	15.9	1413.3	18.9
Oh_074	0.0480	0.0013	0.5584	0.0186	0.0838	0.0011	0.391	0.0194	0.0003	96.0	62.9	450.5	12.1	518.7	6.5	387.8	6.0
Oh_075	0.0902	0.0020	2.8261	0.0985	0.2218	0.0029	0.374	0.0637	0.0011	1430.5	40.9	1362.5	26.1	1291.1	15.3	1248.8	20.6
Oh_076	0.0661	0.0014	1.7667	0.0542	0.1971	0.0025	0.414	0.0502	0.0009	810.8	43.2	1033.3	19.9	1159.8	13.5	990.6	17.1
Oh_077	0.0762	0.0016	2.0534	0.0644	0.1986	0.0025	0.408	0.0565	0.0009	1100.2	41.4	1133.4	21.4	1167.8	13.7	1110.4	17.5
Oh_078	0.0719	0.0020	1.7643	0.0718	0.1678	0.0023	0.335	0.0543	0.0012	984.4	54.4	1032.4	26.4	1000.1	12.6	1068.2	22.8
Oh_079	0.0720	0.0016	1.7337	0.0571	0.1653	0.0021	0.393	0.0506	0.0010	986.6	44.9	1021.1	21.2	986.2	11.8	997.5	18.7
Oh_080	0.0781	0.0019	1.8007	0.0645	0.1698	0.0023	0.370	0.0542	0.0009	1149.9	47.2	1045.7	23.4	1010.7	12.4	1067.6	18.0
Oh_089	0.0876	0.0014	2.6191	0.0625	0.2169	0.0026	0.510	0.0436	0.0007	1373.7	31.0	1306.0	17.5	1265.4	14.0	862.9	12.9
Oh_091	0.0752	0.0015	1.8127	0.0527	0.1761	0.0022	0.430	0.0515	0.0008	1073.0	39.4	1050.0	19.0	1045.6	12.1	1014.3	15.8
Oh_092	0.0785	0.0016	2.0001	0.0585	0.1782	0.0022	0.428	0.0513	0.0008	1159.6	38.7	1115.5	19.8	1057.3	12.2	1011.4	15.2
Oh_093	0.0846	0.0016	2.6028	0.0767	0.2254	0.0028	0.423	0.0632	0.0010	1305.8	37.1	1301.4	21.6	1310.2	14.8	1238.9	18.2
Oh_094	0.0748	0.0016	1.7095	0.0525	0.1700	0.0021	0.410	0.0527	0.0009	1064.0	41.8	1012.1	19.7	1011.9	11.8	1038.1	17.4
Oh_095	0.0578	0.0012	0.5493	0.0152	0.0679	0.0008	0.448	0.0201	0.0003	522.4	45.0	444.5	9.9	423.7	5.1	403.1	6.4
Oh_096	0.0627	0.0013	0.7269	0.0210	0.0853	0.0011	0.431	0.0222	0.0004	698.1	44.5	554.7	12.3	527.7	6.3	444.1	7.7
Oh_097	0.0863	0.0018	2.7589	0.0876	0.2331	0.0029	0.396	0.0650	0.0011	1345.8	39.7	1344.5	23.7	1350.5	15.3	1272.5	21.0
Oh_098	0.0731	0.0017	1.6196	0.0546	0.1624	0.0021	0.378	0.0495	0.0009	1016.9	46.2	977.8	21.2	969.9	11.5	976.6	18.0
Oh_107	0.0713	0.0012	1.5888	0.0397	0.1628	0.0020	0.489	0.0472	0.0007	967.3	35.1	965.8	15.6	972.0	11.1	931.5	13.8
Oh_109	0.0559	0.0012	0.5011	0.0142	0.0661	0.0008	0.449	0.0174	0.0003	449.4	47.1	412.4	9.6	412.4	5.1	349.6	5.3
Oh_110	0.0718	0.0013	1.5823	0.0419	0.1604	0.0020	0.471	0.0489	0.0008	980.9	36.4	963.3	16.5	958.8	11.1	964.0	14.7
Oh_111	0.0705	0.0013	1.7152	0.0461	0.1798	0.0023	0.466	0.0506	0.0007	941.5	36.8	1014.2	17.2	1065.7	12.3	996.8	14.2
Oh_112	0.0842	0.0017	2.7528	0.0844	0.2310	0.0030	0.418	0.0619	0.0011	1296.6	37.7	1342.8	22.8	1339.5	15.5	1214.4	20.2
Oh_113	0.0715	0.0014	1.6576	0.0495	0.1720	0.0022	0.431	0.0489	0.0009	971.8	40.1	992.4	18.9	1022.9	12.1	964.5	16.5
Oh_114	0.0715	0.0014	1.5820	0.0475	0.1608	0.0021	0.429	0.0347	0.0006	972.2	40.2	963.2	18.7	961.2	11.5	688.4	11.5
Oh_115	0.0861	0.0018	3.0170	0.0999	0.2446	0.0032	0.396	0.0692	0.0012	1339.2	39.7	1411.9	25.2	1410.6	16.6	1352.6	22.3
Oh_116	0.0760	0.0018	1.9194	0.0706	0.1828	0.0025	0.367	0.0536	0.0010	1096.2	46.8	1087.9	24.6	1082.1	13.5	1054.4	18.5
Oh_125	0.0865	0.0016	2.8194	0.0764	0.2348	0.0030	0.470	0.0695	0.0011	1348.3	34.2	1360.7	20.3	1359.7	15.6	1358.0	19.8
Oh_126	0.0884	0.0015	2.7839	0.0705	0.2313	0.0029	0.497	0.0489	0.0007	1391.3	32.4	1351.2	18.9	1341.3	15.2	965.4	13.5
Oh_127	0.0930	0.0017	3.1654	0.0885	0.2489	0.0032	0.456	0.0740	0.0011	1487.2	34.2	1448.8	21.6	1432.6	16.4	1443.1	21.1
Oh_129	0.0726	0.0015	1.7860	0.0535	0.1803	0.0023	0.429	0.0521	0.0009	1003.8	41.3	1040.4	19.5	1068.5	12.7	1026.0	16.4

Anal. #	$^{207}Pb/^{206}Pb$	1 σ	$^{207}Pb/^{235}U$	1 σ	$^{206}Pb/^{238}U$	1 σ	rho	$^{208}Pb/^{232}Th$	1 σ	$^{207}Pb/^{206}Pb$ Age (Ma)	1 σ	$^{207}Pb/^{235}U$ Age (Ma)	1 σ	$^{206}Pb/^{238}U$ Age (Ma)	1 σ	$^{208}Pb/^{232}Th$ Age (Ma)	1 σ
Oh_130	0.0837	0.0019	2.4508	0.0878	0.2086	0.0028	0.372	0.0682	0.0013	1285.6	44.5	1257.6	25.8	1221.6	14.8	1334.2	24.4
Oh_131	0.0910	0.0017	2.9759	0.0831	0.2353	0.0030	0.454	0.0594	0.0009	1447.0	35.5	1401.5	21.2	1362.0	15.5	1165.8	17.4
Oh_132	0.0737	0.0017	1.7786	0.0582	0.1734	0.0023	0.399	0.0483	0.0009	1034.0	44.6	1037.7	21.3	1030.5	12.4	953.1	17.0
Oh_133	0.0704	0.0014	1.7828	0.0527	0.1881	0.0024	0.432	0.0463	0.0008	940.2	41.4	1039.2	19.2	1110.9	13.0	914.0	15.3
Oh_134	0.0756	0.0017	1.8904	0.0639	0.1849	0.0024	0.388	0.0541	0.0010	1084.6	45.4	1077.7	22.4	1093.6	13.2	1065.2	19.3
Oh_143	0.0783	0.0027	2.6706	0.1575	0.2186	0.0033	0.257	0.0589	0.0015	1153.1	67.9	1320.3	43.6	1274.5	17.5	1157.6	29.0
Oh_144	0.0734	0.0013	1.7119	0.0425	0.1709	0.0021	0.498	0.0501	0.0007	1023.7	34.5	1013.0	15.9	1017.1	11.6	988.8	14.0
Oh_145	0.0788	0.0016	1.7829	0.0542	0.1681	0.0021	0.418	0.0553	0.0010	1168.0	40.7	1039.2	19.8	1001.8	11.8	1087.0	18.2
Oh_146	0.0723	0.0014	1.7669	0.0506	0.1820	0.0023	0.438	0.0500	0.0008	994.2	39.5	1033.4	18.6	1078.1	12.5	986.4	16.1
Oh_147	0.0543	0.0015	0.5489	0.0183	0.0737	0.0010	0.390	0.0217	0.0004	385.1	58.5	444.2	12.0	458.1	5.8	432.9	7.4
Oh_148	0.0831	0.0016	1.9106	0.0523	0.1689	0.0021	0.454	0.0319	0.0005	1271.1	36.2	1084.8	18.3	1006.0	11.6	634.7	10.7
Oh_149	0.0569	0.0014	0.5671	0.0184	0.0713	0.0009	0.398	0.0210	0.0003	485.4	54.8	456.1	11.9	443.8	5.6	420.1	6.7
Oh_150	0.0559	0.0012	0.5360	0.0157	0.0680	0.0009	0.432	0.0186	0.0003	447.2	48.2	435.8	10.4	423.9	5.2	372.9	6.1
Oh_151	0.0870	0.0021	2.7223	0.1020	0.2252	0.0030	0.351	0.0631	0.0011	1361.1	44.6	1334.6	27.8	1309.4	15.6	1236.2	20.7
Oh_152	0.0721	0.0016	1.4687	0.0479	0.1478	0.0019	0.392	0.0398	0.0008	989.1	45.3	917.6	19.7	888.4	10.6	788.7	14.5
Oh_161	0.0742	0.0014	1.8733	0.0534	0.1767	0.0022	0.439	0.0477	0.0007	1047.8	38.7	1071.7	18.9	1048.7	12.1	942.3	13.1
Oh_162	0.0713	0.0017	1.5664	0.0524	0.1631	0.0021	0.388	0.0469	0.0009	966.5	46.6	957.0	20.8	974.2	11.7	926.1	17.0
Oh_163	0.0559	0.0013	0.5717	0.0163	0.0731	0.0009	0.445	0.0203	0.0003	448.9	48.8	459.1	10.6	454.8	5.6	405.6	6.4
Oh_164	0.0842	0.0016	2.8399	0.0869	0.2374	0.0030	0.415	0.0724	0.0011	1296.7	37.3	1366.1	23.0	1372.9	15.7	1412.2	19.8
Oh_165	0.0894	0.0016	3.3549	0.0947	0.2621	0.0033	0.443	0.0746	0.0011	1413.1	34.0	1493.9	22.1	1500.6	16.8	1453.3	21.4
Oh_166	0.0811	0.0019	2.1429	0.0771	0.1944	0.0026	0.368	0.0543	0.0010	1224.2	45.3	1162.8	24.9	1144.9	13.9	1068.2	18.8
Oh_167	0.0740	0.0017	1.7990	0.0630	0.1667	0.0022	0.377	0.0473	0.0009	1040.3	46.6	1045.1	22.9	993.6	12.1	934.9	17.0
Oh_168	0.0852	0.0016	2.7175	0.0752	0.2233	0.0028	0.455	0.0571	0.0009	1319.8	35.1	1333.2	20.6	1299.2	14.8	1122.1	16.6
Oh_169	0.0763	0.0015	1.9905	0.0573	0.1811	0.0023	0.441	0.0453	0.0007	1103.3	38.1	1112.3	19.5	1073.1	12.6	895.4	14.3
Oh_170	0.0705	0.0015	1.6950	0.0551	0.1683	0.0022	0.400	0.0487	0.0008	943.3	44.2	1006.6	20.8	1002.9	12.1	961.2	16.2
Oh_179	0.0728	0.0023	1.8016	0.0842	0.1707	0.0025	0.311	0.0509	0.0012	1009.0	61.9	1046.0	30.5	1016.0	13.6	1003.1	23.2
Oh_180	0.0718	0.0014	1.6561	0.0447	0.1707	0.0022	0.473	0.0453	0.0008	980.0	37.9	991.9	17.1	1015.8	12.0	894.5	15.4
Oh_181	0.0771	0.0014	2.1062	0.0568	0.2085	0.0027	0.473	0.0602	0.0009	1123.6	35.8	1150.8	18.6	1220.7	14.2	1181.1	17.6
Oh_182	0.0848	0.0015	2.6806	0.0732	0.2220	0.0028	0.467	0.0593	0.0009	1310.9	34.2	1323.1	20.2	1292.6	14.9	1165.2	16.4
Oh_183	0.0771	0.0015	2.1478	0.0632	0.2033	0.0026	0.439	0.0549	0.0011	1123.6	38.5	1164.3	20.4	1193.1	14.1	1079.2	21.7
Oh_184	0.0565	0.0012	0.5364	0.0139	0.0692	0.0009	0.498	0.0164	0.0002	471.9	44.9	436.0	9.2	431.3	5.3	328.0	4.6
Oh_185	0.0746	0.0019	1.8080	0.0690	0.1783	0.0025	0.360	0.0504	0.0011	1058.1	50.8	1048.4	25.0	1057.4	13.4	993.1	20.2
Oh_186	0.0560	0.0014	0.5679	0.0181	0.0708	0.0009	0.416	0.0199	0.0003	451.3	55.8	456.6	11.8	440.7	5.7	397.9	6.2

Anal. #	$^{207}Pb/^{206}Pb$	1 σ	$^{207}Pb/^{235}U$	1 σ	$^{206}Pb/^{238}U$	1 σ	rho	$^{208}Pb/^{232}Th$	1 σ	$^{207}Pb/^{206}Pb$ Age (Ma)	1 σ	$^{207}Pb/^{235}U$ Age (Ma)	1 σ	$^{206}Pb/^{238}U$ Age (Ma)	1 σ	$^{208}Pb/^{232}Th$ Age (Ma)	1 σ
Oh_187	0.0531	0.0014	0.5382	0.0170	0.0714	0.0010	0.422	0.0215	0.0003	334.8	56.4	437.2	11.2	444.7	5.7	430.6	6.8
Oh_188	0.0729	0.0014	1.5218	0.0420	0.1591	0.0021	0.467	0.0392	0.0007	1010.0	38.8	939.2	16.9	952.0	11.4	777.0	13.2
Oh_189	0.0541	0.0014	0.5091	0.0161	0.0730	0.0010	0.420	0.0186	0.0003	374.1	56.0	417.8	10.8	454.5	5.9	373.0	5.9
Oh_190	0.0685	0.0013	1.5776	0.0436	0.1726	0.0022	0.466	0.0343	0.0006	884.7	39.3	961.4	17.2	1026.4	12.2	682.1	11.3
Oh_191	0.0755	0.0020	1.7994	0.0725	0.1837	0.0026	0.347	0.0525	0.0011	1082.2	52.9	1045.3	26.3	1087.4	14.0	1033.6	21.0
Oh_192	0.0721	0.0014	1.5924	0.0439	0.1639	0.0021	0.470	0.0477	0.0007	989.8	38.6	967.2	17.2	978.6	11.7	941.5	14.0
B1_017	0.0850	0.0014	1.5287	0.0334	0.1332	0.0016	0.556	0.0358	0.0005	1315.2	30.5	942.0	13.4	805.9	9.2	711.5	10.0
B1_018	0.0729	0.0013	1.8213	0.0472	0.1745	0.0022	0.478	0.0520	0.0009	1009.8	36.2	1053.2	17.0	1036.9	11.9	1025.0	16.7
B1_019	0.0799	0.0016	1.9715	0.0591	0.1768	0.0022	0.423	0.0463	0.0008	1195.1	39.7	1105.8	20.2	1049.4	12.3	915.0	15.6
B1_020	0.0705	0.0019	1.6047	0.0630	0.1584	0.0021	0.344	0.0466	0.0009	944.1	54.5	972.0	24.6	947.7	11.9	921.4	17.6
B1_021	0.0781	0.0013	2.0216	0.0481	0.1950	0.0024	0.513	0.0545	0.0009	1149.3	33.0	1122.8	16.2	1148.6	12.8	1072.5	16.3
B1_022	0.0796	0.0014	1.7120	0.0439	0.1529	0.0019	0.480	0.0436	0.0007	1186.3	35.4	1013.0	16.4	917.4	10.5	862.7	12.8
B1_023	0.0771	0.0019	1.7973	0.0646	0.1653	0.0022	0.365	0.0449	0.0008	1123.5	48.0	1044.5	23.5	986.1	12.0	888.0	14.9
B1_024	0.0965	0.0022	3.0808	0.1112	0.2217	0.0029	0.361	0.0721	0.0013	1557.5	41.6	1427.9	27.7	1290.9	15.3	1407.6	24.8
B1_025	0.0940	0.0018	2.9351	0.0804	0.2199	0.0027	0.450	0.0555	0.0009	1508.3	34.7	1391.0	20.8	1281.2	14.3	1092.2	16.6
B1_026	0.0716	0.0028	1.0123	0.0525	0.1018	0.0016	0.293	0.0292	0.0006	973.8	77.8	710.0	26.5	624.7	9.1	580.7	11.8
B1_035	0.0639	0.0021	0.3949	0.0154	0.0439	0.0006	0.361	0.0163	0.0004	737.6	69.1	337.9	11.2	277.2	3.8	326.0	7.2
B1_036	0.0790	0.0015	1.4191	0.0365	0.1342	0.0017	0.478	0.0378	0.0006	1170.8	36.0	897.0	15.3	811.9	9.4	749.5	11.4
B1_037	0.0560	0.0018	0.6314	0.0249	0.0787	0.0011	0.345	0.0212	0.0005	450.8	68.8	497.0	15.5	488.2	6.4	423.0	9.1
B1_038	0.0569	0.0014	0.5232	0.0163	0.0663	0.0009	0.411	0.0213	0.0004	486.1	53.6	427.3	10.9	414.0	5.2	426.3	7.3
B1_039	0.0913	0.0019	2.8462	0.0898	0.2353	0.0030	0.403	0.0687	0.0012	1453.5	38.2	1367.8	23.7	1362.0	15.6	1343.0	22.2
B1_040	0.0939	0.0021	2.3097	0.0776	0.1768	0.0023	0.387	0.0714	0.0013	1506.0	41.1	1215.3	23.8	1049.2	12.6	1393.2	25.0
B1_041	0.0954	0.0018	3.3406	0.0963	0.2578	0.0032	0.435	0.0814	0.0013	1535.5	35.1	1490.6	22.5	1478.4	16.6	1582.2	23.9
B1_042	0.0767	0.0019	1.7116	0.0609	0.1672	0.0022	0.372	0.0466	0.0009	1114.3	47.5	1012.9	22.8	996.7	12.2	920.8	17.2
B1_043	0.0752	0.0017	1.4742	0.0466	0.1508	0.0019	0.407	0.0337	0.0006	1072.7	43.5	919.8	19.1	905.5	10.9	669.1	11.7
B1_044	0.0756	0.0017	1.8764	0.0611	0.1895	0.0025	0.397	0.0501	0.0009	1084.4	43.6	1072.8	21.6	1118.8	13.3	987.4	17.3
B1_053	0.0917	0.0020	2.3744	0.0801	0.1940	0.0025	0.385	0.0525	0.0009	1461.7	40.8	1234.9	24.1	1143.2	13.6	1033.5	16.4
B1_054	0.0650	0.0017	0.6084	0.0201	0.0700	0.0009	0.398	0.0229	0.0004	775.1	54.3	482.6	12.7	435.9	5.6	457.9	7.7
B1_055	0.0740	0.0014	1.8372	0.0482	0.1703	0.0021	0.470	0.0523	0.0008	1041.8	36.3	1058.8	17.3	1013.9	11.6	1029.6	16.0
B1_056	0.0768	0.0014	1.7955	0.0453	0.1804	0.0022	0.485	0.0452	0.0007	1115.3	34.8	1043.8	16.5	1069.2	12.1	894.1	13.5
B1_057	0.0791	0.0017	1.0342	0.0305	0.1023	0.0013	0.431	0.0276	0.0005	1173.7	42.0	721.0	15.2	627.9	7.6	550.6	10.6
B1_058	0.0902	0.0018	3.0568	0.0978	0.2522	0.0032	0.394	0.0742	0.0013	1429.9	38.3	1421.9	24.5	1449.6	16.4	1446.5	23.5
B1_059	0.0691	0.0018	1.7082	0.0669	0.1733	0.0023	0.339	0.0464	0.0010	901.9	53.4	1011.6	25.1	1030.0	12.6	915.8	18.4

Anal. #	$^{207}Pb/^{206}Pb$	1 σ	$^{207}Pb/^{235}U$	1 σ	$^{206}Pb/^{238}U$	1 σ	rho	$^{208}Pb/^{232}Th$	1 σ	$^{207}Pb/^{206}Pb$ Age (Ma)	1 σ	$^{207}Pb/^{235}U$ Age (Ma)	1 σ	$^{206}Pb/^{238}U$ Age (Ma)	1 σ	$^{208}Pb/^{232}Th$ Age (Ma)	1 σ
B1_060	0.0744	0.0019	1.3300	0.0473	0.1400	0.0018	0.368	0.0392	0.0009	1051.2	49.5	858.9	20.6	844.4	10.4	776.4	18.3
B1_061	0.0775	0.0020	1.6796	0.0653	0.1565	0.0021	0.342	0.0500	0.0011	1134.5	51.6	1000.8	24.7	937.2	11.6	985.3	20.5
B1_062	0.0753	0.0022	1.7021	0.0754	0.1647	0.0023	0.312	0.0493	0.0013	1076.0	58.4	1009.3	28.3	983.0	12.6	973.3	24.3
B1_071	0.0807	0.0014	2.1148	0.0555	0.1887	0.0023	0.465	0.0490	0.0008	1214.2	34.7	1153.6	18.1	1114.3	12.5	966.8	15.2
B1_072	0.0783	0.0019	1.8157	0.0665	0.1680	0.0022	0.358	0.0507	0.0010	1153.5	47.8	1051.1	24.0	1000.9	12.2	999.8	20.0
B1_073	0.0762	0.0023	1.5934	0.0716	0.1536	0.0022	0.313	0.0391	0.0011	1099.5	60.0	967.6	28.0	921.0	12.1	774.3	21.9
B1_074	0.0827	0.0016	2.6044	0.0771	0.2215	0.0028	0.421	0.0616	0.0010	1261.5	37.2	1301.9	21.7	1289.6	14.6	1208.9	19.4
B1_075	0.0961	0.0019	1.4674	0.0414	0.1156	0.0015	0.445	0.0354	0.0008	1550.3	36.5	917.1	17.0	705.3	8.4	702.8	14.6
B1_076	0.0805	0.0020	1.9364	0.0726	0.1799	0.0024	0.353	0.0562	0.0013	1208.5	48.0	1093.8	25.1	1066.6	13.0	1105.8	25.4
B1_077	0.0879	0.0019	2.5996	0.0884	0.2237	0.0029	0.379	0.0609	0.0011	1380.3	41.3	1300.5	24.9	1301.3	15.2	1194.5	20.4
B1_078	0.0754	0.0021	1.5312	0.0615	0.1481	0.0020	0.338	0.0468	0.0011	1078.6	54.0	943.0	24.7	890.3	11.3	924.0	21.1
B1_079	0.0773	0.0018	1.9718	0.0672	0.1897	0.0025	0.379	0.0454	0.0009	1127.9	44.4	1105.9	23.0	1119.5	13.3	897.5	17.0
B1_080	0.0603	0.0021	0.6190	0.0280	0.0742	0.0011	0.319	0.0235	0.0005	614.4	73.9	489.2	17.6	461.1	6.4	468.8	10.3
B1_089	0.0713	0.0016	1.9058	0.0647	0.1774	0.0023	0.380	0.0500	0.0009	966.5	45.9	1083.1	22.6	1052.8	12.6	985.3	17.6
B1_090	0.0752	0.0015	1.9811	0.0563	0.1828	0.0023	0.441	0.0534	0.0009	1074.6	38.5	1109.1	19.2	1082.4	12.5	1050.6	16.8
B1_091	0.0802	0.0031	2.1981	0.1355	0.2087	0.0033	0.259	0.0592	0.0018	1200.6	74.3	1180.4	43.0	1221.7	17.8	1162.4	33.9
B1_092	0.0567	0.0022	0.5911	0.0276	0.0730	0.0011	0.314	0.0224	0.0005	480.2	82.3	471.6	17.6	453.9	6.4	447.2	9.3
B1_093	0.0796	0.0021	2.1781	0.0869	0.1999	0.0027	0.340	0.0564	0.0012	1186.5	50.2	1174.1	27.8	1175.0	14.6	1109.6	22.7
B1_094	0.0734	0.0029	1.4795	0.0842	0.1452	0.0023	0.276	0.0447	0.0013	1024.1	77.7	922.0	34.5	874.2	12.8	883.3	25.7
B1_095	0.0798	0.0018	2.2152	0.0750	0.2005	0.0026	0.384	0.0445	0.0010	1191.3	43.5	1185.9	23.7	1177.7	14.0	879.6	18.7
B1_096	0.0775	0.0020	1.9950	0.0800	0.1864	0.0025	0.340	0.0488	0.0011	1134.1	51.6	1113.8	27.1	1101.6	13.8	962.1	20.8
B1_097	0.0575	0.0015	0.5997	0.0210	0.0741	0.0010	0.382	0.0207	0.0004	511.2	57.5	477.0	13.3	460.9	5.9	413.2	7.7
B1_098	0.0952	0.0022	3.5168	0.1308	0.2760	0.0037	0.357	0.0753	0.0015	1531.0	42.8	1531.0	29.4	1571.1	18.5	1467.6	27.6
B1_107	0.0715	0.0013	1.6867	0.0427	0.1707	0.0021	0.487	0.0451	0.0007	970.7	35.8	1003.5	16.1	1015.7	11.6	890.6	12.6
B1_108	0.0707	0.0018	1.6461	0.0620	0.1635	0.0022	0.352	0.0480	0.0009	947.8	51.6	988.0	23.8	976.2	12.0	947.5	18.1
B1_109	0.0746	0.0015	1.9413	0.0580	0.1782	0.0022	0.421	0.0539	0.0009	1056.6	40.5	1095.4	20.0	1057.2	12.3	1061.5	17.3
B1_110	0.0582	0.0017	0.5197	0.0192	0.0685	0.0009	0.363	0.0158	0.0003	534.7	64.4	425.0	12.8	427.0	5.6	316.1	6.0
B1_111	0.0883	0.0019	2.3462	0.0762	0.1945	0.0025	0.393	0.0585	0.0011	1389.8	40.2	1226.4	23.1	1145.6	13.4	1148.4	20.1
B1_112	0.0869	0.0020	2.8422	0.1045	0.2456	0.0032	0.354	0.0626	0.0013	1357.6	43.6	1366.7	27.6	1415.5	16.6	1226.6	25.0
B1_113	0.0808	0.0024	2.3568	0.1127	0.2058	0.0029	0.295	0.0634	0.0013	1216.4	57.8	1229.6	34.1	1206.2	15.5	1241.9	24.5
B1_114	0.0864	0.0018	2.4967	0.0797	0.2054	0.0026	0.395	0.0567	0.0011	1346.7	40.2	1271.1	23.2	1204.3	13.9	1115.0	21.3
B1_116	0.0562	0.0050	0.0479	0.0044	0.0060	0.0001	0.255	0.0022	0.0001	458.6	186.8	47.5	4.2	38.8	0.9	44.6	2.3
B1_125	0.0551	0.0015	0.4748	0.0158	0.0670	0.0009	0.389	0.0175	0.0003	414.1	58.7	394.5	10.9	418.2	5.3	349.8	6.2

Anal. #	$^{207}Pb/^{206}Pb$	1 σ	$^{207}Pb/^{235}U$	1 σ	$^{206}Pb/^{238}U$	1 σ	rho	$^{208}Pb/^{232}Th$	1 σ	$^{207}Pb/^{206}Pb$ Age (Ma)	1 σ	$^{207}Pb/^{235}U$ Age (Ma)	1 σ	$^{206}Pb/^{238}U$ Age (Ma)	1 σ	$^{208}Pb/^{232}Th$ Age (Ma)	1 σ
B1_126	0.0600	0.0018	0.6015	0.0230	0.0716	0.0010	0.354	0.0221	0.0004	603.2	64.8	478.2	14.6	445.6	5.8	441.7	8.4
B1_127	0.0775	0.0016	1.6059	0.0490	0.1536	0.0019	0.412	0.0456	0.0014	1134.2	41.5	972.5	19.1	921.2	10.8	901.6	26.3
B1_128	0.0784	0.0016	1.8557	0.0574	0.1698	0.0021	0.407	0.0372	0.0007	1157.5	41.0	1065.5	20.4	1011.1	11.8	737.9	13.2
B1_129	0.0825	0.0018	1.6083	0.0518	0.1445	0.0018	0.396	0.0416	0.0008	1257.6	42.6	973.4	20.2	870.1	10.4	824.2	16.0
B1_130	0.0813	0.0021	2.4024	0.0984	0.2220	0.0030	0.327	0.0547	0.0012	1228.5	49.6	1243.3	29.4	1292.3	15.7	1075.9	22.0
B1_132	0.0600	0.0017	0.6357	0.0240	0.0757	0.0010	0.353	0.0244	0.0005	603.1	61.3	499.7	14.9	470.5	6.1	487.5	9.3
B1_133	0.0757	0.0018	1.8409	0.0666	0.1835	0.0024	0.360	0.0518	0.0011	1086.5	47.7	1060.2	23.8	1086.3	13.0	1021.2	20.9
B1_134	0.0768	0.0020	2.0295	0.0788	0.1927	0.0026	0.341	0.0562	0.0011	1116.1	50.1	1125.4	26.4	1136.0	13.8	1104.6	21.6
B1_143	0.0801	0.0025	1.9479	0.0940	0.1680	0.0024	0.296	0.0534	0.0012	1199.5	60.3	1097.7	32.4	1001.2	13.2	1050.5	22.5
B1_144	0.0710	0.0019	1.6335	0.0632	0.1649	0.0022	0.343	0.0476	0.0009	958.1	52.6	983.2	24.4	984.1	12.1	939.6	16.6
B1_145	0.0707	0.0015	1.6158	0.0501	0.1707	0.0022	0.406	0.0443	0.0009	949.9	43.0	976.4	19.5	1016.0	11.8	876.5	17.0
B1_146	0.1025	0.0018	4.2755	0.1154	0.3060	0.0038	0.454	0.0875	0.0014	1669.8	31.6	1688.7	22.2	1721.1	18.5	1695.1	25.6
B1_147	0.1812	0.0033	13.4655	0.5040	0.5351	0.0068	0.342	0.1383	0.0024	2664.0	30.0	2712.9	35.4	2763.0	28.7	2617.4	43.1
B1_148	0.0577	0.0014	0.6011	0.0192	0.0759	0.0010	0.405	0.0226	0.0004	519.3	52.4	478.0	12.2	471.4	5.9	452.3	7.7
B1_149	0.0755	0.0015	1.7990	0.0511	0.1703	0.0021	0.441	0.0525	0.0009	1082.2	38.1	1045.1	18.5	1013.9	11.7	1034.8	16.8
B1_150	0.0731	0.0014	1.8330	0.0526	0.1781	0.0022	0.438	0.0559	0.0012	1017.9	38.4	1057.4	18.8	1056.8	12.2	1098.7	22.3
B1_151	0.0714	0.0015	1.6970	0.0538	0.1736	0.0022	0.406	0.0502	0.0008	969.4	42.8	1007.4	20.2	1031.7	12.2	989.0	16.1
B1_152	0.0737	0.0015	1.7267	0.0537	0.1766	0.0023	0.411	0.0497	0.0009	1033.5	41.5	1018.5	20.0	1048.5	12.4	980.2	18.0
B1_161	0.0556	0.0013	0.5860	0.0176	0.0751	0.0010	0.425	0.0209	0.0003	436.7	51.3	468.3	11.3	466.8	5.7	418.9	6.6
B1_162	0.0852	0.0015	2.6211	0.0693	0.2166	0.0027	0.466	0.0654	0.0010	1320.0	33.7	1306.6	19.4	1263.9	14.1	1280.4	19.5
B1_163	0.0749	0.0017	1.8868	0.0656	0.1783	0.0023	0.375	0.0558	0.0010	1065.1	45.7	1076.4	23.1	1057.4	12.7	1096.5	18.3
B1_164	0.0861	0.0019	2.9022	0.1064	0.2383	0.0031	0.356	0.0719	0.0012	1340.3	42.8	1382.5	27.7	1377.7	16.2	1403.0	23.1
B1_165	0.0747	0.0017	2.2167	0.0784	0.2106	0.0027	0.367	0.0595	0.0010	1058.9	45.6	1186.3	24.7	1232.0	14.5	1167.7	19.9
B1_166	0.0734	0.0014	1.7544	0.0479	0.1765	0.0022	0.452	0.0509	0.0008	1023.7	37.4	1028.8	17.7	1047.9	12.0	1004.2	16.0
B1_167	0.0538	0.0016	0.5830	0.0218	0.0805	0.0011	0.356	0.0254	0.0005	361.5	64.0	466.4	14.0	499.4	6.4	507.3	10.3
B1_168	0.0762	0.0017	1.8139	0.0586	0.1735	0.0022	0.394	0.0523	0.0009	1101.3	42.8	1050.5	21.2	1031.3	12.2	1029.8	18.0
B1_169	0.0585	0.0022	0.6185	0.0301	0.0772	0.0011	0.303	0.0217	0.0005	549.9	81.5	488.9	18.9	479.5	6.8	433.2	9.3
B1_179	0.0563	0.0020	0.5531	0.0235	0.0714	0.0010	0.333	0.0206	0.0004	461.6	76.5	447.0	15.4	444.5	6.1	411.9	8.3
B1_180	0.0560	0.0017	0.5221	0.0190	0.0686	0.0009	0.368	0.0202	0.0005	451.2	65.8	426.6	12.7	427.7	5.6	404.5	9.7
B1_181	0.0594	0.0026	0.5477	0.0285	0.0650	0.0010	0.299	0.0212	0.0005	581.6	91.5	443.5	18.7	405.8	6.1	424.2	10.4
B1_182	0.0733	0.0014	1.7152	0.0456	0.1688	0.0021	0.463	0.0500	0.0008	1023.4	37.0	1014.2	17.1	1005.7	11.5	986.9	15.1
B1_183	0.0736	0.0016	1.6318	0.0497	0.1623	0.0021	0.414	0.0508	0.0008	1031.4	42.0	982.5	19.2	969.8	11.4	1002.1	15.5
B1_184	0.0806	0.0017	1.2374	0.0349	0.1072	0.0014	0.447	0.0480	0.0010	1211.4	39.9	817.7	15.8	656.4	7.9	947.9	18.9

Anal. #	$^{207}Pb/^{206}Pb$	1 σ	$^{207}Pb/^{235}U$	1 σ	$^{206}Pb/^{238}U$	1 σ	rho	$^{208}Pb/^{232}Th$	1 σ	$^{207}Pb/^{206}Pb$ Age (Ma)	1 σ	$^{207}Pb/^{235}U$ Age (Ma)	1 σ	$^{206}Pb/^{238}U$ Age (Ma)	1 σ	$^{208}Pb/^{232}Th$ Age (Ma)	1 σ
B1_185	0.0592	0.0012	0.5412	0.0138	0.0686	0.0009	0.485	0.0218	0.0003	575.7	43.4	439.2	9.1	427.8	5.1	436.3	6.1
B1_186	0.0783	0.0014	2.2876	0.0598	0.2092	0.0026	0.468	0.0642	0.0010	1154.9	34.5	1208.5	18.5	1224.5	13.7	1258.2	18.3
B1_187	0.0814	0.0020	2.1468	0.0832	0.1939	0.0026	0.344	0.0601	0.0011	1232.1	48.0	1164.0	26.8	1142.3	14.0	1179.5	20.4
B1_188	0.0592	0.0017	0.5691	0.0200	0.0682	0.0009	0.379	0.0220	0.0004	576.1	60.6	457.4	13.0	425.0	5.5	440.0	7.3
B1_189	0.0593	0.0038	0.6252	0.0488	0.0829	0.0016	0.246	0.0219	0.0010	576.2	134.5	493.1	30.5	513.4	9.5	437.3	20.6
B1_190	0.0751	0.0013	1.8390	0.0456	0.1832	0.0022	0.491	0.0540	0.0008	1072.3	34.3	1059.5	16.3	1084.3	12.2	1062.9	16.0
B1_191	0.0822	0.0019	2.6943	0.0978	0.2475	0.0032	0.357	0.0690	0.0012	1250.1	43.4	1326.9	26.9	1425.5	16.6	1348.2	22.3
B2_017	0.0502	0.0051	0.0348	0.0035	0.0051	0.0001	0.250	0.0016	0.0001	204.3	219.7	34.7	3.5	33.0	0.8	31.8	1.5
B2_018	0.0885	0.0019	1.9285	0.0602	0.1618	0.0020	0.396	0.0373	0.0007	1392.3	39.4	1091.0	20.9	966.9	11.1	740.4	14.1
B2_019	0.0550	0.0014	0.4871	0.0155	0.0632	0.0008	0.392	0.0221	0.0004	411.6	57.0	402.9	10.6	395.2	4.8	441.6	7.9
B2_020	0.0535	0.0013	0.4457	0.0128	0.0618	0.0008	0.422	0.0128	0.0003	348.9	52.6	374.3	9.0	386.8	4.6	256.5	5.4
B2_021	0.0863	0.0021	2.7574	0.1100	0.2353	0.0030	0.323	0.0673	0.0012	1345.5	45.5	1344.1	29.7	1362.0	15.8	1316.1	22.0
B2_022	0.0654	0.0014	1.5156	0.0478	0.1652	0.0020	0.388	0.0462	0.0010	788.4	45.1	936.7	19.3	985.4	11.2	912.8	19.9
B2_023	0.0978	0.0018	2.8920	0.0810	0.2095	0.0025	0.426	0.0478	0.0008	1582.0	33.3	1379.8	21.1	1225.9	13.3	943.1	14.8
B2_024	0.0950	0.0026	2.7307	0.1259	0.2162	0.0030	0.296	0.0485	0.0009	1527.1	50.6	1336.8	34.3	1261.5	15.6	956.6	17.6
B2_026	0.0537	0.0016	0.3856	0.0138	0.0546	0.0007	0.360	0.0158	0.0004	360.2	64.9	331.2	10.1	342.4	4.3	317.7	7.7
B2_035	0.0817	0.0016	2.2073	0.0677	0.1955	0.0024	0.395	0.0456	0.0007	1238.1	38.4	1183.4	21.4	1151.2	12.8	900.6	14.4
B2_036	0.0581	0.0064	1.4624	0.2307	0.1637	0.0046	0.176	0.0530	0.0055	533.4	226.4	915.0	95.1	977.1	25.2	1044.2	105.3
B2_037	0.0866	0.0019	2.7914	0.1043	0.2292	0.0029	0.337	0.0621	0.0011	1351.1	42.7	1353.2	27.9	1330.3	15.2	1217.0	20.2
B2_038	0.0570	0.0020	0.5068	0.0214	0.0669	0.0009	0.325	0.0165	0.0003	490.3	75.3	416.3	14.4	417.7	5.5	331.5	6.3
B2_039	0.1879	0.0037	11.1021	0.5095	0.4759	0.0062	0.285	0.1201	0.0019	2723.5	32.2	2531.7	42.8	2509.3	27.2	2292.5	33.9
B2_040	0.0881	0.0015	2.6555	0.0703	0.2224	0.0026	0.447	0.0595	0.0010	1385.1	33.1	1316.2	19.5	1294.5	13.9	1168.5	19.0
B2_041	0.1081	0.0021	3.1847	0.1007	0.2175	0.0027	0.388	0.0614	0.0010	1766.9	35.3	1453.5	24.4	1268.4	14.1	1203.5	18.8
B2_042	0.0739	0.0018	1.4668	0.0515	0.1514	0.0019	0.361	0.0426	0.0008	1039.7	47.7	916.8	21.2	908.9	10.7	842.5	14.9
B2_043	0.0819	0.0019	1.2353	0.0407	0.1040	0.0013	0.383	0.0149	0.0003	1242.2	44.3	816.8	18.5	638.0	7.6	298.3	6.0
B2_044	0.0492	0.0038	0.0813	0.0065	0.0116	0.0002	0.247	0.0029	0.0002	157.9	171.7	79.4	6.1	74.2	1.5	58.8	3.2
B2_053	0.0851	0.0023	2.5568	0.1144	0.2229	0.0030	0.299	0.0685	0.0013	1317.2	51.2	1288.4	32.7	1296.9	15.7	1338.8	24.7
B2_055	0.0597	0.0018	0.6675	0.0257	0.0809	0.0011	0.344	0.0243	0.0004	593.5	64.5	519.2	15.6	501.7	6.4	484.7	8.2
B2_057	0.0738	0.0014	1.3319	0.0344	0.1313	0.0016	0.457	0.0248	0.0004	1035.9	36.8	859.7	15.0	795.3	8.8	495.6	7.8
B2_058	0.0539	0.0044	0.0670	0.0056	0.0088	0.0002	0.258	0.0027	0.0001	367.0	174.8	65.8	5.3	56.5	1.2	55.3	2.0
B2_059	0.0548	0.0027	0.1873	0.0101	0.0260	0.0004	0.293	0.0082	0.0002	404.8	106.7	174.3	8.6	165.2	2.6	164.4	4.2
B2_062	0.0797	0.0020	2.2350	0.0861	0.2000	0.0026	0.331	0.0483	0.0009	1188.5	47.5	1192.1	27.0	1175.2	13.7	953.0	17.0
B2_071	0.0575	0.0017	0.5428	0.0198	0.0642	0.0008	0.354	0.0187	0.0003	510.1	64.9	440.3	13.1	401.1	5.1	373.8	6.6

Anal. #	$^{207}Pb/^{206}Pb$	1 σ	$^{207}Pb/^{235}U$	1 σ	$^{206}Pb/^{238}U$	1 σ	rho	$^{208}Pb/^{232}Th$	1 σ	$^{207}Pb/^{206}Pb$ Age (Ma)	1 σ	$^{207}Pb/^{235}U$ Age (Ma)	1 σ	$^{206}Pb/^{238}U$ Age (Ma)	1 σ	$^{208}Pb/^{232}Th$ Age (Ma)	1 σ
B2_072	0.0800	0.0017	1.3402	0.0398	0.1208	0.0015	0.412	0.0123	0.0003	1197.7	41.2	863.3	17.3	735.3	8.5	246.9	5.3
B2_073	0.0790	0.0016	1.8396	0.0569	0.1532	0.0019	0.397	0.0460	0.0008	1171.7	40.6	1059.7	20.3	918.6	10.5	908.7	15.4
B2_074	0.1071	0.0019	3.0880	0.0893	0.2076	0.0025	0.418	0.0733	0.0013	1750.7	32.8	1429.7	22.2	1215.9	13.4	1429.1	23.8
B2_075	0.0577	0.0055	0.1016	0.0100	0.0122	0.0003	0.251	0.0041	0.0002	517.0	198.0	98.3	9.2	78.0	1.9	82.8	3.2
B2_076	0.0454	0.0053	0.0959	0.0114	0.0162	0.0004	0.222	0.0055	0.0004	0.1	225.4	93.0	10.6	103.9	2.7	111.2	7.2
B2_077	0.0725	0.0018	1.4290	0.0523	0.1472	0.0019	0.353	0.0250	0.0009	1000.0	50.5	901.1	21.9	885.1	10.7	499.9	16.9
B2_078	0.0787	0.0017	1.7554	0.0551	0.1615	0.0020	0.396	0.0400	0.0008	1164.1	41.4	1029.1	20.3	965.3	11.1	793.1	15.3
B2_079	0.0454	0.0044	0.0714	0.0071	0.0117	0.0003	0.231	0.0042	0.0002	0.1	188.1	70.1	6.8	75.0	1.7	85.5	3.7
B2_080	0.0707	0.0018	1.3422	0.0501	0.1390	0.0018	0.351	0.0085	0.0004	948.4	52.1	864.2	21.7	839.0	10.3	170.7	7.4
B2_089	0.0836	0.0017	2.4153	0.0769	0.2155	0.0027	0.392	0.0584	0.0010	1283.6	39.2	1247.1	22.9	1257.8	14.3	1147.6	18.3
B2_090	0.0925	0.0017	2.9860	0.0884	0.2500	0.0031	0.416	0.0704	0.0012	1478.3	34.7	1404.1	22.5	1438.6	15.9	1374.6	22.9
B2_091	0.0966	0.0022	2.2067	0.0791	0.1645	0.0022	0.365	0.0667	0.0012	1559.9	42.8	1183.2	25.1	981.8	11.9	1305.4	21.8
B2_092	0.0528	0.0013	0.2889	0.0086	0.0419	0.0005	0.425	0.0113	0.0002	318.4	56.3	257.7	6.8	264.4	3.3	226.2	4.6
B2_093	0.0557	0.0014	0.4183	0.0126	0.0549	0.0007	0.416	0.0094	0.0002	440.8	53.9	354.9	9.1	344.4	4.2	189.8	4.4
B2_094	0.0610	0.0013	0.4805	0.0130	0.0588	0.0007	0.459	0.0133	0.0002	639.1	45.2	398.4	8.9	368.4	4.4	267.1	3.9
B2_095	0.0664	0.0027	0.3801	0.0180	0.0414	0.0006	0.321	0.0142	0.0003	820.4	83.1	327.1	13.2	261.4	3.9	284.4	6.0
B2_096	0.0867	0.0030	2.7199	0.1639	0.2309	0.0036	0.255	0.0623	0.0017	1353.4	66.1	1333.9	44.7	1339.4	18.6	1222.1	31.3
B2_097	0.0699	0.0018	0.7991	0.0277	0.0834	0.0011	0.380	0.0230	0.0004	924.3	52.9	596.3	15.7	516.6	6.5	460.3	8.7
B2_098	0.0355	0.0050	0.0804	0.0115	0.0163	0.0005	0.197	0.0051	0.0002	0.1	0.0	78.5	10.8	104.3	2.9	102.8	4.8
B2_107	0.0644	0.0076	0.1072	0.0128	0.0118	0.0004	0.256	0.0034	0.0003	754.2	230.0	103.4	11.8	75.4	2.3	69.5	6.0
B2_108	0.0838	0.0015	2.5835	0.0724	0.2279	0.0028	0.434	0.0656	0.0010	1287.1	35.1	1296.0	20.5	1323.5	14.6	1283.9	19.2
B2_109	0.0608	0.0015	0.7781	0.0240	0.0915	0.0012	0.408	0.0243	0.0004	630.5	50.5	584.4	13.7	564.2	6.8	485.9	7.4
B2_110	0.1915	0.0032	11.7329	0.3810	0.4507	0.0055	0.378	0.1106	0.0018	2754.9	26.8	2583.3	30.4	2398.5	24.6	2119.8	33.3
B2_111	0.0614	0.0018	0.4429	0.0160	0.0532	0.0007	0.370	0.0117	0.0003	654.3	63.1	372.3	11.3	334.4	4.3	236.0	5.8
B2_112	0.0822	0.0014	2.2146	0.0546	0.2013	0.0024	0.484	0.0484	0.0007	1250.6	32.8	1185.7	17.2	1182.4	12.9	955.0	13.9
B2_113	0.0852	0.0016	2.3465	0.0634	0.2010	0.0024	0.445	0.0533	0.0008	1319.0	35.0	1226.5	19.3	1180.5	13.0	1050.2	15.4
B2_114	0.0769	0.0019	1.9897	0.0761	0.1906	0.0025	0.339	0.0523	0.0009	1118.5	49.2	1112.0	25.8	1124.5	13.4	1030.0	16.7
B2_115	0.0820	0.0024	1.6161	0.0700	0.1474	0.0020	0.316	0.0332	0.0008	1244.8	56.4	976.5	27.2	886.5	11.4	660.5	16.4
B2_116	0.0732	0.0015	1.7524	0.0525	0.1767	0.0022	0.408	0.0511	0.0009	1018.4	40.7	1028.0	19.4	1048.9	11.8	1007.8	16.4
B2_125	0.0745	0.0020	1.7611	0.0687	0.1793	0.0024	0.336	0.0520	0.0011	1055.1	52.2	1031.2	25.3	1063.1	12.8	1024.6	20.4
B2_126	0.1145	0.0021	4.6831	0.1498	0.2911	0.0036	0.384	0.0740	0.0012	1871.4	33.0	1764.2	26.8	1647.1	17.9	1442.0	23.3
B2_127	0.0518	0.0066	0.0333	0.0042	0.0046	0.0001	0.220	0.0014	0.0001	277.9	268.9	33.3	4.2	29.8	0.9	27.4	1.6
B2_128	0.0971	0.0019	3.2758	0.1067	0.2418	0.0030	0.381	0.0532	0.0010	1568.4	37.0	1475.3	25.3	1396.1	15.6	1047.4	18.8

Anal. #	$^{207}Pb/^{206}Pb$	1 σ	$^{207}Pb/^{235}U$	1 σ	$^{206}Pb/^{238}U$	1 σ	rho	$^{208}Pb/^{232}Th$	1 σ	$^{207}Pb/^{206}Pb$ Age (Ma)	1 σ	$^{207}Pb/^{235}U$ Age (Ma)	1 σ	$^{206}Pb/^{238}U$ Age (Ma)	1 σ	$^{208}Pb/^{232}Th$ Age (Ma)	1 σ
B2_130	0.0669	0.0034	0.3523	0.0206	0.0356	0.0006	0.294	0.0082	0.0003	833.9	103.5	306.5	15.5	225.3	3.8	165.5	5.0
B2_132	0.0552	0.0024	0.4491	0.0236	0.0587	0.0009	0.289	0.0184	0.0005	419.0	95.4	376.7	16.5	367.4	5.4	368.6	9.4
B2_133	0.0512	0.0061	0.0775	0.0094	0.0102	0.0003	0.228	0.0034	0.0002	250.1	252.1	75.8	8.8	65.2	1.8	68.2	3.0
B2_134	0.0564	0.0018	0.4891	0.0195	0.0607	0.0008	0.340	0.0177	0.0004	467.6	68.9	404.3	13.3	379.8	5.0	354.4	7.6
B2_143	0.0561	0.0030	0.4170	0.0256	0.0514	0.0009	0.270	0.0128	0.0005	457.7	114.2	353.9	18.3	323.1	5.2	257.4	9.5
B2_144	0.0647	0.0014	0.6627	0.0188	0.0772	0.0010	0.434	0.0201	0.0003	764.0	46.3	516.3	11.5	479.4	5.7	401.3	6.4
B2_145	0.0750	0.0028	0.3478	0.0148	0.0317	0.0005	0.348	0.0271	0.0006	1069.7	72.9	303.1	11.1	201.4	2.9	540.1	11.7
B2_146	0.0519	0.0052	0.0383	0.0039	0.0058	0.0001	0.242	0.0017	0.0001	281.5	214.4	38.1	3.8	36.9	0.9	34.0	2.3
B2_147	0.0751	0.0029	1.5899	0.0922	0.1562	0.0024	0.265	0.0483	0.0015	1070.7	76.6	966.3	36.2	935.6	13.4	952.5	29.7
B2_149	0.1118	0.0020	2.8682	0.0778	0.1896	0.0023	0.442	0.0416	0.0007	1828.2	32.4	1373.6	20.4	1119.1	12.3	824.6	13.6
B2_150	0.0606	0.0050	0.0898	0.0076	0.0108	0.0002	0.264	0.0036	0.0002	623.1	167.6	87.3	7.0	69.4	1.6	72.9	4.3
B2_151	0.0549	0.0017	0.3930	0.0150	0.0526	0.0007	0.348	0.0123	0.0003	406.0	68.3	336.6	10.9	330.7	4.3	247.0	6.4
B2_152	0.0572	0.0035	0.4224	0.0296	0.0596	0.0011	0.256	0.0289	0.0017	498.5	128.0	357.8	21.1	373.2	6.5	576.6	33.2
B2_162	0.0574	0.0044	0.0756	0.0059	0.0101	0.0002	0.269	0.0028	0.0001	507.3	159.8	74.0	5.5	64.5	1.4	55.5	2.7
B2_164	0.0744	0.0018	1.6323	0.0575	0.1557	0.0020	0.361	0.0443	0.0009	1052.3	47.7	982.7	22.2	933.0	11.1	875.2	16.7
B2_165	0.0518	0.0057	0.0706	0.0079	0.0100	0.0003	0.241	0.0037	0.0003	277.2	235.4	69.2	7.5	64.0	1.7	74.2	5.4
B2_166	0.0754	0.0020	1.5877	0.0618	0.1476	0.0019	0.338	0.0292	0.0005	1078.9	52.3	965.4	24.3	887.7	10.9	580.9	10.4
B2_168	0.0721	0.0020	1.6762	0.0697	0.1620	0.0022	0.319	0.0472	0.0010	989.9	55.6	999.5	26.4	967.8	12.0	932.7	19.6
B2_169	0.0874	0.0019	2.5553	0.0887	0.2126	0.0027	0.363	0.0664	0.0013	1370.0	41.7	1287.9	25.3	1242.5	14.2	1299.4	24.4
B2_170	0.0884	0.0021	2.5408	0.0959	0.2113	0.0027	0.341	0.0615	0.0012	1391.5	44.7	1283.8	27.5	1235.6	14.5	1206.7	22.9
B2_179	0.0782	0.0024	2.0722	0.0999	0.1872	0.0026	0.289	0.0519	0.0009	1152.7	59.3	1139.7	33.0	1106.2	14.2	1021.9	18.1
B2_180	0.0884	0.0015	2.7516	0.0742	0.2231	0.0027	0.444	0.0556	0.0008	1390.1	33.0	1342.5	20.1	1298.1	14.1	1093.4	15.5
B2_181	0.0795	0.0014	1.2640	0.0307	0.1139	0.0014	0.492	0.0336	0.0005	1184.0	34.7	829.7	13.8	695.2	7.9	668.5	9.1
B2_182	0.0867	0.0016	2.3727	0.0655	0.1955	0.0024	0.437	0.0394	0.0006	1353.1	34.7	1234.4	19.7	1151.0	12.7	780.6	12.2
B2_183	0.0757	0.0014	1.5959	0.0426	0.1526	0.0018	0.451	0.0499	0.0008	1086.4	37.1	968.6	16.7	915.7	10.3	984.7	15.7
B2_184	0.0730	0.0018	1.5750	0.0563	0.1670	0.0021	0.358	0.0457	0.0010	1015.0	49.0	960.4	22.2	995.8	11.8	902.7	19.6
B2_185	0.0784	0.0014	2.0287	0.0536	0.1769	0.0021	0.453	0.0429	0.0007	1156.1	35.2	1125.2	18.0	1049.8	11.6	848.2	13.5
B2_186	0.0864	0.0014	2.6979	0.0643	0.2155	0.0025	0.494	0.0591	0.0008	1347.7	30.7	1327.9	17.7	1257.9	13.5	1160.8	15.1
B2_187	0.0880	0.0015	2.4650	0.0610	0.2111	0.0025	0.480	0.0503	0.0008	1383.0	31.7	1261.8	17.9	1234.8	13.4	991.4	14.4
B2_188	0.0822	0.0017	2.1151	0.0672	0.1814	0.0023	0.390	0.0528	0.0009	1249.3	40.2	1153.8	21.9	1074.7	12.3	1040.1	17.7
B2_189	0.0782	0.0015	1.6331	0.0447	0.1562	0.0019	0.445	0.0311	0.0005	1152.0	37.3	983.0	17.2	935.7	10.6	619.9	10.5
B2_190	0.0786	0.0015	1.9679	0.0550	0.1894	0.0023	0.434	0.0534	0.0008	1161.1	37.1	1104.6	18.8	1118.3	12.5	1050.8	15.4
B2_191	0.0548	0.0016	0.4749	0.0168	0.0671	0.0009	0.366	0.0192	0.0004	405.6	62.5	394.5	11.6	418.7	5.3	385.3	7.9

Anal. #	$^{207}Pb/^{206}Pb$	1 σ	$^{207}Pb/^{235}U$	1 σ	$^{206}Pb/^{238}U$	1 σ	rho	$^{208}Pb/^{232}Th$	1 σ	$^{207}Pb/^{206}Pb$ Age (Ma)	1 σ	$^{207}Pb/^{235}U$ Age (Ma)	1 σ	$^{206}Pb/^{238}U$ Age (Ma)	1 σ	$^{208}Pb/^{232}Th$ Age (Ma)	1 σ
B2_192	0.0859	0.0024	2.7080	0.1266	0.2320	0.0032	0.294	0.0645	0.0012	1336.3	53.0	1330.6	34.7	1345.0	16.7	1262.6	22.0
MFP_017	0.0529	0.0033	0.4846	0.0352	0.0714	0.0013	0.256	0.0201	0.0008	324.2	134.5	401.2	24.1	444.8	8.0	402.4	16.1
MFP_018	0.0691	0.0022	1.7657	0.0848	0.1708	0.0025	0.303	0.0560	0.0020	903.0	64.3	1032.9	31.1	1016.5	13.7	1101.2	37.6
MFP_019	0.0607	0.0027	0.7385	0.0406	0.0878	0.0014	0.292	0.0290	0.0006	628.8	92.0	561.5	23.7	542.5	8.3	577.0	12.3
MFP_020	0.0788	0.0017	1.9911	0.0654	0.2008	0.0027	0.403	0.0551	0.0012	1165.9	42.5	1112.5	22.2	1179.5	14.3	1084.5	22.8
MFP_021	0.1474	0.0043	1.7637	0.0755	0.0868	0.0014	0.366	0.0440	0.0008	2316.1	49.4	1032.2	27.7	536.3	8.1	870.6	16.3
MFP_022	0.0616	0.0026	0.7227	0.0388	0.0766	0.0012	0.297	0.0243	0.0007	659.7	88.9	552.3	22.8	475.8	7.3	484.5	14.1
MFP_023	0.1213	0.0071	3.2940	0.3545	0.1988	0.0048	0.223	0.1091	0.0046	1976.0	101.3	1479.6	83.8	1168.9	25.7	2092.0	83.2
MFP_024	0.0556	0.0016	0.3990	0.0143	0.0546	0.0008	0.384	0.0144	0.0003	437.3	64.1	341.0	10.4	342.8	4.6	288.5	6.8
MFP_025	0.0938	0.0024	3.4045	0.1533	0.2746	0.0039	0.315	0.0698	0.0015	1503.3	48.0	1505.4	35.3	1563.8	19.7	1363.0	27.6
MFP_026	0.0723	0.0023	1.4735	0.0670	0.1620	0.0024	0.322	0.0492	0.0014	993.7	62.1	919.6	27.5	968.0	13.2	971.6	26.7
MFP_035	0.0790	0.0023	2.1750	0.1008	0.1953	0.0028	0.312	0.0562	0.0012	1173.2	57.0	1173.1	32.2	1150.0	15.2	1105.6	23.2
MFP_037	0.0763	0.0030	1.4621	0.0826	0.1542	0.0025	0.285	0.0475	0.0013	1102.1	76.6	914.9	34.1	924.6	13.9	938.0	25.1
MFP_038	0.0574	0.0016	0.5478	0.0191	0.0697	0.0010	0.391	0.0160	0.0005	505.6	61.0	443.5	12.5	434.3	5.7	320.6	10.1
MFP_039	0.0548	0.0025	0.5196	0.0287	0.0737	0.0012	0.290	0.0230	0.0006	403.9	99.5	424.9	19.2	458.1	7.1	459.6	10.8
MFP_054	0.0580	0.0021	0.5358	0.0238	0.0703	0.0010	0.331	0.0189	0.0004	527.5	78.8	435.6	15.7	437.6	6.2	378.4	8.4
MFP_055	0.0906	0.0021	2.8434	0.1089	0.2433	0.0033	0.355	0.0700	0.0016	1437.8	44.0	1367.1	28.8	1403.8	17.2	1366.7	30.5
MFP_056	0.0717	0.0030	1.7618	0.1115	0.1592	0.0026	0.259	0.0482	0.0016	976.2	82.6	1031.5	41.0	952.3	14.5	951.4	31.5
MFP_057	0.0567	0.0017	0.5128	0.0192	0.0629	0.0009	0.369	0.0163	0.0004	477.4	66.5	420.3	12.9	393.3	5.3	327.2	7.0
MFP_058	0.0800	0.0016	1.8601	0.0536	0.1734	0.0023	0.450	0.0441	0.0010	1197.1	38.3	1067.0	19.0	1031.0	12.3	872.8	18.8
MFP_059	0.0845	0.0030	2.4717	0.1446	0.2192	0.0035	0.271	0.0625	0.0017	1305.0	67.8	1263.8	42.3	1277.5	18.4	1225.2	31.5
MFP_060	0.0786	0.0016	2.1739	0.0639	0.1986	0.0026	0.442	0.0571	0.0010	1162.1	38.6	1172.7	20.5	1167.8	13.9	1121.6	19.2
MFP_061	0.0780	0.0021	1.5937	0.0620	0.1597	0.0022	0.359	0.0500	0.0012	1145.7	51.9	967.7	24.3	954.9	12.4	985.9	22.7
MFP_062	0.1885	0.0090	6.3369	0.6670	0.2638	0.0061	0.221	0.1493	0.0048	2728.9	76.1	2023.6	92.3	1509.2	31.3	2813.1	83.9
MFP_071	0.1519	0.0122	3.0311	0.4264	0.1237	0.0040	0.230	0.0417	0.0014	2367.3	130.9	1415.5	107.4	752.0	23.0	824.7	27.2
MFP_072	0.0791	0.0019	1.7517	0.0616	0.1665	0.0023	0.388	0.0440	0.0010	1174.0	46.6	1027.8	22.7	992.6	12.6	870.8	18.8
MFP_073	0.0589	0.0017	0.4312	0.0147	0.0539	0.0007	0.404	0.0148	0.0004	563.2	60.1	364.1	10.4	338.2	4.6	297.1	8.5
MFP_074	0.0746	0.0020	1.9390	0.0786	0.1809	0.0025	0.347	0.0503	0.0010	1058.5	53.2	1094.6	27.2	1071.8	13.9	991.0	19.6
MFP_075	0.0525	0.0018	0.4733	0.0198	0.0665	0.0010	0.346	0.0172	0.0005	305.2	76.6	393.5	13.6	414.9	5.8	344.1	9.2
MFP_076	0.0764	0.0019	1.8731	0.0685	0.1847	0.0025	0.376	0.0483	0.0009	1105.8	48.0	1071.6	24.2	1092.6	13.8	953.4	17.9
MFP_077	0.0850	0.0025	2.5636	0.1203	0.2192	0.0032	0.312	0.0598	0.0013	1316.4	55.2	1290.3	34.3	1277.6	17.0	1173.9	24.0
MFP_078	0.1845	0.0038	11.7352	0.4978	0.4908	0.0068	0.327	0.1028	0.0021	2694.0	33.3	2583.5	39.7	2574.1	29.4	1978.0	38.0
MFP_079	0.0525	0.0018	0.4472	0.0187	0.0641	0.0009	0.348	0.0173	0.0006	306.0	75.3	375.3	13.1	400.5	5.6	345.6	11.2

Anal. #	$^{207}Pb/^{206}Pb$	1 σ	$^{207}Pb/^{235}U$	1 σ	$^{206}Pb/^{238}U$	1 σ	rho	$^{208}Pb/^{232}Th$	1 σ	$^{207}Pb/^{206}Pb$ Age (Ma)	1 σ	$^{207}Pb/^{235}U$ Age (Ma)	1 σ	$^{206}Pb/^{238}U$ Age (Ma)	1 σ	$^{208}Pb/^{232}Th$ Age (Ma)	1 σ
MFP_080	0.0879	0.0019	2.3234	0.0756	0.2012	0.0027	0.412	0.0474	0.0010	1379.9	40.6	1219.5	23.1	1181.7	14.5	935.5	19.1
MFP_089	0.0542	0.0015	0.5279	0.0178	0.0714	0.0010	0.402	0.0201	0.0003	379.1	60.5	430.4	11.8	444.8	5.8	402.7	6.5
MFP_090	0.0808	0.0018	2.1712	0.0715	0.2096	0.0028	0.404	0.0518	0.0011	1217.5	42.1	1171.8	22.9	1226.8	14.9	1020.1	20.2
MFP_091	0.0600	0.0025	0.5920	0.0296	0.0725	0.0011	0.312	0.0209	0.0005	604.5	86.5	472.1	18.9	450.9	6.8	417.8	9.5
MFP_092	0.0527	0.0017	0.4367	0.0168	0.0646	0.0009	0.363	0.0166	0.0003	316.0	71.3	367.9	11.9	403.4	5.5	331.7	6.6
MFP_093	0.0784	0.0027	2.0850	0.1134	0.1722	0.0026	0.282	0.0490	0.0013	1155.8	67.4	1143.9	37.3	1024.4	14.5	966.1	24.1
MFP_094	0.0775	0.0022	1.2387	0.0481	0.1239	0.0017	0.362	0.0280	0.0010	1134.0	54.6	818.3	21.8	753.0	10.0	558.1	18.8
MFP_096	0.0955	0.0027	2.2678	0.1002	0.1776	0.0026	0.326	0.0475	0.0011	1538.1	52.3	1202.3	31.2	1053.9	14.0	937.7	21.5
MFP_097	0.0849	0.0023	2.4759	0.1069	0.2215	0.0031	0.325	0.0635	0.0015	1312.6	52.0	1265.0	31.2	1289.6	16.4	1244.7	28.2
MFP_098	0.0556	0.0022	0.4013	0.0186	0.0559	0.0008	0.321	0.0139	0.0004	436.3	83.9	342.6	13.5	350.7	5.1	278.5	8.7
MFP_107	0.0908	0.0018	3.1578	0.0986	0.2476	0.0032	0.413	0.0671	0.0011	1443.2	36.3	1446.9	24.1	1426.0	16.5	1312.3	20.9
MFP_108	0.0826	0.0035	2.2440	0.1564	0.2225	0.0038	0.248	0.0543	0.0017	1260.5	81.6	1194.9	49.0	1294.9	20.2	1068.9	33.4
MFP_109	0.0523	0.0022	0.5001	0.0255	0.0710	0.0011	0.298	0.0217	0.0007	297.3	94.6	411.8	17.3	442.2	6.5	433.5	13.1
MFP_112	0.0597	0.0015	0.8006	0.0273	0.0954	0.0013	0.391	0.0268	0.0005	591.8	54.7	597.2	15.4	587.2	7.5	534.0	9.4
MFP_113	0.1923	0.0037	12.9641	0.5293	0.4932	0.0065	0.323	0.1209	0.0021	2761.9	31.0	2677.0	38.5	2584.3	28.1	2307.5	37.4
MFP_114	0.0562	0.0016	0.5415	0.0194	0.0681	0.0009	0.377	0.0187	0.0005	458.5	61.1	439.4	12.8	424.5	5.5	374.6	9.5
MFP_115	0.0544	0.0016	0.4912	0.0183	0.0647	0.0009	0.364	0.0192	0.0004	385.8	64.4	405.8	12.5	404.3	5.3	383.8	7.0
MFP_116	0.0844	0.0025	2.2418	0.1021	0.1961	0.0028	0.314	0.0541	0.0010	1302.2	55.4	1194.2	32.0	1154.5	15.1	1065.5	18.3
MFP_125	0.0893	0.0018	3.1173	0.1015	0.2547	0.0033	0.399	0.0669	0.0010	1409.7	37.8	1437.0	25.0	1462.8	17.0	1308.7	19.8
MFP_126	0.0739	0.0016	1.9097	0.0609	0.1837	0.0024	0.408	0.0431	0.0008	1039.5	42.6	1084.5	21.3	1087.0	13.0	853.5	15.1
MFP_127	0.0574	0.0017	0.5776	0.0216	0.0748	0.0010	0.369	0.0216	0.0004	507.6	65.1	462.9	13.9	465.1	6.2	432.7	7.7
MFP_128	0.0936	0.0018	3.5225	0.1117	0.2481	0.0032	0.408	0.0695	0.0010	1500.1	36.3	1532.3	25.1	1428.6	16.6	1357.2	19.2
MFP_129	0.0655	0.0014	1.3838	0.0423	0.1468	0.0019	0.425	0.0427	0.0008	791.6	44.3	882.1	18.0	882.9	10.7	844.4	15.6
MFP_130	0.0893	0.0019	2.8296	0.0968	0.2237	0.0030	0.387	0.0611	0.0011	1410.7	40.4	1363.4	25.7	1301.3	15.6	1198.2	20.4
MFP_131	0.0679	0.0019	1.1971	0.0458	0.1291	0.0018	0.361	0.0389	0.0008	865.9	55.6	799.2	21.2	782.8	10.2	771.6	15.8
MFP_132	0.0710	0.0016	1.4270	0.0466	0.1433	0.0019	0.406	0.0350	0.0006	956.5	45.4	900.3	19.5	863.4	10.7	695.3	11.9
MFP_133	0.0806	0.0019	1.9304	0.0676	0.1858	0.0025	0.384	0.0363	0.0008	1211.0	45.0	1091.7	23.4	1098.4	13.6	719.9	16.4
MFP_134	0.0745	0.0021	1.4864	0.0617	0.1513	0.0022	0.342	0.0389	0.0010	1055.2	56.4	924.8	25.2	908.3	12.0	770.9	18.5
MFP_143	0.0553	0.0017	0.5877	0.0224	0.0768	0.0011	0.365	0.0216	0.0004	425.4	67.1	469.4	14.3	476.9	6.4	432.3	8.5
MFP_144	0.0567	0.0015	0.4428	0.0141	0.0583	0.0008	0.421	0.0123	0.0004	478.2	56.7	372.2	9.9	365.0	4.8	247.7	7.0
MFP_145	0.0786	0.0016	1.6512	0.0493	0.1609	0.0021	0.439	0.0287	0.0008	1160.7	40.4	990.0	18.9	961.7	11.7	572.1	15.8
MFP_146	0.0843	0.0021	2.6245	0.1044	0.2344	0.0032	0.347	0.0606	0.0012	1298.9	47.2	1307.5	29.2	1357.3	16.9	1189.9	22.3
MFP_147	0.0787	0.0016	1.9570	0.0593	0.1835	0.0024	0.431	0.0439	0.0008	1165.5	40.0	1100.8	20.4	1086.2	13.1	869.0	15.2

Anal. #	$^{207}Pb/^{206}Pb$	1 σ	$^{207}Pb/^{235}U$	1 σ	$^{206}Pb/^{238}U$	1 σ	rho	$^{208}Pb/^{232}Th$	1 σ	$^{207}Pb/^{206}Pb$ Age (Ma)	1 σ	$^{207}Pb/^{235}U$ Age (Ma)	1 σ	$^{206}Pb/^{238}U$ Age (Ma)	1 σ	$^{208}Pb/^{232}Th$ Age (Ma)	1 σ
MFP_150	0.0876	0.0017	2.2830	0.0658	0.1903	0.0025	0.449	0.0549	0.0009	1373.5	36.9	1207.1	20.4	1122.8	13.3	1079.8	17.8
MFP_151	0.0802	0.0017	2.1185	0.0667	0.1951	0.0026	0.417	0.0475	0.0009	1201.3	41.1	1154.9	21.7	1148.8	13.8	937.1	17.5
MFP_152	0.0761	0.0017	1.3878	0.0455	0.1309	0.0017	0.406	0.0319	0.0006	1098.8	45.0	883.8	19.3	792.8	9.9	633.7	11.1
MFP_162	0.2280	0.0046	2.6530	0.0815	0.0860	0.0012	0.451	0.1016	0.0016	3037.9	32.2	1315.5	22.7	531.6	7.1	1954.9	28.7
MFP_163	0.0590	0.0015	0.5601	0.0175	0.0680	0.0009	0.429	0.0160	0.0003	568.3	52.8	451.6	11.4	423.9	5.5	320.2	5.0
MFP_164	0.0581	0.0015	0.6203	0.0201	0.0779	0.0010	0.411	0.0216	0.0004	533.8	55.0	490.0	12.6	483.5	6.2	431.8	7.1
MFP_166	0.0820	0.0017	2.3069	0.0716	0.2043	0.0027	0.422	0.0533	0.0010	1245.6	39.4	1214.4	22.0	1198.3	14.4	1050.2	19.5
MFP_167	0.0588	0.0017	0.5193	0.0194	0.0640	0.0009	0.373	0.0173	0.0005	558.8	63.3	424.7	13.0	399.6	5.4	346.0	9.4
MFP_168	0.0742	0.0016	1.3932	0.0435	0.1432	0.0019	0.425	0.0279	0.0005	1046.1	43.0	886.0	18.5	862.6	10.7	556.0	10.7
MFP_169	0.0544	0.0018	0.4345	0.0176	0.0578	0.0008	0.354	0.0161	0.0004	389.0	70.8	366.4	12.5	362.4	5.0	322.8	7.5
MFP_170	0.0756	0.0017	1.8452	0.0613	0.1751	0.0023	0.402	0.0457	0.0010	1084.9	44.0	1061.7	21.9	1040.1	12.8	903.1	20.1
MFP_179	0.0785	0.0023	2.3360	0.1107	0.2133	0.0031	0.309	0.0551	0.0015	1158.6	57.6	1223.3	33.7	1246.2	16.6	1084.8	28.0
MFP_180	0.0740	0.0022	1.7652	0.0778	0.1888	0.0027	0.328	0.0462	0.0011	1040.4	58.6	1032.7	28.6	1114.6	14.8	913.4	20.8
MFP_181	0.0599	0.0028	0.6620	0.0373	0.0793	0.0013	0.291	0.0208	0.0005	601.4	96.5	515.9	22.8	491.7	7.8	416.6	10.7
MFP_182	0.0771	0.0015	1.5733	0.0441	0.1486	0.0019	0.466	0.0360	0.0006	1122.8	38.8	959.7	17.4	892.9	10.9	714.6	12.6
MFP_183	0.1715	0.0026	8.6318	0.2142	0.3836	0.0049	0.513	0.1003	0.0014	2572.0	25.5	2299.9	22.6	2093.0	22.8	1932.5	26.5
MFP_184	0.0817	0.0021	1.5369	0.0568	0.1319	0.0018	0.378	0.0073	0.0004	1239.2	49.5	945.2	22.7	798.5	10.5	146.3	8.6
MFP_186	0.0570	0.0017	0.5494	0.0200	0.0711	0.0010	0.383	0.0200	0.0004	492.0	64.2	444.6	13.1	442.7	6.0	399.5	7.8
MFP_187	0.0828	0.0023	2.0848	0.0883	0.1721	0.0025	0.338	0.0492	0.0011	1265.0	52.7	1143.8	29.1	1023.5	13.5	970.0	21.9
MFP_188	0.0561	0.0028	0.3909	0.0225	0.0512	0.0009	0.292	0.0125	0.0005	454.8	107.7	335.0	16.4	321.6	5.3	251.0	9.4
MFP_189	0.0600	0.0022	0.4143	0.0179	0.0531	0.0008	0.344	0.0132	0.0003	601.7	77.2	352.0	12.9	333.4	4.9	264.7	5.6